TESTING OF A REPAIRED MICRO-CONCRETE MODEL OF A COOLING TOWER SHELL

by

HOSSEIN MOZAFFARIAN

B.S., Kansas State University, 1980

A MASTER'S THESIS

submitted in partial fulfillment of

the requirements for the degree

MASTER OF SCIENCE

Department of Civil Engineering

KANSAS STATE UNIVERSITY

Manhattan, Kansas

1983

Approved by

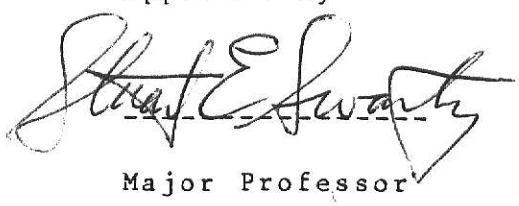

Major Professor

Table of Contents

List of Tables

List of Figures

List of Figures (Continued)

THIS BOOK
CONTAINS
NUMEROUS PAGES
WITH THE ORIGINAL
PRINTING BEING
SKEWED
DIFFERENTLY FROM
THE TOP OF THE
PAGE TO THE
BOTTOM.

THIS IS AS RECEIVED
FROM THE
CUSTOMER.

List of Figures (Continued)

List of Figures (Continued)

SYNOPSIS

In the past ten years the use of natural-draft cooling towers in Europe and North America has increased. These hyperboloids of revolution have increased in size from 115 ft. (35 m) in 1914 to 495 ft. (151 m) in 1979 with 656 ft. (200 m) contemplated for the near future.

Following the catastrophic collapse of three of the eight towers in Ferrybridge, England, in 1965 (5), an intensified research was initiated to understand the behavior of this type of shell and to find answers to these spectacular structural failures. Further interest and need for more and better understanding of the structural behavior of hyperbolic natural-draft cooling towers became urgent after the failure of the cooling tower in 1973 at Ardeer, Scotland, some eight years after construction. This structural tragedy at Ardeer inspired research in the effects of geometry imperfections in cooling towers especially. Most of the experimental work has been on small elastic models and very little information is available on the results of physical testing of concrete models. Consequently, there appears to be a gap between theoretical and true behavior of these giant concrete structures.

The work described herein, is on the testing procedure, behavior, and effects of imperfections on the response of a reinforced concrete cooling tower model subjected to axisymmetric loading (vacuum).

The shell is nominally 0.5 in. (13 mm) thick, 12 ft. (3.65 m) high, and 9.33 ft. (2.84 m), 6 ft. (1.82 m), and 6.45 ft. (1.96 m) in diameter at the base, throat, and top, respectively.

CHAPTER I

INTRODUCTION

Hyperbolic, natural-draft cooling towers are probably the largest reinforced concrete thin-shell structures being built today. Because of the growing need for electric power in the industrialized societies, the use of taller and larger cooling towers with higher cooling capacities has become continually necessary to dissipate large quantities of heat in power stations. Since 1914 the size of these towers has increased from 115 ft. (35 m) to 495 ft. (151 m) in 1979 and towers as high as 656 ft. (200 m) are being considered for the near future.

The basic reason for using the hyperbolic shape for cooling towers is that it is highly efficient in producing a natural draft of air compared to the cylindrical or conical shapes. Besides, the hyperbolic shape provides much greater structural strength due to the double curvature of the shell.

The principal function of a cooling tower is to cool and reuse large quantities of water. The general operational system can be summarized as followes: hot water is pumped to a certain height and then through a piping system it reaches nozzels which splash it over a system called filling or stacking. the function of the filling or stacking is to scatter the water into films or droplets which will provide a larger surface area for the cooling air and hot water to contact. The air, which enters into the base of the tower, is forced upward by

atmospheric pressure difference or the so-called chimney effect. The rising air passes through the droplets or films of hot water and cools them by evaporation and convection. The cooled water is then collected in a pond at the bottom of the tower and is ready to be returned into the condenser system for use.

Even though natural-draft cooling towers consist of several structural units, the shell part (hyperboloid of revolution) remains in the center of attention and demands most of the work and analysis in design and construction.

As a result, and due to collapse of three cooling towers at Ferrybridge, England, and one at Ardeer, Scotland, researchers have become more concerned about the true behavior of these giant reinforced concrete structures. Unfortunately, most of the work is analytical and very few buckling experiments have been carried out on concrete or micro-concrete models subject to axisymmetric or asymmetric loads. Even the experimental results available are mostly for metal or plastic models.

The experiment reported here is on a simple, non-offset, and repaired micro-concrete hyperboloid of revolution. The goals of this study are to obtain some experimental evidence on the buckling behavior of this type of concrete shell and the effects of geometry imperfections under axisymmetric pressure (vacuum).

CHAPTER II

REVIEW OF LITERATURE

Although hyperbolic natural-draft cooling towers are probably the largest reinforced thin-shell structures being built today, there has been very little experimental research on the behavior and stability of this type of shell (2). Perhaps, the most extensive experimental study of model cooling towers has been carried out by Der and Fidler (13). Their electroformed copper and PVC (Polyvinyl Chloride) models were subjected to wind loading in a compressed air tunnel. All the models failed by a snap-through of the upper rim with little noticeable progressive deflection prior to buckling.

In Reference 4, Billington and Harris review tests used to investigate the buckling of roof shells and shell walls. They categorize hyperbolic cooling towers as shell walls where the primary loads causing buckling are horizontal and transient (wind or seismic).

Even though, wind loadings are the governing design criteria for hyperbolic natural-draft cooling towers, there seems to be a lack of experimental evidence regarding the stability of concrete shells for this type of loadings. Most of the pertinent tests of this nature have been conducted on plastic or metal models (13). Nevertheless, Abel and Gould in their paper (2) identify three methods for the stability analysis of large concrete hyperboloids subject to wind

loadings based on axisymmetry (15,29). In References 14 and 15, Ewing gives a complete analytical treatment of cooling tower stability. He uses a linearized theory to analyze hyperboloids of constant thickness without stiffening rings or flexible supports both under axisymmetric pressures and non-axisymmetric wind loads. His conclusion is that the theoretical axisymmetric buckling pressures are smaller than the peak wind pressure associated with bifurcation of the same hyperboloid. Langhaar and Miller (22) also reached the same conclusion for fixed-free cylinders subjected to both axisymmetric and asymmetric radial pressures.

Veronda and Weingarten (33) have written computer programs for linear buckling and linear and nonlinear prebuckling analysis of hyperboloidal shells using the finite element method. Cole, Abel, and Billington (7,8) have also developed a finite-element computer program to study the problems encountered in design when cosidering stability. In Reference 8 the authors describe in their work those parameters which are characteristic of actual cooling towers to estimate the bifurcation buckling loads.

However, it should be mentioned that neither of the three methods given in Reference 2 has been accepted or used universally by designers and researchers who differ on such matters as local buckling versus global stability treatment, bifurcation analyses versus limit-point analyes, reduced shell theories versus full shell theories, and axisymmetric analyses versus non-axisymmetric analyses.

Be that as it may, Abel and Gould (2) say that for routine design purposes bifurcation calculations with approximate methods based on axisymmetry can supply reasonable estimates for buckling pressure of hyperboloids subject to wind loading.

In two recent studies (19,23), a reinforced concrete cooling tower built in Port Gibson, Miss., USA subjected to wind loading is investigated in detail. The investigators believe that failure of a reinforced concrete cooling tower would not be initiated by buckling but rather by rapid propagation of cracks in the tensile zone followed by temporary stiffening and, finally, by yielding of the reinforcement. For that matter, the tensile strength of concrete is considered to be of critical importance in the safety of the shell against collapse. In Reference 23, Mang, et al., conclude that results based on an equivalent axisymmetric pressure are on the unsafe side of corresponding results for the actual wind load. It is also believed in both studies that linear-elastic non-axisymmetric analysis is an appropriate tool for the design of cooling towers subject to wind loads.

Since the collapse of the 350 ft. high Ardeer cooling tower in Scotland, more research and study has been conducted in order to gain better knowledge of the effects of imperfections in the geometry of reinforced concrete cooling towers.

In Reference 11, Croll, Kaleli, and Kemp analyze a cooling tower model with axisymmetric geometry imperfections represented as a series of piecewise continuous second-order

rotationally symmetric shells of the same general form as that of the perfect shell. Their analysis yields hoop forces due to imperfections and meridional bending moments. This analysis is based on the assumption that flexural failure due to the imperfection generated meridional moments will not precipitate collapse, but that the shell has sufficient ductility to enable a redistribution from bending to membrane action to occur. It is also stated that variations in the elevation of the imperfection are found to have a significant influence on the stress changes.

Croll and Kemp have two approaches to examine changes in hoop tensions that occur in an axisymmetric meridionally imperfect shell. The first approach (10) is the same as that given in Reference 11 and a finite difference discretisation is used to solve the appropriate equations for shell bending. In the second approach (12), however, a normal pressure distribution is chosen to simulate the geometric imperfection so that it is statically equivalent to the out-of-balance forces that would be present when it is considered that the membrane stresses of the perfect shell act on the geometrically imperfect shell.

Mungan (26) tested several shell models made of a cold epoxy resin and hardner to determine the primary buckling stresses of nearly perfect hyperboloidal-type shells and he concluded that buckling depends primarily on the local imperfections, wall thickness, and the stress state acting in

the model. He also reached the conclusion that buckling is always initiated at a point with an imperfection resulting from a reduced thickness. Mungan in a later study (25) shows that the buckling behavior of shells can be improved by placing stiffening rings in the models.

In a recent paper (24) Mungan states that model tests showed that buckling always began locally. According to him cooling tower shells buckle locally in presence of even slight imperfections and the influence of initial imperfections is more than the influence of boundary conditions on local buckling. He emphasizes that in the buckling design of reinforced concrete cooling tower shells local buckling has to be prevented everywhere within a certain safety margin in order to fulfill global or overall stability of the shell. This is the idea behind what he calls the Buckling Stress States (BSS) approach developed by him.

The preceding approach, which is recommended by the International Association for Shell and Spatial Structures (IASS), is critisized by Abel, et al. (1). They question the applicability of the approach to actual cooling tower design and list three problems associated with it: (1) factoring of boundary-condition sensitivity into the approach in an uncertain way; (2) lacking a way to include the important influence of concrete cracking; and (3) applying a safety factor of five to both wind and dead load and in turn creating an unrealistic stress condition.

Gupta and Al-Dabbagh have also studied the effects of meridional imperfections in cooling towers. In Reference 3 they assume that the meridional shape of imperfection is a combination of two straight lines. Later Gupta, et al. (18) assumed a general shape which would have the straight line or circular configuration as two extremes.

Furthermore, they state that: (a) hoop stresses are increased as a result of imperfections; (b) meridional moment plays an important role in the safety of the tower; and (c) imperfection stresses should be considered in the design of cooling towers.

On the other hand, there are those who believe that shells of negative Gaussian curvature, hyperboloids of revolution, under axisymmetric loadings are not significantly sensitive to geometric imperfections (21,33).

In Reference 6, the results of the first test of the shell under consideration here are discussed. The failure is reported to be similar to that of a spherical concrete shell. The author states that this type of failure has never been reported for hyperbolic shells before. The geometry and thickness imperfections are considered to have produced additional stresses and moments. The author also states that the structure responded unsymmetrically and the failure mode was initiated by some mechanism other than by exceeding material limits.

Yet there is no clear and full understanding of the behavior of cooling towers in the real world. Consequently,

more research and effort should be directed in this area considering the effects of such factors as the true shell geometry, realistic support conditions, gravity and thermal loadings, orthotropic materials, and variations of wind pressure.

CHAPTER III

SHELL TEST ARRANGEMENTS

The shell under consideration here has been designed, erected, and tested once previously. The model is 12 ft. (3.65 m) high with throat radius of 36 in. (0.91 m),base radius of 56 in. (1.42 m),and nominal thickness of 0.5 in. (13 mm). The uniform thickness of 0.5 in. was not however accomplished very accurately during construction and various thicknesses were recorded which will be looked at later. Fig. 1 shows the geometry of the shell in more detail.

In References 6,16,30, a complete, detailed, and pictorial description of design and construction of support facilities, assembling of reinforcing wires, form work, model materials, and construction sequence of the shell modell is given. The results of the first buckling test are also discussed in Reference 6.

The hole which occured in the shell as a result of the first experimental test (6) was patched up and later strain gages were mounted on the inside and outside of this patched region. The properties of the patching mix and reinforcing steel are given in Table 1. Table 2 displays the results of the cylinder tests.

STRAIN AND DISPLACEMENT INSTRUMENTATION

Temperature compensated electrical resistance foil strain

gages were used. These were two element rectangular rosettes with a gage length of 0.125 in. (3.18 mm). The gages were positioned to be parallel to the circumferential direction (even-numbered gages) and meridional direction (odd-numbered gages).

Dial gages mounted on a portable beam (6),which could be moved to various circumferential locations, were used to record deflection measurements. These had a least reading of 0.001 in. (0.0254 mm) and travel of 2 in. (50 mm).

Locations for strain, deflection, geometry, and thickness measurements are shown in Fig. 2 and 3. More information on these items can be found in References 6, 16, and 17.

LOADING EQUIPMENT AND TESTING PROCEDURE

The loading equipment essentially consisted of a high vacuum, high capacity pump and three or four lower capacity accessory pumps; lines and fittings; and a mercury manometer. The high capacity pump had a shut off valve which permitted a constant pressure (vacuum) to be maintained.

The testing procedure was:

1. Initialize strain and dial gage data;
2. Apply load to desired level and maintain;
3. Record strain data and dial data;
4. Repeat steps 2 and 3 until the final load level;
5. Move the portable beam to the next location and repeat steps 1-4.

The main difficulty encountered during testing was the leakage of air from the top and bottom cover plates. Hence, more bracing was fastened to the plates to decrease their movement due to suction. The joints and connections were also sealed with different commercial compounds (silicon rubber, liquid nail, resin) where silicon rubber proved the most efficient and air-tight.

CHAPTER IV

TEST RESULTS AND ANALYSIS

SHELL GEOMETRY

After the first testing of the shell (6), measurements of deviation from ideal geometry were taken at 132 locations. The deviation values shown in Table 3 represent the differences from the ideal shell horizontal radius to the outer surface at the locations indicated in Figs. 2 and 3.

It is attemted here to improve the deviation data by considering the actual thickness values given in Reference 6 and shown in Table 4. Sample calculations are given in Appendix C for two throat locations with geometrical description shown in Fig. 4. Table 5 gives the complete list of the improved data of deviation from ideal mid-surface geometry with the maximum deviations in the radii being +3.2%, -2.7%.

The percent deviation in a vertical distance along a meridian expressed as the slope S is found from:

$$S = (2\triangle/H)100$$

where

$$\triangle = \triangle r_{ij} - 1/2\ (\triangle r_{i-1,j} + \triangle r_{i+1,j})$$

H = gage length of 24 in. (60.96 cm)

$\_r_{ij}$ = center line radial deviation at the center of the vertical gage length

$\triangle r_{i-1,j}, \triangle r_{i+1,j}$ = center line radial deviation at the ends of the vertical gage length

i = gage number from 1-11

j = line number from A-L, i.e., from 1-12

The maximum values of S for each vertical line are also presented in Table 5. The overall maximum values of S are about $\pm$ 2.65%.

The data in Table 5 is used to plot circumferential deviation profiles from ideal shell middle surface geometry at all eleven dial gage locations, Figs. 5-15. These display the out-of-roundness of the shell. Notice that they generally follow the same oval pattern.

Hence, the geometry of the model shell is not as accurate as encountered in practice today. Notwithstanding, as geometrical scale becomes smaller (a scale factor of 30 for this model), the chance of achieving corresponding tolerances becomes smaller too,if the model is to represent the prototype.

SHELL THICKNESS

As mentioned previously the shell varied widely in thickness particularly in the first lift (locations of the three lifts are shown in Fig. 2). The reason for this included lack of experience and difficulties encountered during casting of the shell,e.g., form bulging and seperation, etc. (6).

In order to have a better picture of the thickness variation, a thickness contour map of the shell is shown in Fig. 16 with contour intervals of 0.1 in. (2.54 mm). It can be seen from the map that lift one shows great thickness variation

while lifts 2 and 3 show less variation and better uniformity. The percent deviation from mean values of thickness at each elevation for lifts 2 and 3 are given in Table 6. It is observed that the largest deviations from the mean are +82% and -60%. Corresponding deviations for Mungan's large plastic models (26) are +26% and -22% as given in Table 7. Thickness deviations on a concrete model of a cylindrical shell reported by Harris, et al. (28) are +46%, -24%.

Geometry and thickness imperfections produce additional forces and moments which will be discussed later.

STRUCTURAL RESPONSE AND FAILURE

After a long and cumbersome buckling test the shell finally failed at a pressure (vacuum) of 3.7 Psi (25.53 KPa). This is about 20% greater than the pressure of 3.1 Psi (21.4 KPa) that caused failure in the first test (6). The load that commenced failure is slightly more than half that predicted using the method of Reference 17. The method of Reference 20 using a grid analogy and considering linear material response gave a buckling load of 3.2 Psi (22 KPa).

Strain versus load curves up to the failure load of 3.7 Psi (25.53 KPa) are presented in Figs. 17-24. The overall response is linear and no indication of buckling is observed. Fig. 24 shows the curves for the patched region which is the failure region of the first test. These plots do not show any sudden jump of the strain and are generally linear up to the failure pressure. Also shown in the figures are the theoretical

curves based on membrane theory amended by meridional imperfection. These are plotted using the following equations:

$$\varepsilon_\theta = (N_\theta - \mu N_\phi)/t E_c$$

$$\varepsilon_\phi = (N_\phi - \mu N_\theta)/t E_c$$

where

Poisson's ratio, μ, and Young's modulus of concrete, E_c, are 0.16 and 3.62×10^6 Psi (24.9 GPa), respectively (6).

In calculating the membrane forces N_ϕ and N_θ it was assumed that the shell carried 5/9 of the load from the top plate (16). In addition the method given by Gupta and Al-Dabbagh (18) was followed in order to include the effects of measured surface geometry imperfections which caused additional hoop force and meridional bending moment. This process is demonstrated in Appendix C through sample calculations at the throat on vertical line H.

The load-strain curves show good agreement between average (membrane) values and theoretical values. For example, at 4 ft. (1.22 m) below the throat, Fig. 22, the deviation between the average and theoretical curves becomes very small while at the base, Fig. 23, this deviation is almost zero.

Evidently the structural failure did not initiate by exceeding material limits because the maximum negative strain recorded --169×10^{-6} in./in.,Fig. 21-- is equivalent to a concrete compressive stress of about 690 Psi (4.76 MPa).

Values of the experimental forces and bending moments at the locations of the strain gages, including the patched region, are given in Table 8 for the failure load of 3.7 Psi (25.53 KPa). The equations and sample calculations for computing these forces and moments are presented in Appendix C. From Table 8 it can be observed that,

1. The patched region does not have the largest forces and moments.
2. The forces at the three throat locations (90 degree apart circumferentialy) are not equal; hence the structural response is unsymmetrical.
3. At all locations except that just below the top ring N_θ predominates.
4. At the base and top of the shell M_θ and M_ϕ are significant, respectively.

Figure 25 displays the experimental and theoretical plots for the compressive support column loads. The curves are plotted from the equations:

Experimental, $P = 1/2\ (\varepsilon_{c_1} + \varepsilon_{c_2}) E_s\ A$

Theoretical, $P = 4/9\ \pi r^2 q$

In which,

ε_{c_1} and ε_{c_2} are the recorded strains for the column;

E_s is the modulus of elasticity of steel, 29 x 10^6 Psi (200 GPa);

A is the cross sectional area of the column given in Table 1;

r is the radius of the top plate;

In plotting the theoretical curve it was assumed that the column carried 4/9 of the top cover load (16).

Deflection profiles along the twelve meridional lines,A-L, are displayed in Figs. 26-34. Local perturbations can be noticed on lines B, E, and L which might suggest development of cracks or failure on or close to these lines. However, neither cracks nor failure occured at these locations. The failure location of the first buckling test (patched region) appears to act as an inflection point because line G has outward displacement while line H moved inward. Deflection in the region of the hole seems to be the largest along line J. Also the direction of of the deflection curve is the same as the failure - inward. The two deflection profiles for line F --Figs. 28 and 29-- are for loads of 2.8 Psi (19.3 KPa) and 3.7 Psi (25.53 KPa), respectively. Notice that Fig. 29 is plotted up to the failure pressure of 3.7 Psi. Although the data for the two plots were taken at different times the resemblance is very good.

The circumferential plots of the displacements for all eleven dial gage locations are presented in Figs. 35-45 for a load of 2.8 Psi (19.3 KPa). This same oval pattern was obtained for virtually all of the load stages. This deflection pattern is not associated with buckling but is probably caused by the

shell imperfections, particularly the out-of-roundness. It is interesting and worthwhile to mention that these circumferential deflection profiles essentially have the same pattern as the geometry deviation profiles, Figs. 5-15.

It was desired to find a function of θ (circumferential angle from 0-2) expressed as a series that would fit the circumferential deviation plots and pass through all twelve data points,i.e., A-L. For that matter a number of different functions were tried as given below

$$e = \sum_{n=o}^{N} A_n \cos(n\theta/2) \quad \ldots\ldots\ldots\ldots\ldots\ldots\ldots \quad (1)$$

$$e = \sum_{n=o}^{N} A_n \cos(n\theta) \quad \ldots\ldots\ldots\ldots\ldots\ldots\ldots \quad (2)$$

$$e = \sum_{n=o}^{N} [\, A_n \cos(n\theta) + B_n \sin(n\theta)] \quad \ldots\ldots \quad (3)$$

where

e = theoretical circumferential deviation (+ inward)

A_n, B_n = coefficients in the series

The first two functions did not give any acceptable results; however, the third function with N=6 fitted the deviation plots perfectly and passed through all twelve data points. A computer program with least square method was used to evaluate the coefficients A_n and B_n. Using this series the deviations were calculated at the throat, 4 ft. (1.22 m) below the throat, and 7 ft. (2.13 m) below the throat at ten degree intervals with plots shown in Figs. 8, 12, and 15, respectively. the values of the coefficients for these locations are presented in

Table 9.

Now the question in mind is: would the deflection function found using the given series for circumferential deviation as a basis fit the experimental deflection curves? To find that out, first, the deflection function is derived as follows:

From Reference 31 the differential equation for the deflection curve for a thin bar with circular center line is

$$d^2w/ds^2 + w/r^2 = -M/EI \quad \ldots\ldots\ldots\ldots\ldots\ldots \quad (4)$$

where w is the radial deflection (+ inward)

and $ds^2 = r^2 d\theta^2$

Hence

$$d^2w/d\theta^2 + w = -Mr^2/EI \quad \ldots\ldots\ldots\ldots\ldots \quad (5)$$

The moment is given by

$$M = qrh\,(e + w) \quad \ldots\ldots\ldots\ldots\ldots\ldots\ldots\ldots \quad (6)$$

Neglect w in equations 5 and 6 by assuming that at low loads it is small compared to the imperfection, e, and has secondary effects.

Therefore,

$$d^2w/d\theta^2 = -Mr^2/EI$$

and $M = qrhe$

where

q = uniform external pressure (vacuum)

r = radius of the ring

h = width of the ring

$$e = \sum_{h=o}^{6} [\, A_n \cos(n\theta) + B_n \sin(n\theta)]$$

or

$$e = A_o + \sum_{n=1}^{6} [\, A_n \cos(n\theta) + B_n \sin(n\theta)]$$

$$d^2w/d\theta^2 = -KA_o - K \sum_{n=1}^{6} [A_n \cos(n\theta) + B_n \sin(n\theta)]$$

$$K = qr^3h/EI$$

$$dw/d\theta = -KA_o\theta - K \sum_{n=1}^{6} 1/n \, [A_n \sin(n\theta) - B_n \cos(n\theta)] + C_1$$

$$w = -1/2 \; KA_o\theta^2 + K \sum_{n=1}^{6} 1/n^2 \, [A_n \cos(n\theta) + B_n \sin(n\theta)] + C_1\theta + C_2$$

From the boundary condition $w(\theta=0) = w(\theta=2\pi)$

$$C_1 = K\pi A_o$$

The relationship between radial displacement (w) and tangential displacement (v) is given by (27)

$$dv/d\theta - w = 0 \quad \ldots\ldots\ldots\ldots\ldots\ldots\ldots\ldots\ldots\ldots \quad (7)$$

Therefore,

$$v = -1/6 \; KA_o\theta^3 + K \sum_{n=1}^{6} 1/n^3 \, [A_n \sin(n\theta) - B_n \cos(n\theta)] + 1/2 \; C_1\theta^2 + C_2\theta + C_3$$

and $v(\theta=0) = v(\theta=2\pi)$

Hence

$$C_2 = -1/3 \; K\pi^2 A_o$$

Or,

$$w = qr^3h/EI\{(-1/3 \; \pi^2 + \pi\theta - 1/2 \; \theta^2)A_o + \sum_{n=1}^{6} 1/n^2 \, [A_n \cos(n\theta) + B_n \sin(n\theta)]\}$$

The above deflection function is plotted at the throat, 4

ft. (1.22 m) below the throat, and 7 ft. (2.13 m) below the throat as shown in Figs. 38, 42, and 45, respectively. Notice that the theoretical deflection plots do not fit the experimental curves very well and show almost kind of a circular deflection pattern.

The shell failed explosively at a vacuum pressure of 3.7 Psi (25.53 KPa) in a similar manner to the first test (6) but at a different location. The failure region is shown in Figs. 46 - 49. Figs. 48 and 49 present drawings of the hole when viewed from outside and inside the shell, respectively. The hole is kind of oval in shape with its long axis in the circumferential direction and centered on line J, 12.5 in. (31.75 cm) above the base. Unlike the failure region of the first test there were a good number of cracks surrounding the hole. Fig. 49 displays a vertical crack which propagated into lift 2. The wire reinforcing, which had some concrete attached to, was basicly bent with one broken wire. Hence the wires provided much more support in restraining the concrete as opposed to the first test where the wires provided almost no support and remained essentially straight.

Although this type of failure was unexpected one should have foreseen the occurance of local buckling due to the presence of imperfections and absence of deformation control (24).

In Reference 6 it is stated that in the first test the shell failed in a manner quite similar to unreinforced concrete spherical caps. The writer beleives that this is not quite true

for the second test. First, the failed region is not quite like those shown in References 6 and 32. Secondly, the reinforcement provided support in retaining the concrete which resulted in the failed area being about double in size that of the first test.

The shell was analyzed at the location of the hole to determine a critical pressure associated with possible local buckling using Mungan's Buckling Stress State approach with modified equations presented in Reference 17. These are

$$0.80\left(\frac{\tilde{\sigma}_\theta}{\sigma_{\theta_o}}+\frac{\tilde{\sigma}_\phi}{\sigma_{\phi_o}}\right)+0.20\left[\left(\frac{\tilde{\sigma}_\theta}{\sigma_{\theta_o}}\right)^2+\left(\frac{\tilde{\sigma}_\phi}{\sigma_{\phi_o}}\right)^2\right]=1$$

in which

$$\tilde{\sigma}_\phi = -N_\phi/t\ ,\quad \tilde{\sigma}_\theta = -N_\theta/t$$

$$\sigma_{\phi_o} = Q_\phi E_T\ ,\quad \sigma_{\theta_o} = Q_\theta E_T$$

and the geometry buckling parameters Q_θ , Q_ϕ are given by

$$\begin{Bmatrix} Q_\theta \\ Q_\phi \end{Bmatrix} = \frac{1}{(1-\mu^2)^{3/4}}(t/a)^{4/3}\begin{Bmatrix} K_{G\theta} & F_\theta \\ K_{G\phi} & F_\phi \end{Bmatrix}$$

where $K_{G\theta}$, $K_{G\phi}$, F_θ, and F_ϕ are buckling coefficients which depend on the geometry, boundary conditions, and imperfections of the shell considered. The instantaneous tangent modulus, E_T, is given by one of the two E_T values associated with strain in the circumferential or in the meridional direction. For the linear results E_T is replaced by E_C, Young's modulus of concrete.

The results of these calculations are presented in Table 10 in which one would notice that buckling pressure associated with the meridional direction strain is more critical but only by a slight percentage. For the first test the calculated critical pressure was minimum at the location of the hole. However, a comparison between these results and those of Table 6 of Reference 6 show that this is not true for the second test. In other words there are locations in the shell with thinner wall thicknesses which have smaller critical loads than the hole of the second test. It should be noted however that the actual average thickness in the failed area is not known. the average thickness was estimated from values measured at the edge of the hole. One can also see in Table 10 that both linear and non-linear analyses gave results considerably larger than the actual failure pressure.

CHAPTER V

CONCLUSIONS

The shell tested and analyzed in this investigation was the first micro-concrete model cooling tower shell built using double-walled forms and a pump mix. The results reported here are for the second test conducted on the model, i.e., the model had been tested to failure in the first test and later repaired.

Improvements in the testing procedure made it possible to obtain more complete and consistent data. However, some problems regarding air leakage were still encountered during testing which were eventually taken care of by using commercial sealing compounds.

The second failure reported here occured in lift one on line J at a vacuum pressure of 3.7 Psi (25.53 KPa). This type of failure could be due to imperfections, the out-of-roundness of the shell, and small amount of reinforcing. It was also noticed that the shell behaved unsymmetrically under axisymmetric pressure (vacuum) which could have been caused by the geometry imperfections. Furthermore the experimental failure load was much lower than the theoretical ones.

Thickness imperfections produced additional moments and stresses which were taken into account in the analysis. As it was shown, the thickness variation was especially large in the first lift.

Circumferential plots of deviation and displacement showed that radial displacement generally followed the same oval pattern of the deviation. Since the load carrying mechanism of a cooling tower under axisymmetric pressure is dominated by ring action (23) a series was chosen that would fit the circumferential deviation curves.

Although this model is not similar to prototype cooling towers in loading procedure, support conditions, geometry and thickness accuracy, and although it is not intended that the results reported here be used to deduce prototype behavior, one could utilize the results of this model to verify general methods of analysis.

At the present time both the outer forms and the inner forms are being repaired for the future models. The repairs include

1. more bracing in order to stop bulging of the forms;
2. surface finishing in order to accomplish smoother surface and better uniform curvature;

The overall objective is to improve the thickness and geometry imperfections in the future models.

It is recommended that for the future work the effects of wind loading alone and/or in combination with vacuum pressure be tested and analyzed. Furthermore, the models should have more realistic boundary conditions and less geometry imperfections so that direct similitude extrapolation to prototype shells is possible.

Appendix A : Tables

Table 1. Properties of the Patching Mix,
Steel Reinforcing, and Support Column

Micro-Concrete for Patching

Sieve Analysis of Kaw River Sand,
Percent Retained :

No. 16 = 0

No. 30 = 17

No. 50 = 78

No. 100 = 98

No. 200 = 99

Fineness Modulus = 2.92

Quantities Per cu. ft. Mix :

Cement (Type I)	30.76 lb (136.88 N)
Sand	76.92 lb (342.29 N)
Water	15.38 lb (68.44 N)
HEC 400	0.069 lb(0.31 N)
Unit Weight	123.05 lb/cu. ft. (19.25 KN/m^3)
Slump	0.00

Cylinder Strength, f'_c = 4547 Psi (31.37 MPa)

Reinforcing Steel

Diameter = 0.105 in. (2.7 mm)

Average Yield Stress = 81.9 Ksi (564 MPa)

Average Modulus of Elasticity, E_s=29.8 x 10^6 Psi (206 GPa)

40 wires per ruling direction evenly spaced (80 wires total)

Nominal Steel Ratio = 0.35 %

Support Column

HP 10 x 42

A=12.4$in.^2$(80 cm^2)

E=29 x 10^6Psi(200GPa)

Table 2. Cylinder Test Results, Shell No. 1

Casting Date	Testing Date	Load lb (KN)	Compressive Strength f'_c Psi (MPa)	Age at Test Days
10 April 81[a]	19 May 82	53000 (236.85)	7496 (51.72)	404
17 April 81[b]	19 May 82	41150 (183.12)	5820 (40.16)	397
27 April 81[c]	19 May 82	39800 (177.11)	5629 (38.84)	387
21 Dec. 81[d]	20 May 82	32150 (143.07)	4547 (31.37)	150

a - Lift 1

b - Lift 2

c - Lift 3

d - Patch

Note: Cylinders are 3in. x 6in. (76 mm x 152 mm), A = 7.07 $in.^2$(45.6 cm^2). Curing was done in ambient conditions adjacent to the shell.

Table 3. Origional Surface Deviation From Ideal Geometry, Shell No. 1

Deviations, inches (horizontal component)

Merid. Location	Theo. Radius r, in.	A	B	C	D	E	F	G	H	I	J	K	L	Dist. From Throat Z, in.
1	38.4	-.21	+.15	+.42	+.20	-.13	-.41	-.93	-.19	-.06	-.22	-.63	-.47	- 33
2	37.24	-.12	+.12	+.55	+.58	+.07	-.42	-.84	+.06	-.09	-.19	-.68	-.50	- 24
3	36.31	-.54	+.30	+.61	+.53	+.09	-.68	-.81	-.01	+.04	-.36	-.86	-.77	- 12
4	36.00	-.83	-.16	+.67	+.62	+.19	-.80	-.88	+.13	+.20	-.61	-.81	-1.01	0
5	36.31	-.86	+.05	+.74	+1.02	+.45	-.54	-.62	+.45	+.73	-.29	-.46	-.84	+ 12
6	37.24	-.70	+.05	+.74	+.91	+.45	-.64	-.47	+.31	+.78	-.08	-.34	-.89	+ 24
7	38.74	-.64	+.19	+.80	+1.12	+.73	-.39	-.21	+.58	+.80	+.32	-.15	-.68	+ 36
8	40.74	-1.14	-.17	+.39	+.60	+.48	-.68	-.45	+.14	+.20	+.10	-.45	-.92	+ 48
9	43.17	-.53	-.18	+.18	+.81	+.51	-.57	-.18	+.13	+.70	+.46	+.05	-.28	+ 60
10	45.98	-.25	-.66	-.82	+.98	+.46	-.40	-.32	+.05	+.39	+.66	-.20	+.12	+ 72
11	49.08	-.74	-1.56	-1.15	+.09	+.69	-.41	-.14	-.03	+.56	+.57	+.26	-.01	+ 84
Max. Deviation in 24 in., S%		-4.6	2.1	3.3	4.4	2.2	-2.7	-2.1	3.0	-4.6	2.6	3.1	-3.7	

(-) = outward (+) = inward 1 in. = 25.4 mm

Table 4. Shell Thicknesses, Shell No. 1

Thickness, inches

Merid. Location	A	B	C	D	E	F	G	H	I	J	K	L	Dist. From Throat Z, in.
1	0.41	1.02	0.37	0.56	0.71	0.48	0.45	0.58	0.72	0.51	0.25	0.68	- 33
2	0.25	0.75	0.61	0.32	0.61	0.43	0.31	0.41	0.74	0.48	0.29	0.18	- 24
3	0.61	0.54	0.42	0.75	0.97	0.58	0.79	0.78	0.85	0.58	0.58	0.73	- 12
4	0.60	0.52	0.33	0.76	0.41	0.64	0.46	0.49	0.65	0.61	0.57	0.59	0
5	0.72	0.47	0.38	0.65	0.54	0.65	0.61	0.32	0.59	0.42	0.49	0.69	+ 12
6	0.41	0.40	0.31	0.96	0.75	0.89	0.67	0.61	0.62	0.51	0.32	0.78	+ 24
7	0.33	0.61	0.42	0.72	0.86	0.81	0.42	0.62	0.65	0.36	0.51	0.73	+ 36
8	1.45	1.11	1.15	1.07	1.24	0.85	0.78	1.44	1.45	0.58	1.61	1.28	+ 48
9	0.83	1.27	1.27	0.87	1.05	1.10	0.73	1.45	0.57	0.68	0.95	0.60	+ 60
10	0.75	2.21	2.57	0.44	0.97	1.07	1.35	1.48	0.79	0.65	0.86	0.81	+ 72
11	1.07	3.30	2.70	0.91	0.72	1.28	1.31	1.81	0.78	0.52	0.68	1.01	+ 84

1 in. = 25.4 mm

Table 5. Improved Data of Deviation From Ideal Mid-Surface Geometry Considering Actual Thicknesses, Shell No.1

Deviations, inches (horizontal component)

Merid. Location	A	B	C	D	E	F	G	H	I	J	K	L
1	-.26	+.41	+.36	+.23	-.02	-.42	-.96	-.15	+.05	-.22	-.76	-.38
2	-.24	+.24	+.60	+.49	+.12	-.46	-.49	+.01	+.03	-.02	-.78	-.66
3	-.48	+.05	+.57	+.66	+.32	-.64	-.66	+.13	+.22	-.32	-.82	-.66
4	-.78	-.15	+.58	+.75	+.14	-.73	-.90	+.12	+.28	-.56	-.78	-.96
5	-.75	+.04	+.68	+1.10	+.47	-.46	-.56	+.36	+.78	-.33	-.46	-.74
6	-.74	0.00	+.64	+1.14	+.58	-.44	-.38	+.36	+.84	-.08	-.43	-.75
7	-.72	+.24	+.76	+1.23	+.91	-.24	-.25	+.64	+.88	+.25	-.14	-.56
8	-.66	+.14	+.72	+.88	+.85	-.50	-.31	+.61	+.68	+.41	+.10	-.53
9	-.36	+.20	+.56	+1.00	+.78	-.27	-.06	+.60	+.74	+.55	+.28	-.23
10	-.12	+.20	+.22	+.95	+.70	-.12	-.10	+.54	+.54	+.74	-.02	+.28
11	-.46	-.16	-.05	+.30	+.80	-.02	+.26	+.62	+.70	+.58	+.35	+.24
Max. Deviation in 24 in., S %	2.38	-1.60	1.19	2.54	-2.10	-2.10	-2.38	1.27	-1.83	-1.92	-2.77	2.23

(-) = outward (+) = inward 1 in. = 25.4 mm

Table 6. Percent Deviation From Mean Thickness for Lifts 2 and 3 of Shell No. 1

Merid. Location	Avg. Thickness, inches	A	B	C	D	E	F	G	H	I	J	K	L
1	0.56	-27	82	-34	0	26	-15	-20	3	28	- 9	-55	21
2	0.45	-44	67	36	-29	36	- 4	-31	-9	65	7	-35	-60
3	0.68	-11	-21	-38	10	42	-15	16	14	25	-15	-15	7
4	0.55	8	- 6	-40	38	-26	16	-17	-11	18	10	3	7
5	0.54	32	-14	-30	19	- 1	19	12	-41	8	-23	-10	27
6	0.60	-32	-34	-49	59	24	48	11	1	3	-15	-47	29
7	0.59	-44	4	-28	23	47	38	-28	6	11	-39	-13	24

1 in. = 25.4 mm

Table 7. Percent Deviation From Mean Thickness

for Mungan's Plastic Models (26)

	Avg. Thickness	θ , in degrees								
Z/H_{SM}	in mm	40	80	120	160	200	240	280	320	360
Model 1: 1/2*	2.06	10	12	4	6	-3	-8	- 8	-10	-5
Model 2: 1/9	1.96	6	15	-.5	- 6	-7	.5	- 3	.5	-3
Model 3: 5/9	1.85	-16	-13	-14	1	6	16	14	10	-5
Model 4: 5/9	1.53	- 8	-.6	7	4	3	.6	.6	- 2	-2
4/9	1.59	4	4	-.6	6	0	-9	-.6	- 2	-1
Model 5: 1/2*	1.14	- 8	-22	-22	-20	1	10	26	24	10

1 mm = 0.0394 in.

* - Throat

Table 8. Experimental Forces and Bending Moments at The Location of Strain Gages at Max. Load of 3.7 Psi, Shell No.1

Location	N_θ lb/in. (KN/m)	N_ϕ lb/in. (KN/m)	M_θ lb-in./in. (N-m/m)	M_ϕ lb-in./in. (N-m/m)
Top of Shell Just Below Ring, Line H	103.5 (18.1)	152.4 (26.7)	-1.6 (-7.1)	136.5 (607.4)
Throat, Line H	-104.2 (-18.2)	-41.8 (-7.3)	-7.9 (-35.2)	-3.1 (-13.8)
4 ft. Below Throat, Line H	-125.8 (-22.0)	30.1 (5.3)	-123.1 (-547.8)	15.2 (67.6)
Base, Line H	-180.8 (-31.7)	-55.0 (-9.6)	-124.5 (-554.0)	-27.4 (-121.9)
Throat, Line E	-221.9 (-38.9)	-14.8 (-2.6)	2.3 (10.2)	-4.8 (-21.4)
Throat, Line B	-277.4 (-48.6)	-118.2 (-20.7)	23.1 (102.8)	8.5 (37.8)
Patched Region	-192.6 (-33.7)	66.2 (11.6)	-22.6 (-100.6)	-27.4 (-121.9)

Tensile hoop force is positive and positive moment causes tension in the outer layer of the shell.

Table 9. Values of The Coefficients for The Deviation Function, $e = \sum_{n=0}^{6} [A_n \cos(n\theta) + B_n \sin(n\theta)]$

Coefficient	Throat	4ft. Below Throat Gage No. 8	7ft. Below Throat Gage No. 11
A_o	-0.2479	0.1979	0.2646
A_1	-0.2863	-0.2421	-0.1664
A_2	-0.6325	-0.5758	-0.1025
A_3	0.2242	0.1542	0.1275
A_4	0.0392	-0.1092	-0.0458
A_5	-0.0554	0.0754	0.1714
A_6	-0.0062	-0.0304	-0.0017
B_1	0.2870	0.0392	-0.3019
B_2	-0.1833	-0.3580	-0.2526
B_3	0.1217	0.0583	0.0800
B_4	-0.1198	-0.1992	-0.1342
B_5	-0.0103	0.0392	0.0069
B_6	0.0409	0.1838	0.1782

Table 10. Predicted Pressure Associated With Possible Local Buckling, Shell No. 1

Hole	Vertical Distance Z in. (m)	Avg. Hole Thickness t in. (mm)	Non-Linear Buckling Pressure $q_{cr\phi}$ Psi(KPa)	Non-Linear Buckling Pressure $q_{cr\theta}$ Psi(KPa)	Linear Buckling pressure Psi(KPa)	Experimental Buckling pressure Psi(KPa)
Test No.1	91(2.31)	0.362(9)	6.53(45.0)	6.90(47.6)	7.34(50.6)	3.1(21.4)
Test No.2	95.5(2.42)	0.422(11)	8.93(61.1)	9.53(65.8)	10.23(70.6)	3.7(25.5)

Appendix B : Figures

THIS BOOK CONTAINS NUMEROUS PAGES WITH DIAGRAMS THAT ARE CROOKED COMPARED TO THE REST OF THE INFORMATION ON THE PAGE.

THIS IS AS RECEIVED FROM CUSTOMER.

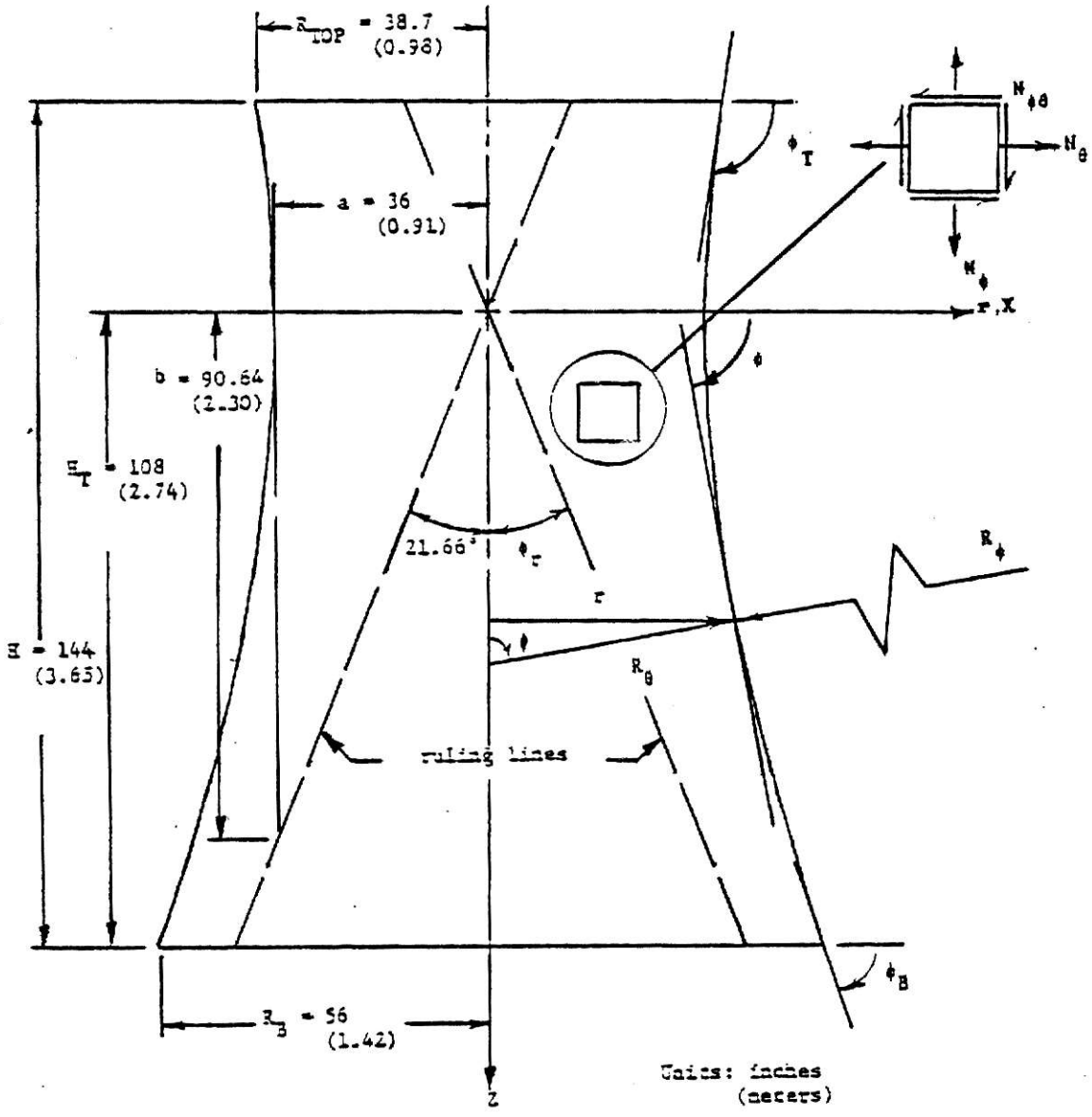

Fig. 1. Shell Geometry

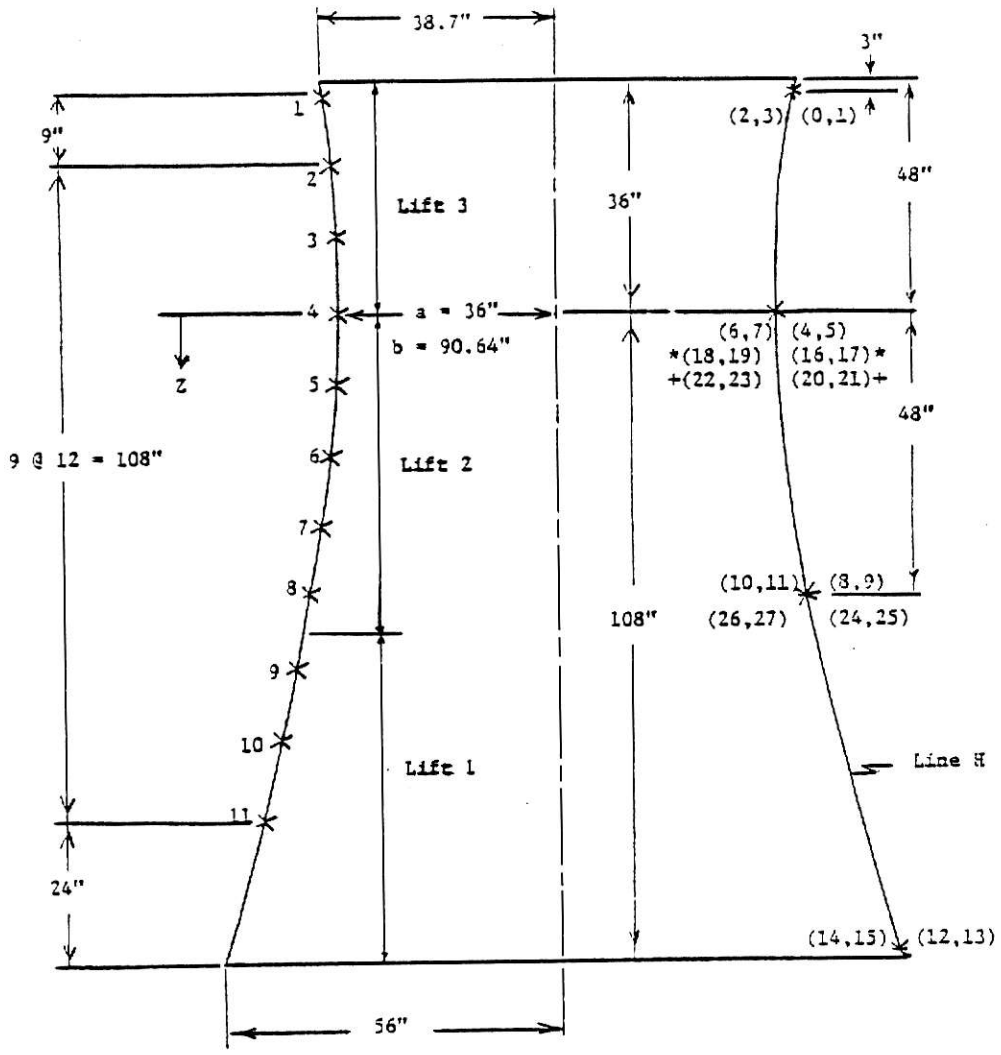

* Throat, Line E + Throat, Line B

⁜ Locations for thickness, geometry, displacement data

( ) = two-element rosettes, even-circumferential; odd-meridional

Refer to Fig. 3 for circumferential locations. 1 in. = 0.0254m

Fig. 2. Meridional Locations for Thickness, Geometry Displacement and Strain Data

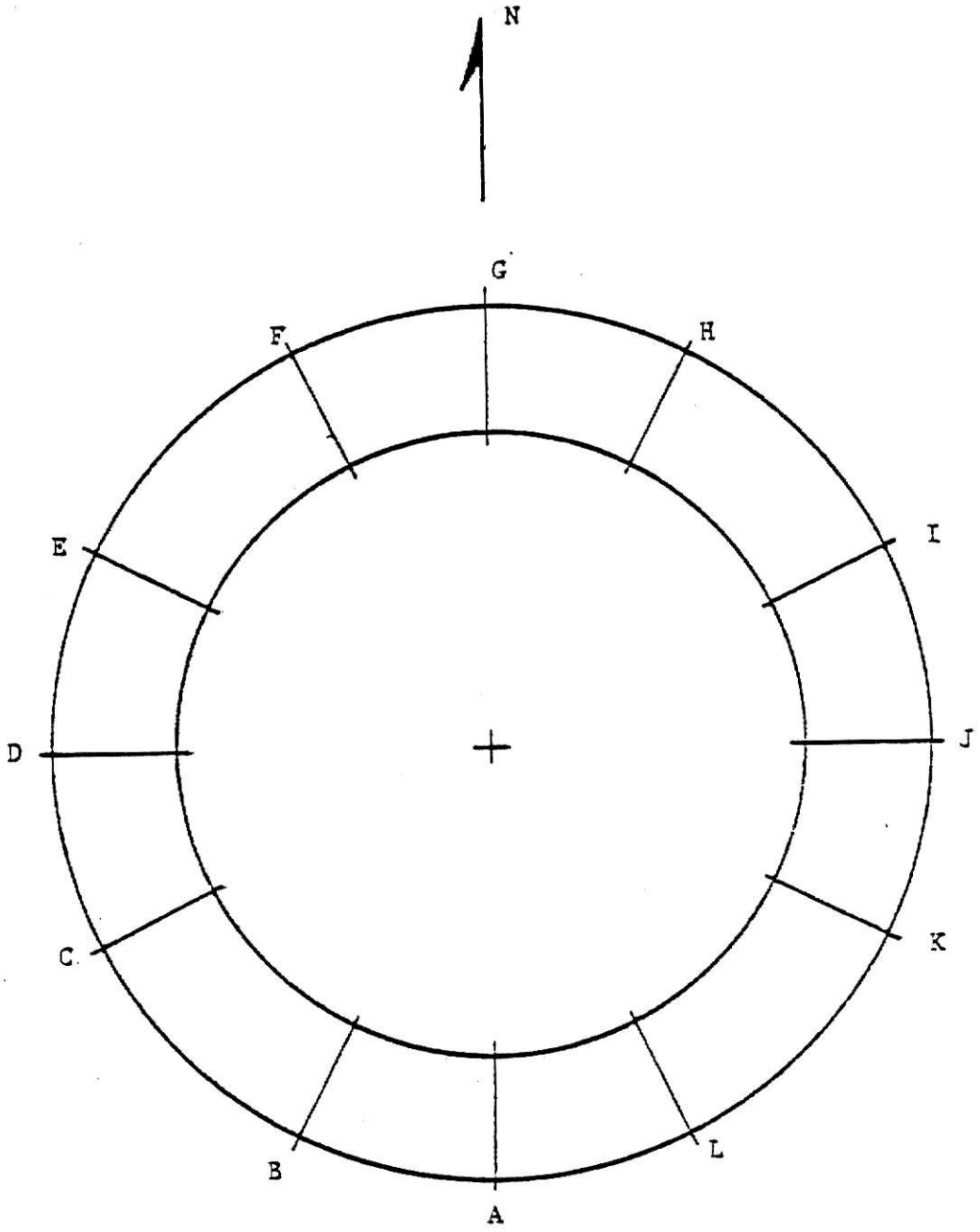

Refer to Fig. 2 for meridional locations.

Fig. 3. Circumferential Locations for Thickness, Geometry and Displacement Data, Shell No. 1

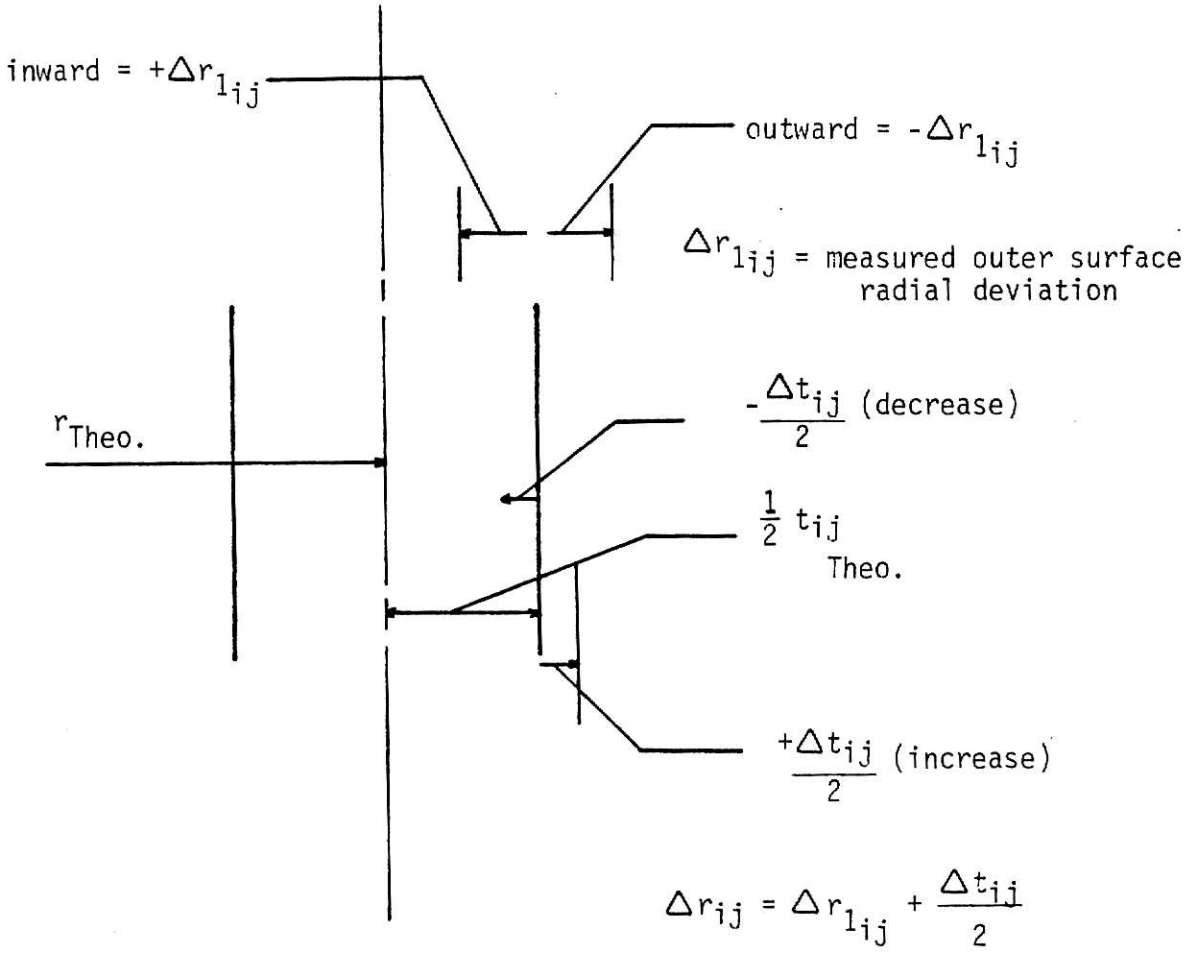

Fig. 4. Geometrical Representation of Deviation Considering Actual Thicknesses

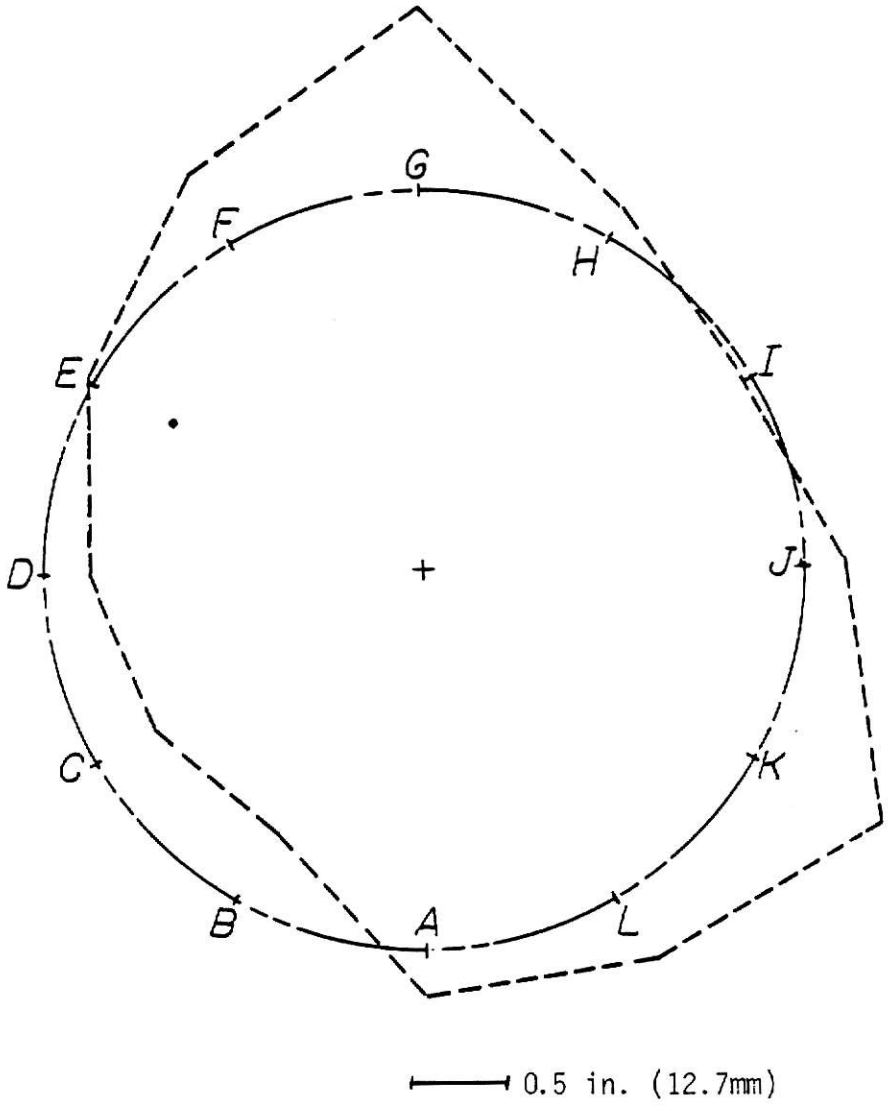

Fig. 5. Deviation Profile from Ideal Geometry for Level No. 1 of Shell No. 1, inches

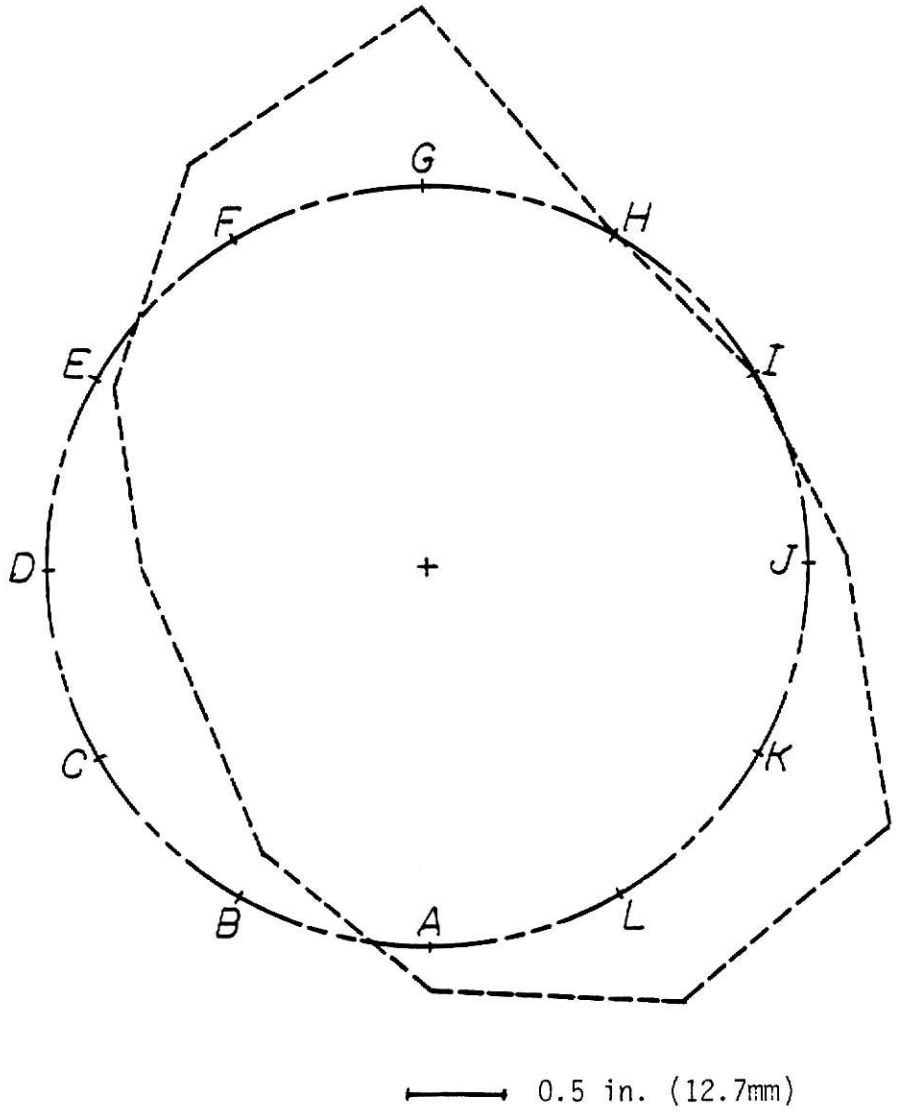

Fig. 6. Deviation Profile from Ideal Geometry for Level No. 2 of Shell No. 1, inches

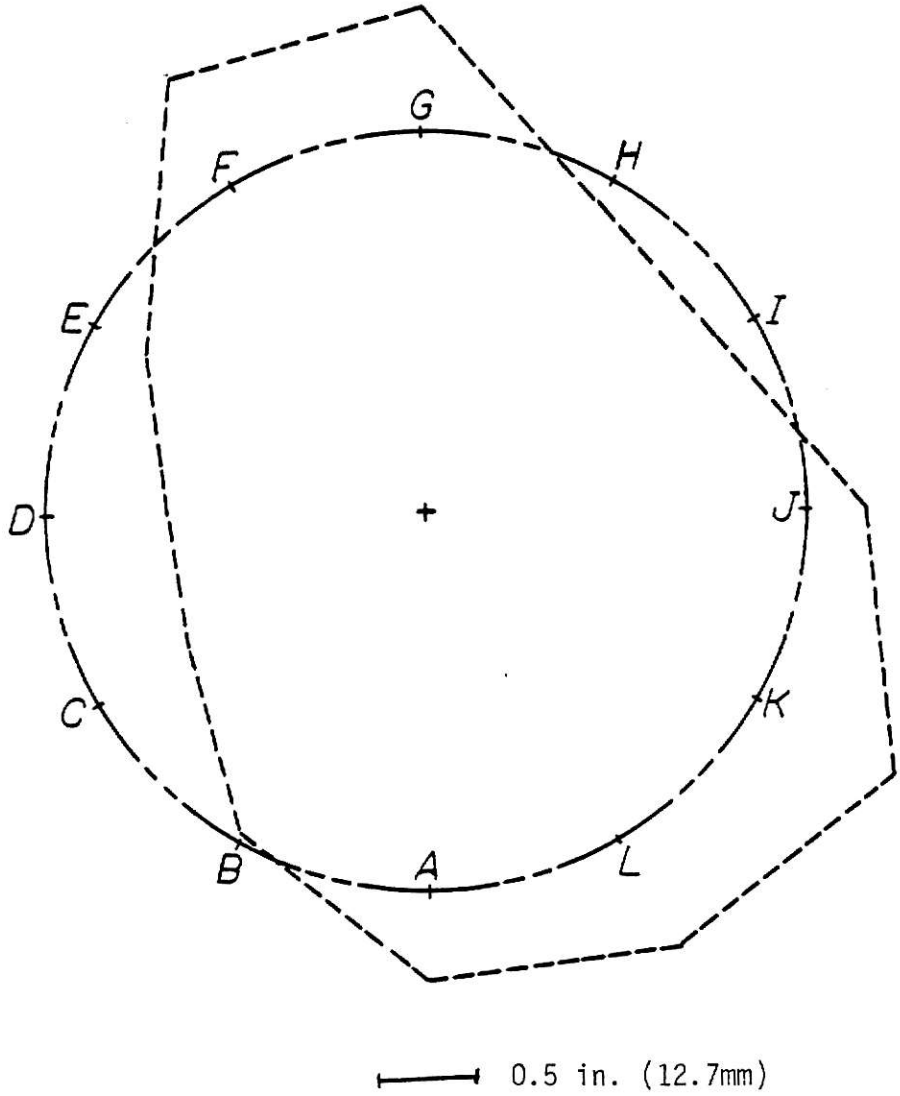

Fig. 7. Deviation Profile from Ideal Geometry for Level No. 3 of Shell No. 1, inches

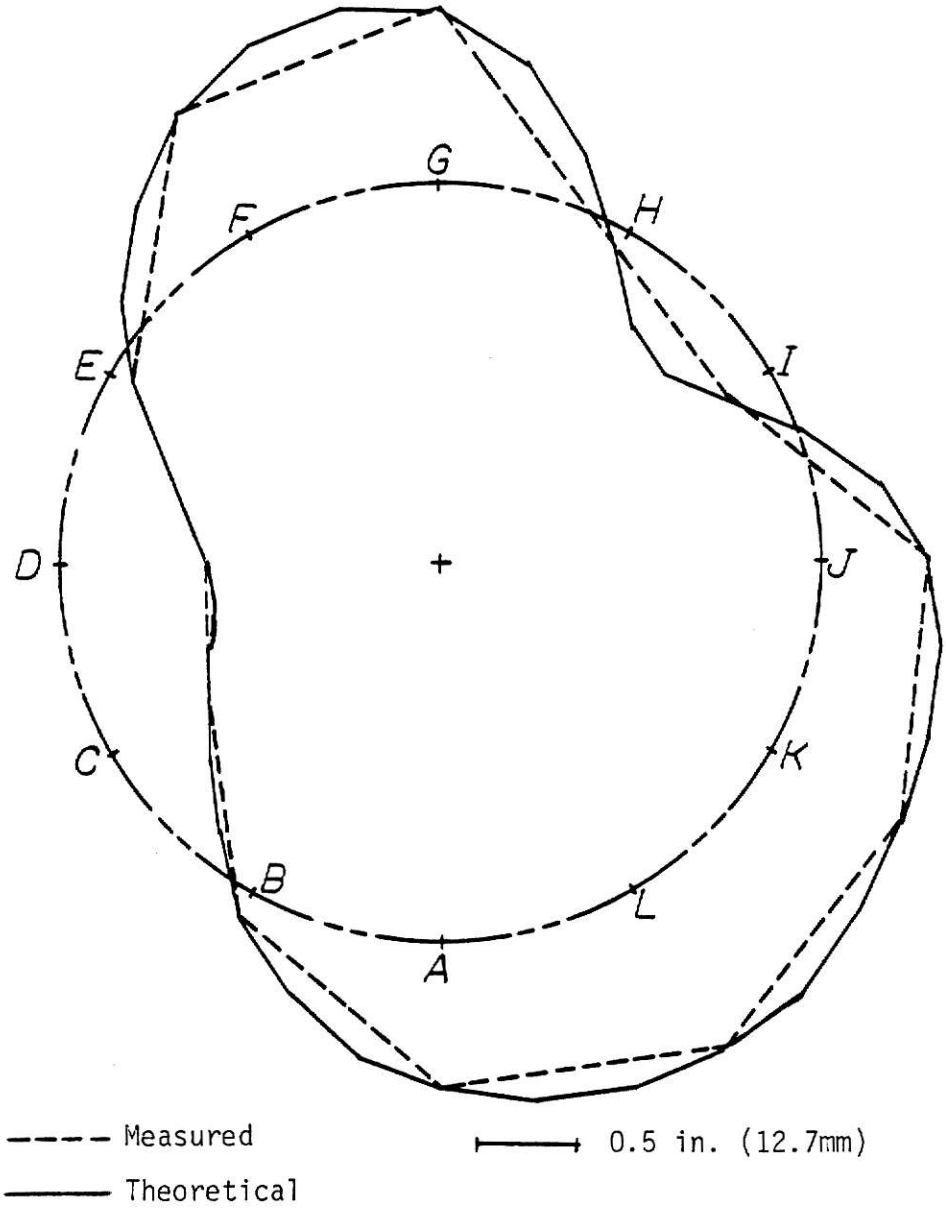

Fig. 8. Deviation Profile from Ideal Geometry for Level No. 4 (Throat) of Shell No. 1, inches

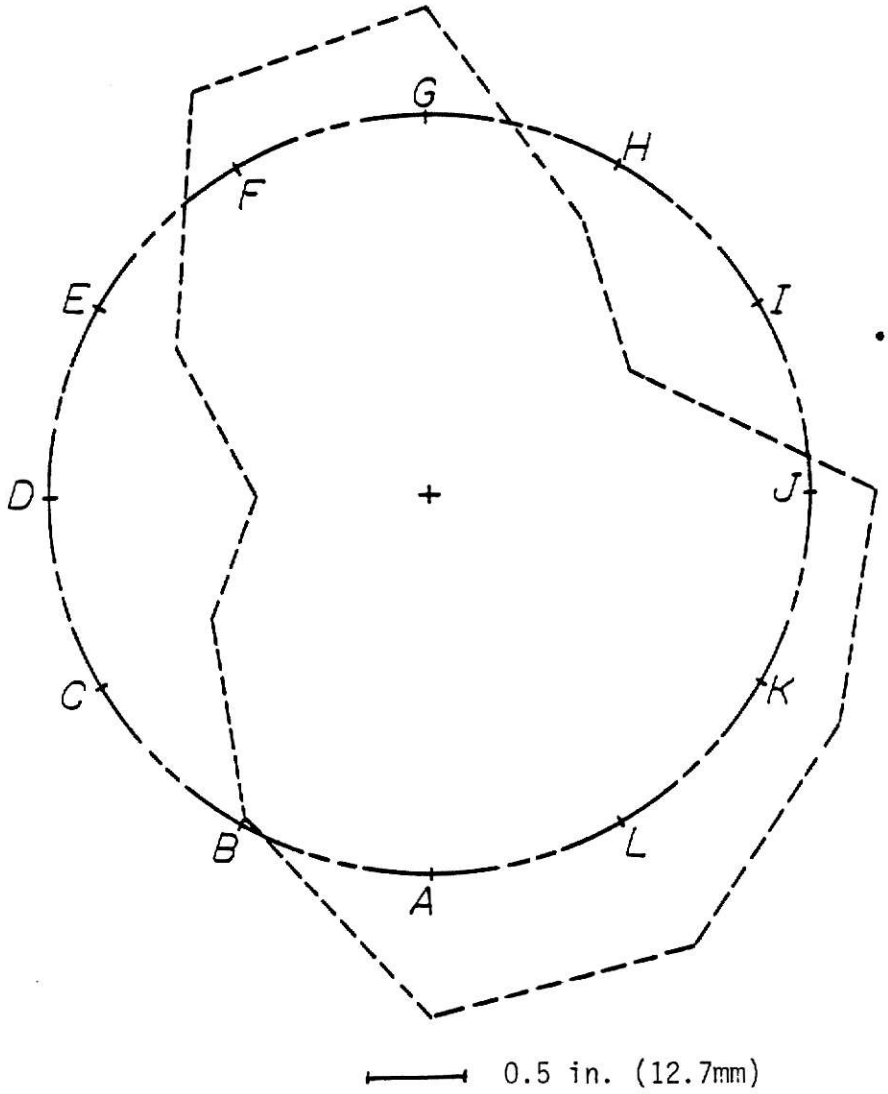

Fig. 9. Deviation Profile from Ideal Geometry for Level No. 5 of Shell No. 1, inches

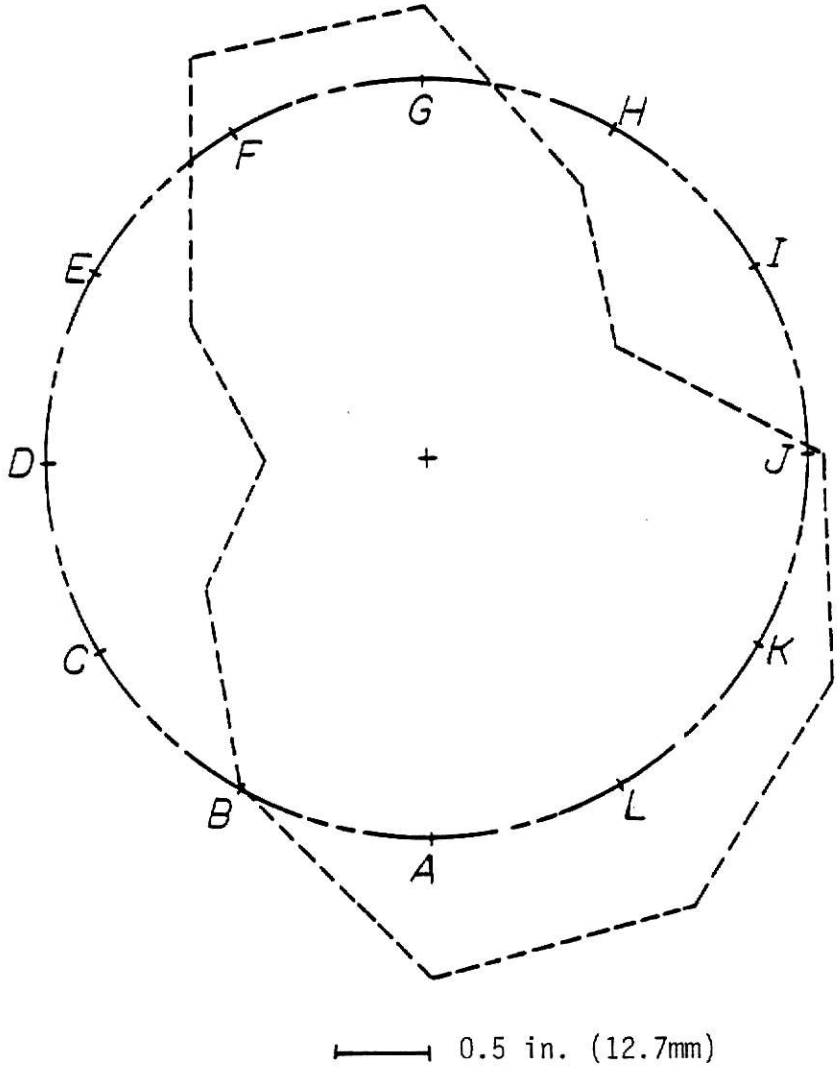

Fig. 10. Deviation Profile from Ideal Geometry for Level No. 6 of Shell No. 1, inches

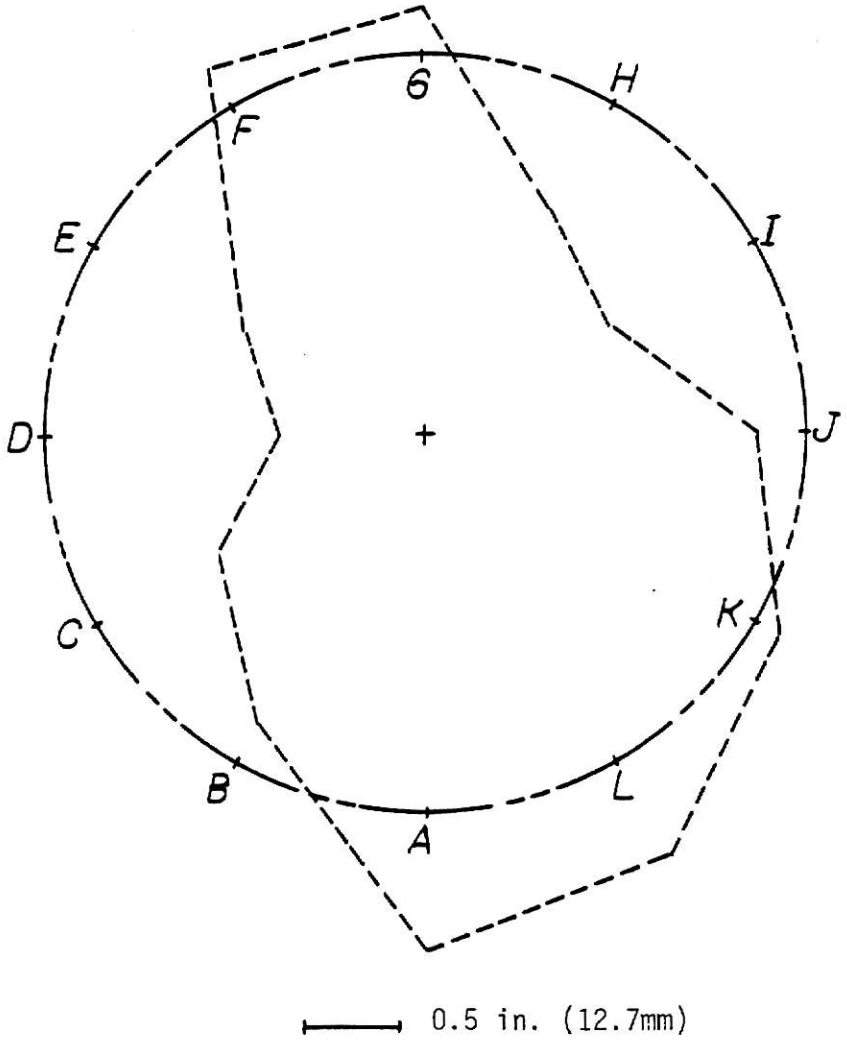

Fig. 11. Deviation Profile from Ideal Geometry for Level No. 7 of Shell No. 1, inches

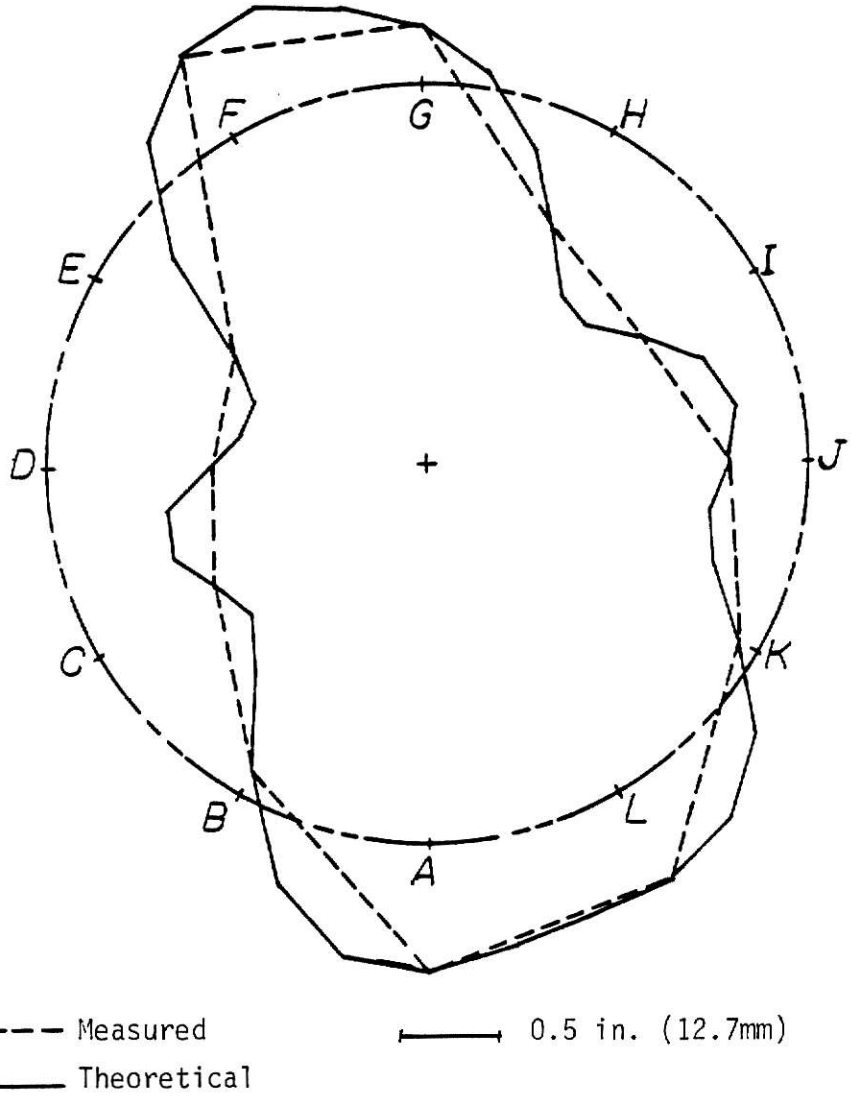

Fig. 12. Deviation Profile from Ideal Geometry for Level No. 8 of Shell No. 1, inches

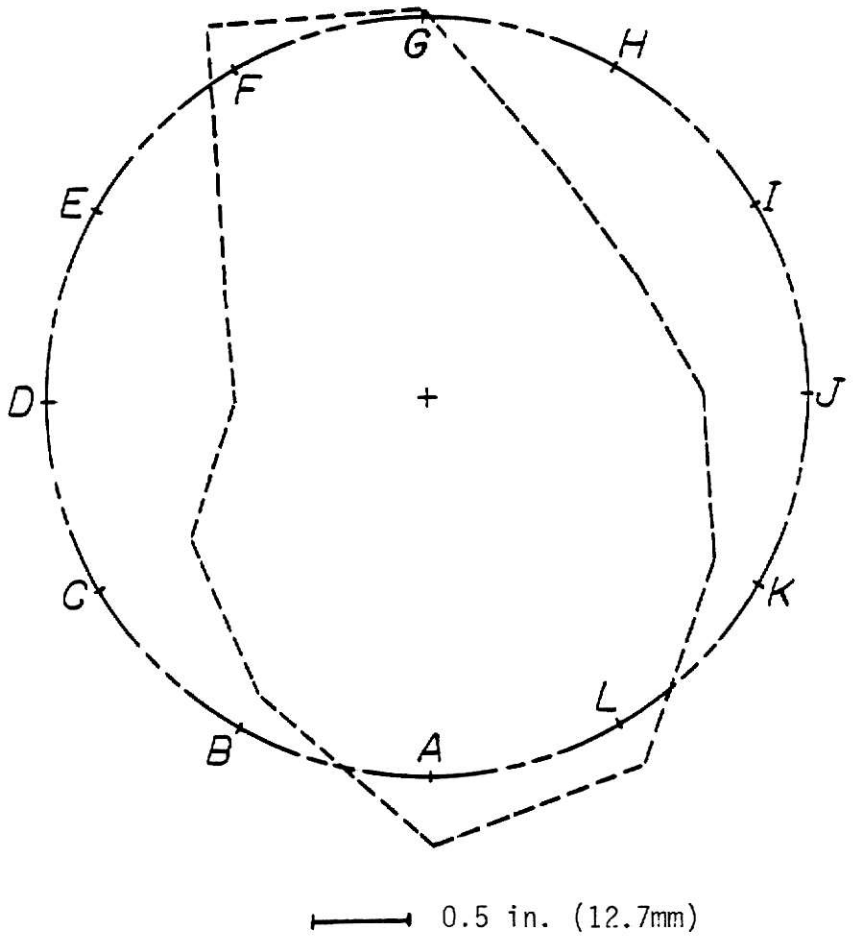

Fig. 13. Deviation Profile from Ideal Geometry for Level No. 9 of Shell No. 1, inches

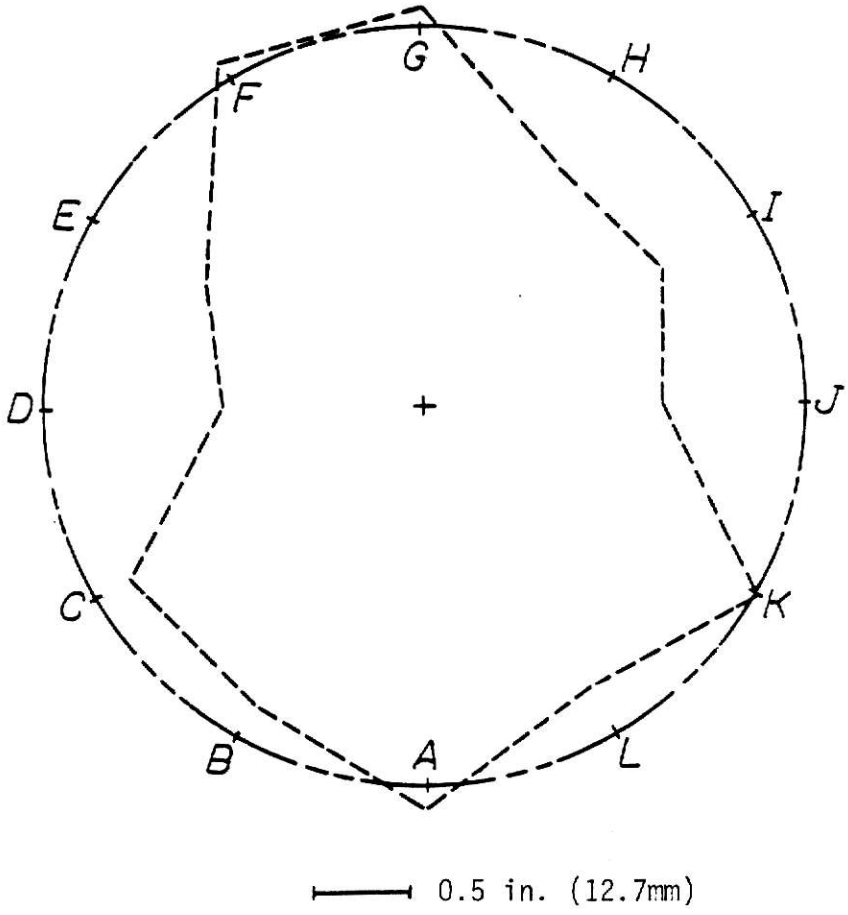

Fig. 14. Deviation Profile from Ideal Geometry for Level No. 10 of Shell No. 1, inches

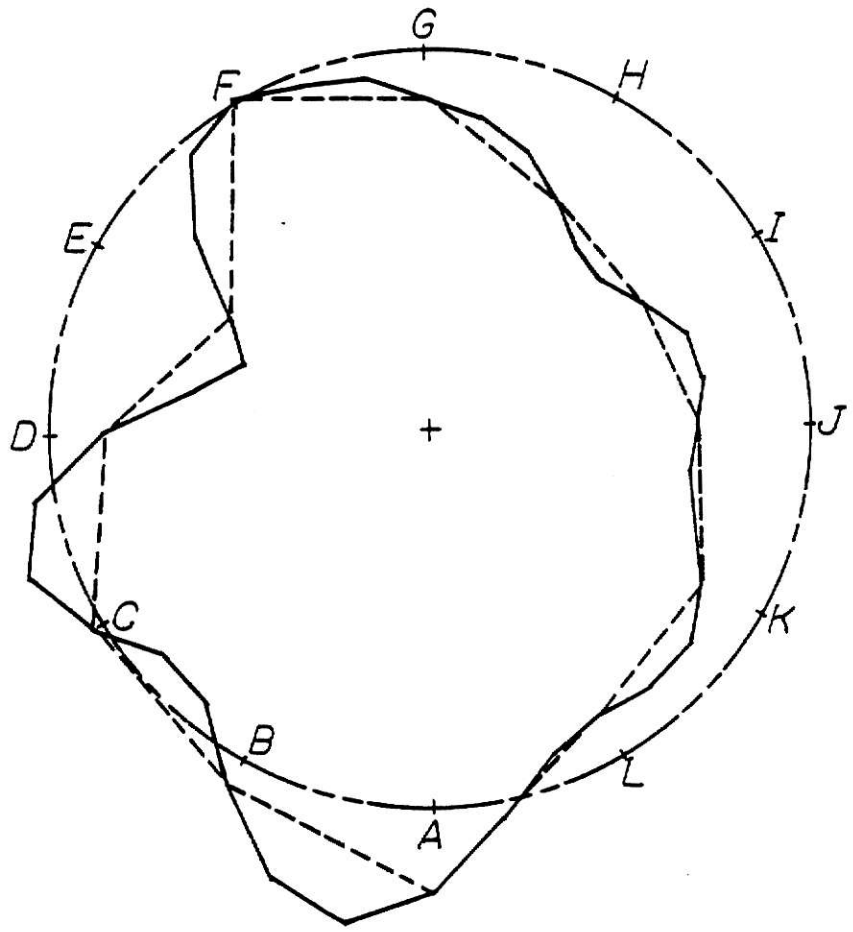

Fig. 15. Deviation Profile from Ideal Geometry for Level No. 11 of Shell No. 1, inches

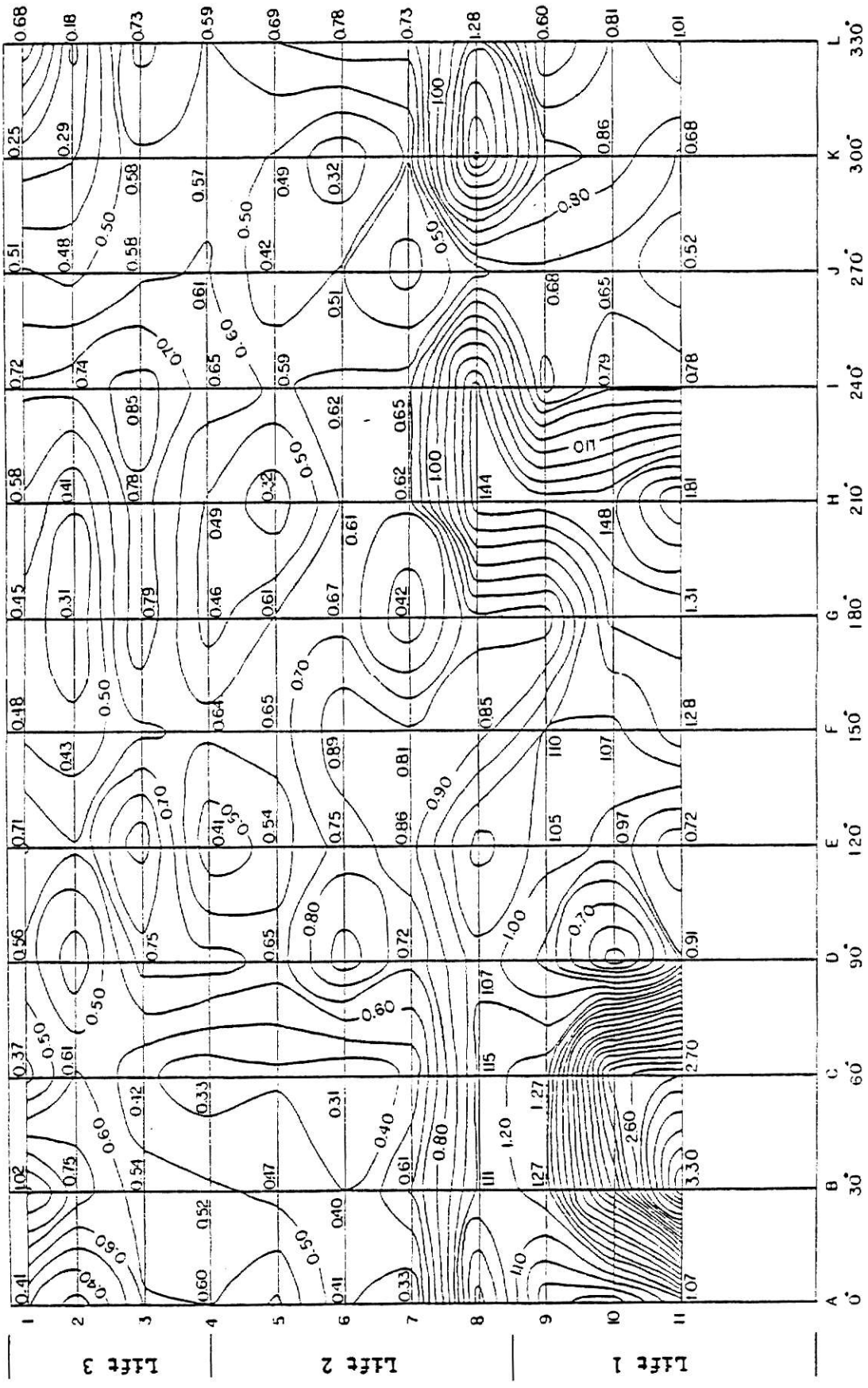

Fig. 16. Thickness Contours, Shell No. 1, Contour Interval = 0.1 in. (2.54mm)

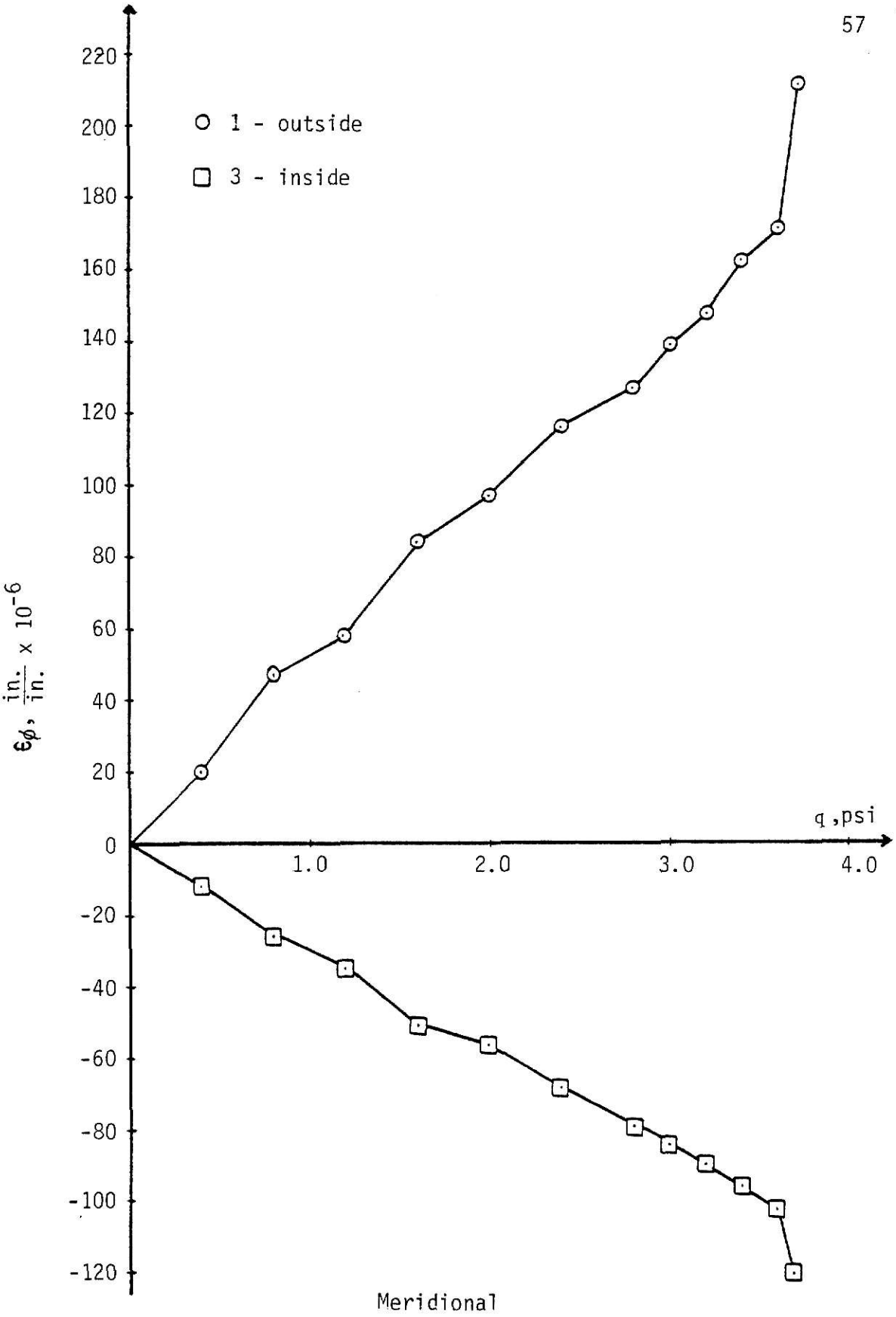

Fig. 17. Strain Versus Load at Line H, Top of Shell - Just Below Ring Beam, Shell No. 1, Tested on 19 Feb., 1982, 1 psi = 6.89 KPa

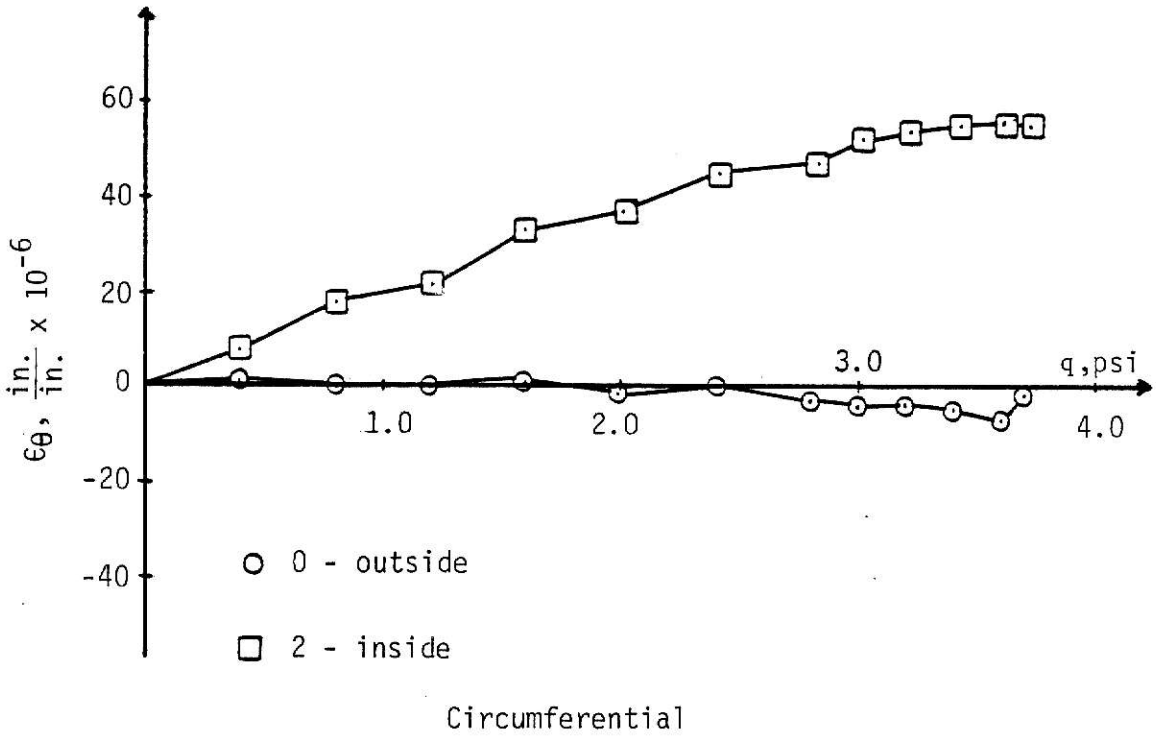

Fig. 18. Strain Versus Load at Line H, Top of Shell - Just Below Ring Beam, Shell No. 1, Tested on 19 Feb., 1982, 1 psi = 6.89 KPa

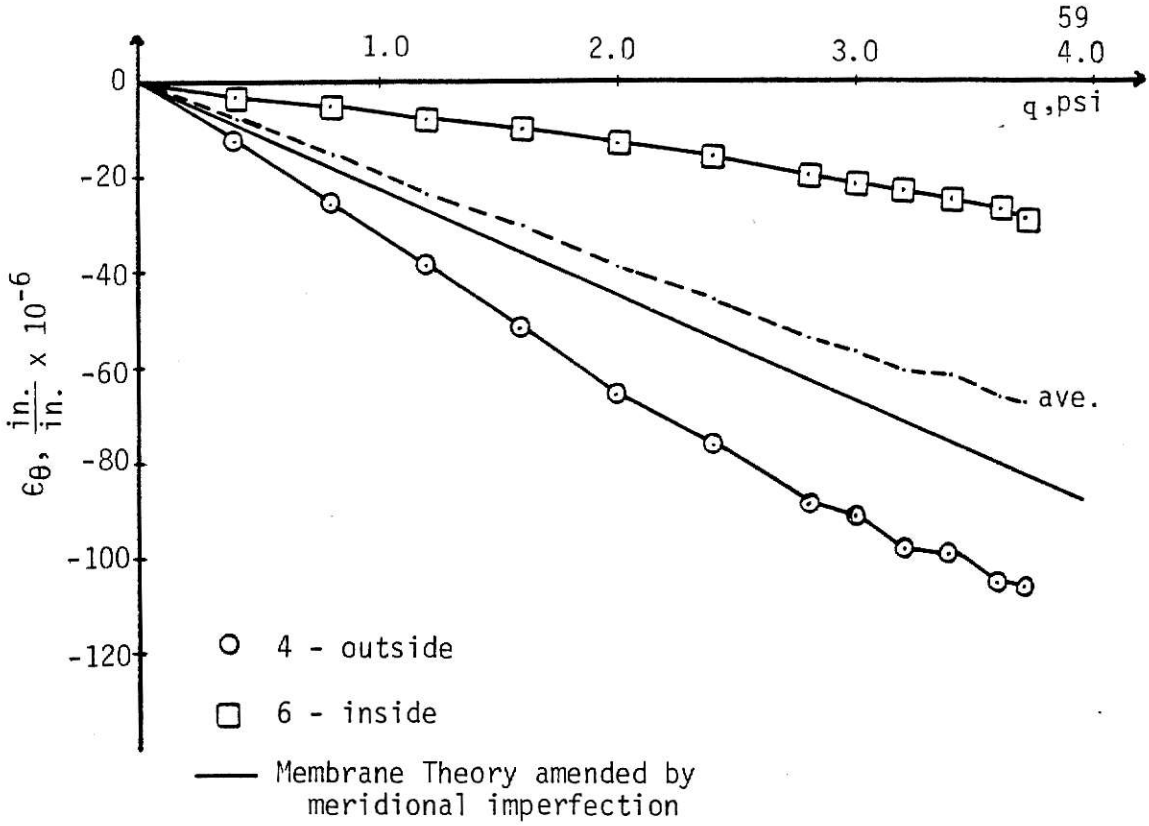

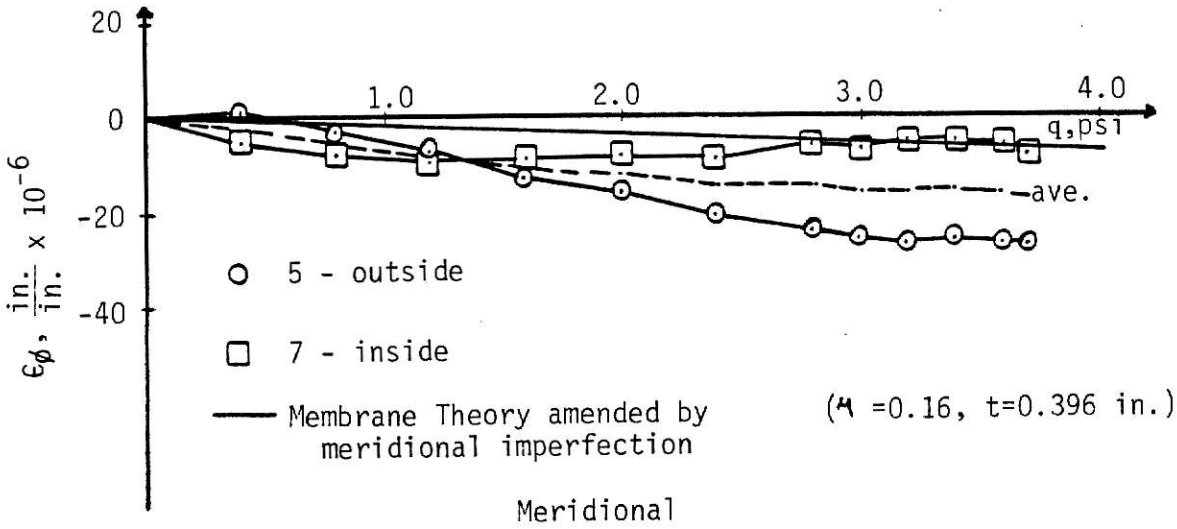

Fig. 19. Strain Versus Load at Throat, Line H, Shell No. 1, Tested on 19 Feb., 1982, 1 psi = 6.89 KPa

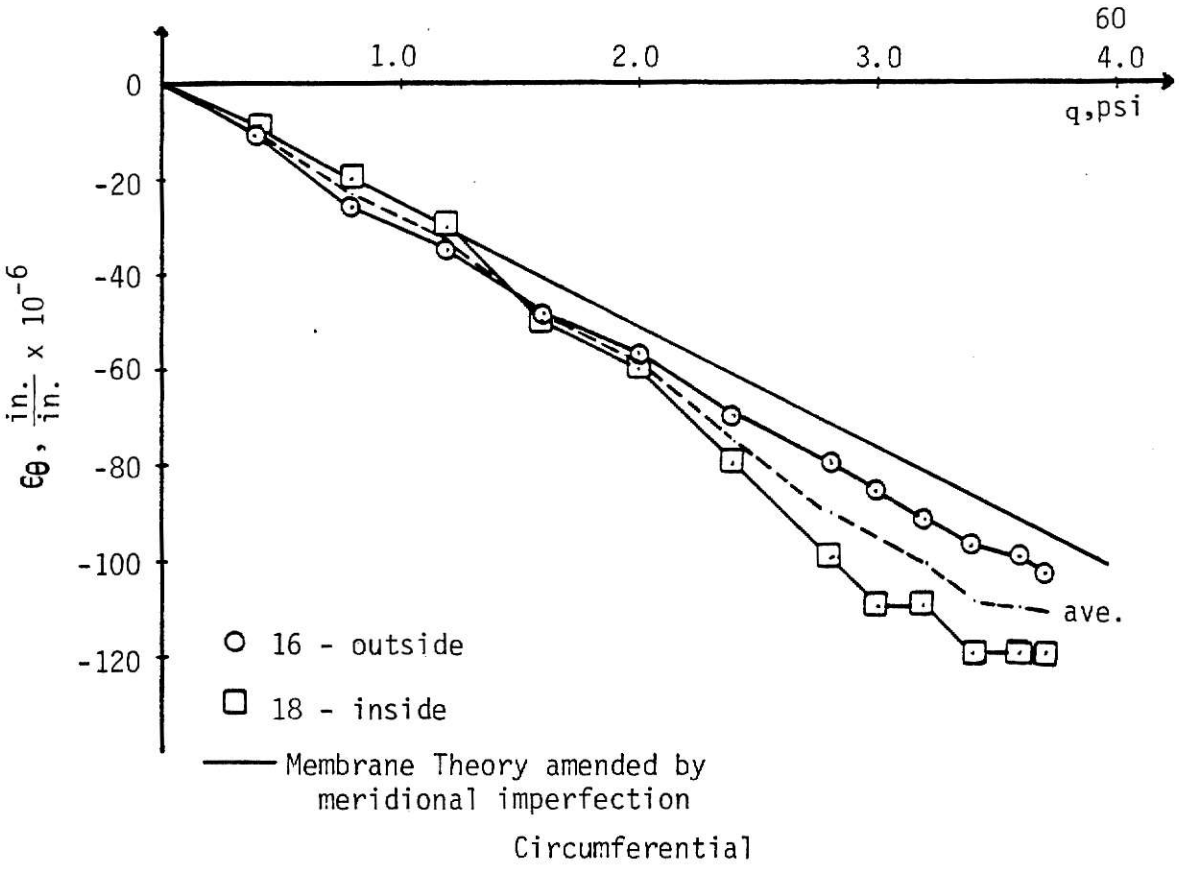

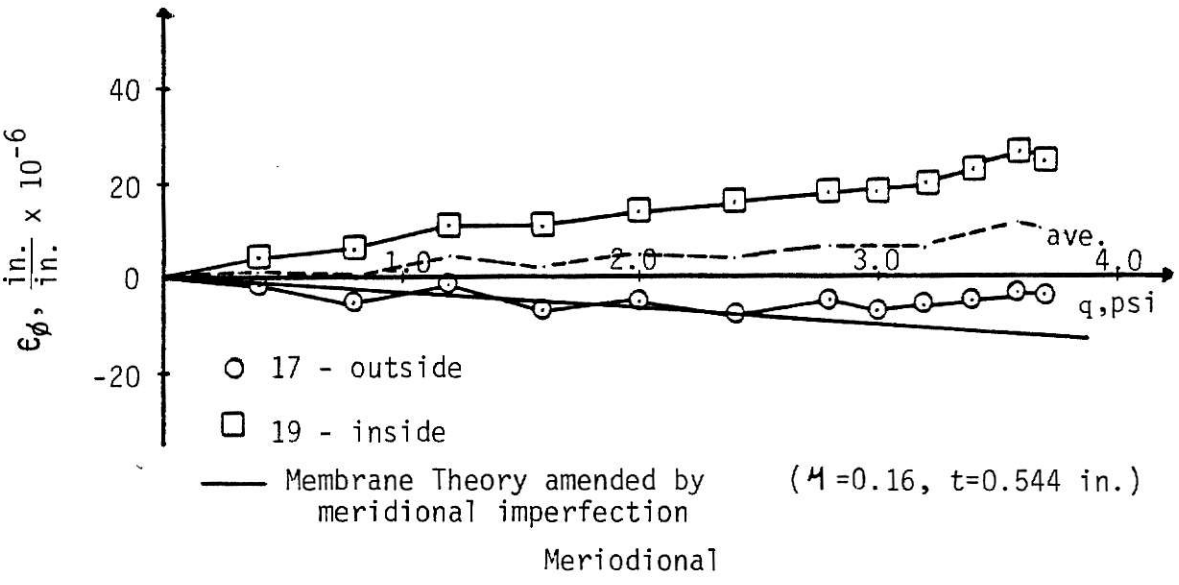

Fig. 20. Strain Versus Load at Throat, Line E, Shell No. 1, Tested on 19 Feb., 1982, 1 psi = 6.89 KPa

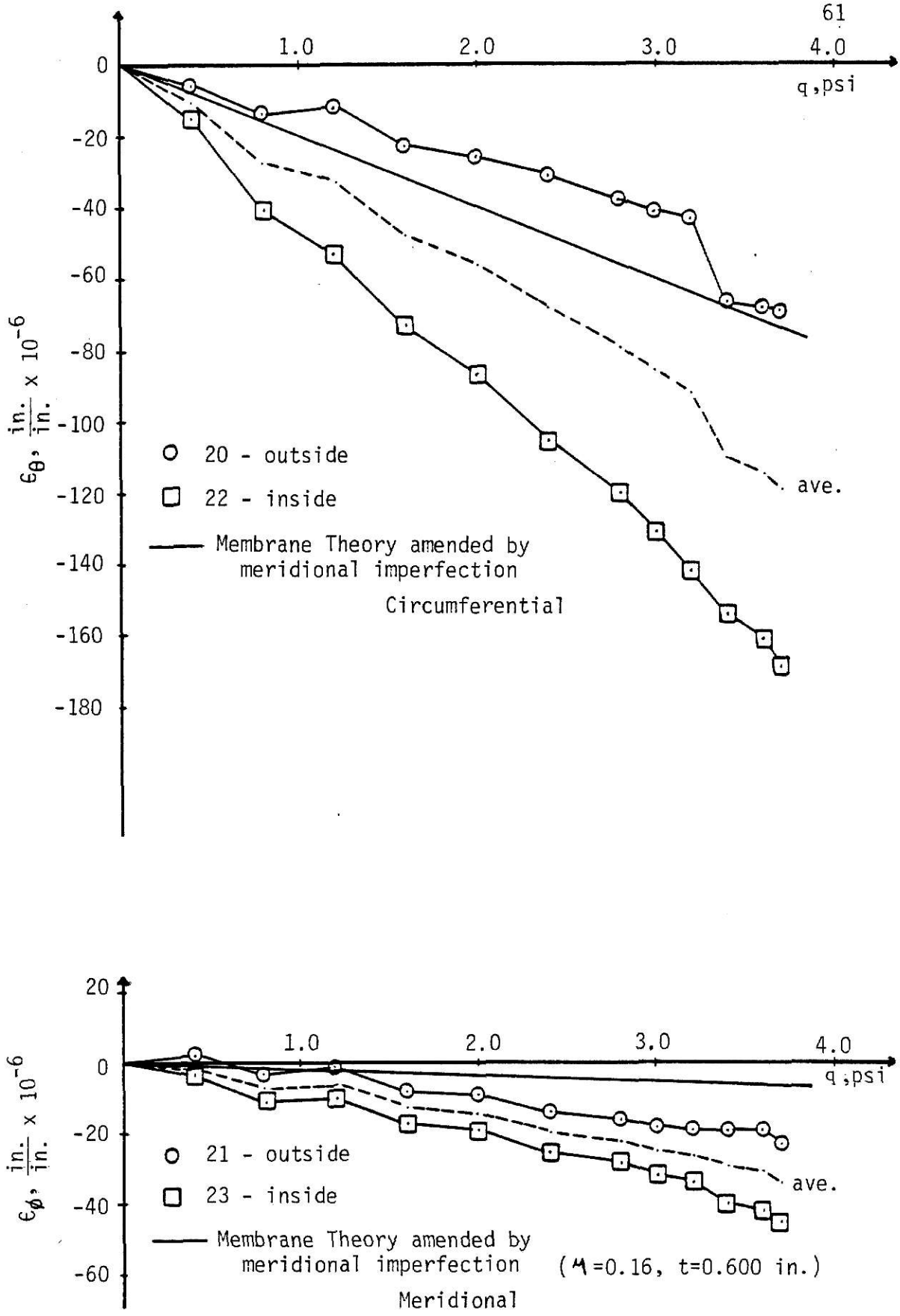

Fig. 21, Strain Versus Load at Throat, Line B, Shell No. 1, Tested on 19 Feb., 1982, 1 psi = 6.89 KPa

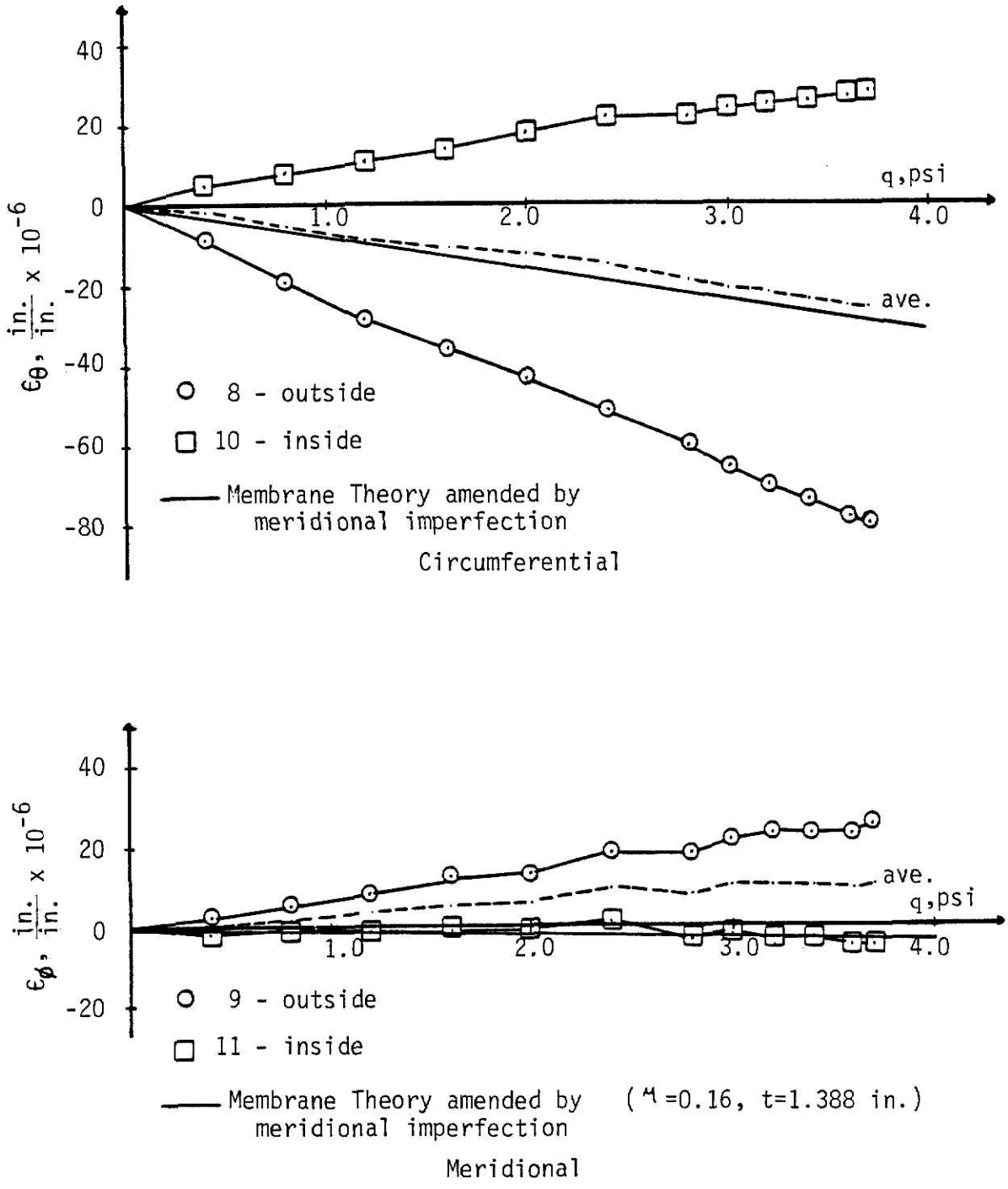

Fig. 22. Strain Versus Load at Four Feet Below Throat, Line H, Shell No. 1, Tested on 19 Feb., 1982, 1 psi = 6.89 KPa

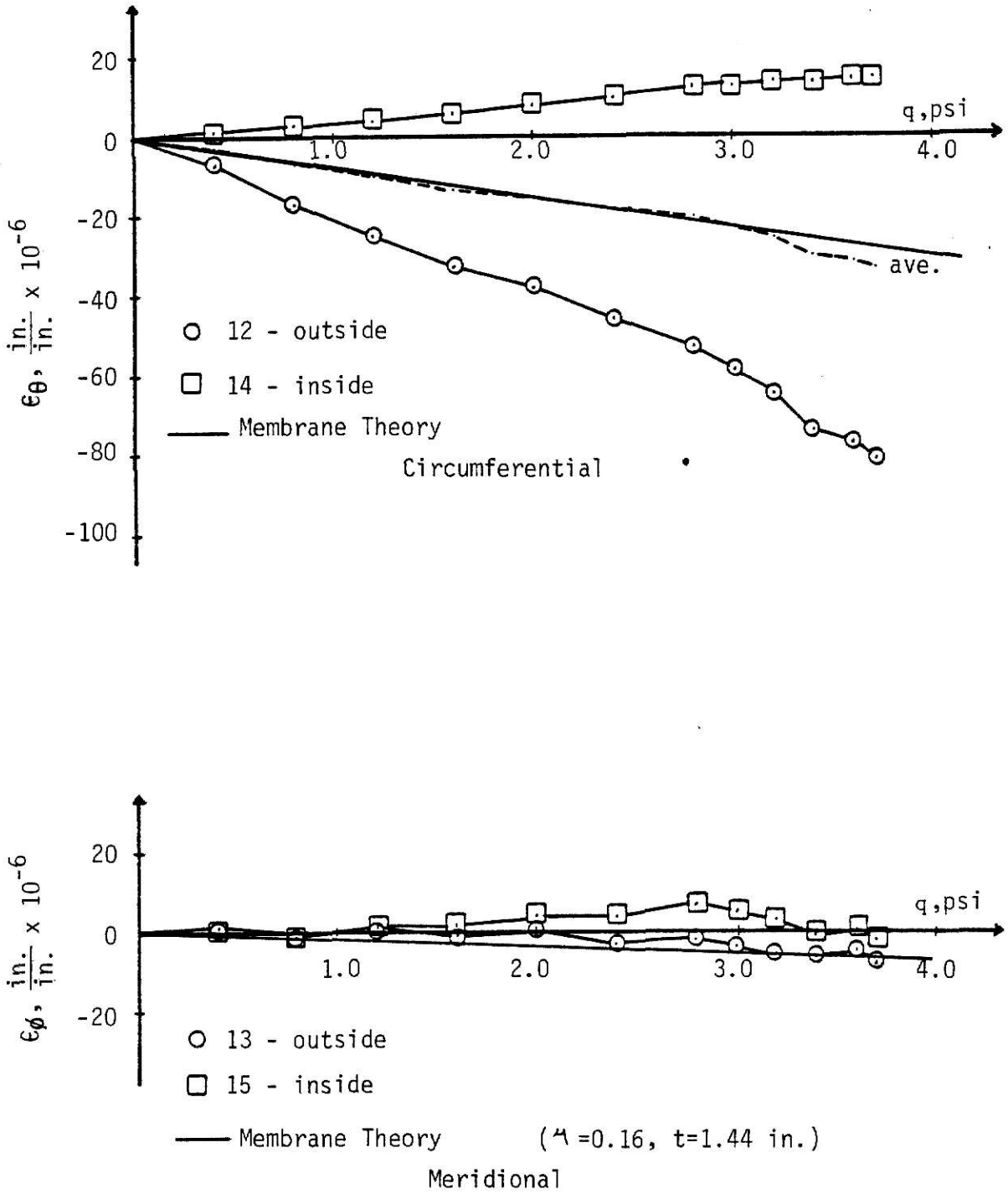

Fig. 23. Strain Versus Load at Base, Line H, Shell No. 1, Tested on 19 Feb., 1982, 1 psi = 6.89 KPa

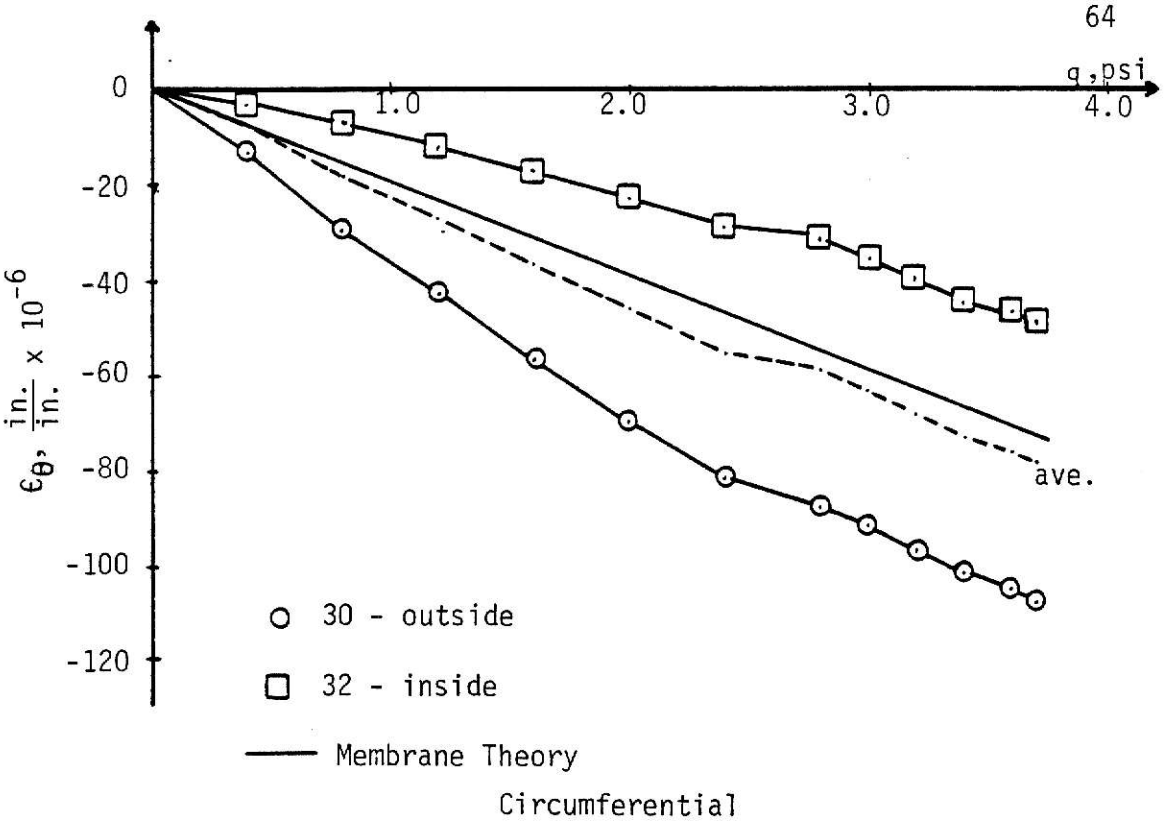

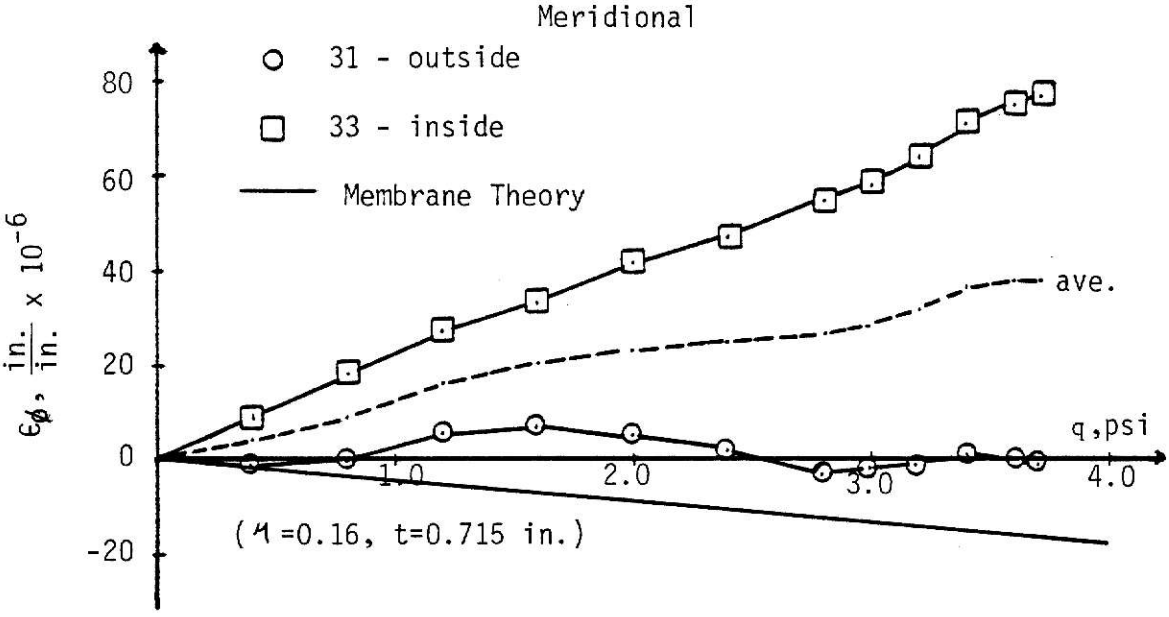

Fig. 24. Strain Versus Load at the Patched Region Between Lines G and H, Tested on 19 Feb., 1982, 1 psi = 6.89 KPa

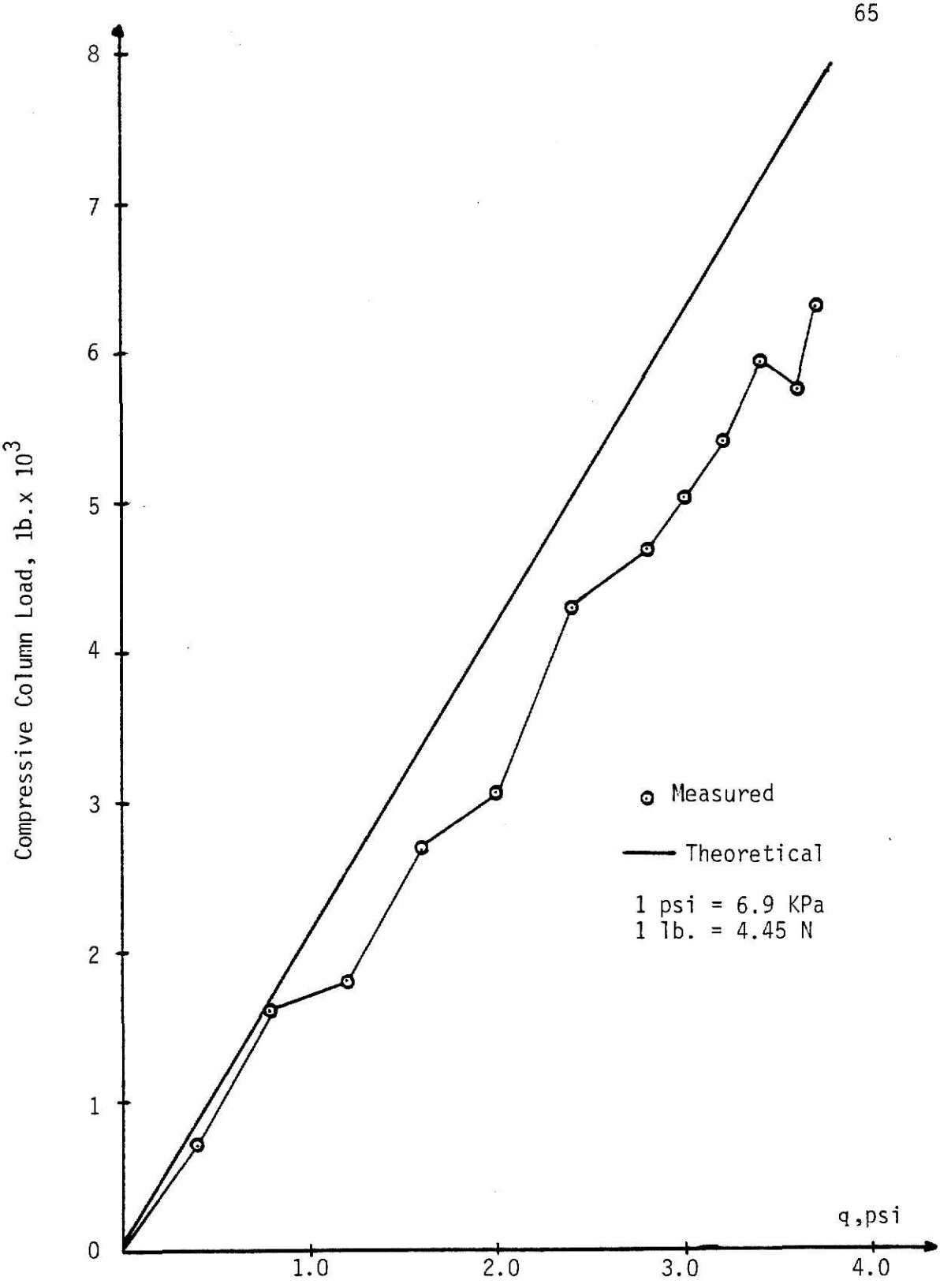

Fig. 25. Measured and Theoretical Loads on Column, Shell No. 1, Tested on 19 Feb., 1982, 1 psi = 6.89 KPa

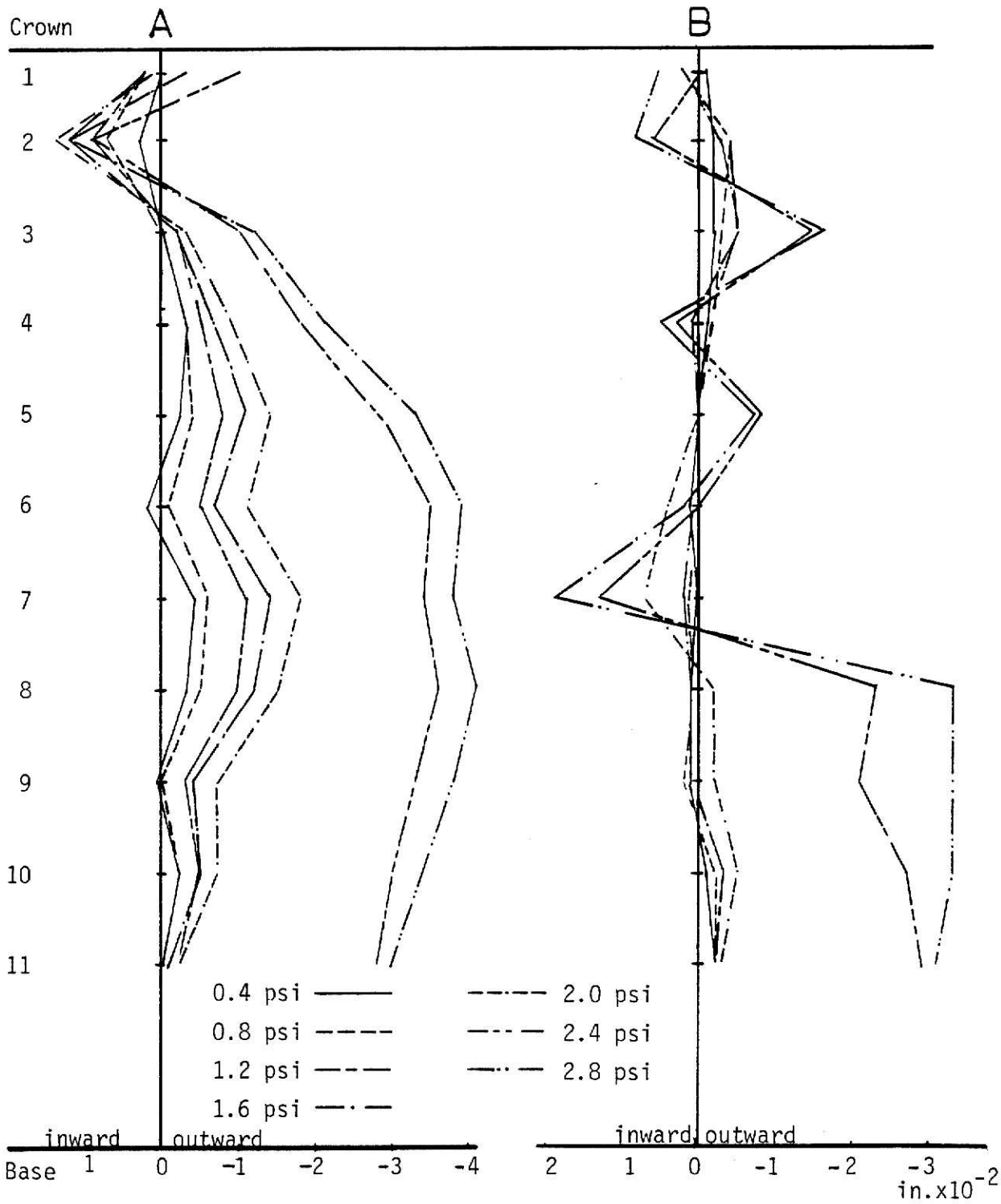

Fig. 26. Deflection Profiles for Lines A and B of Shell No. 1, Tested in Jan.-Feb., 1982, 1 in. = 25.4mm

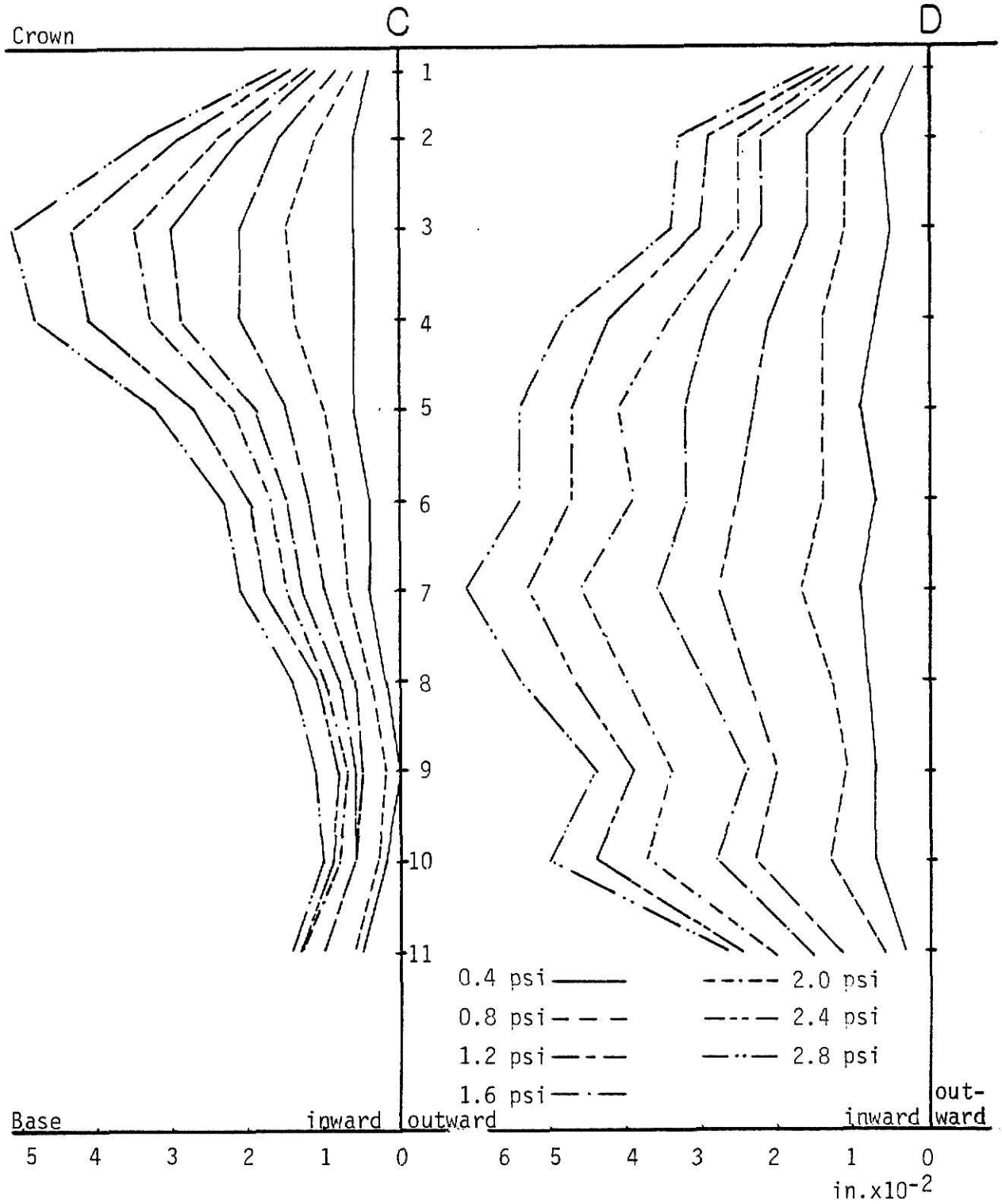

Fig. 27. Deflection Profiles for Lines C and D of Shell No. 1, Tested in Jan.-Feb., 1982, 1 in. = 25.4mm

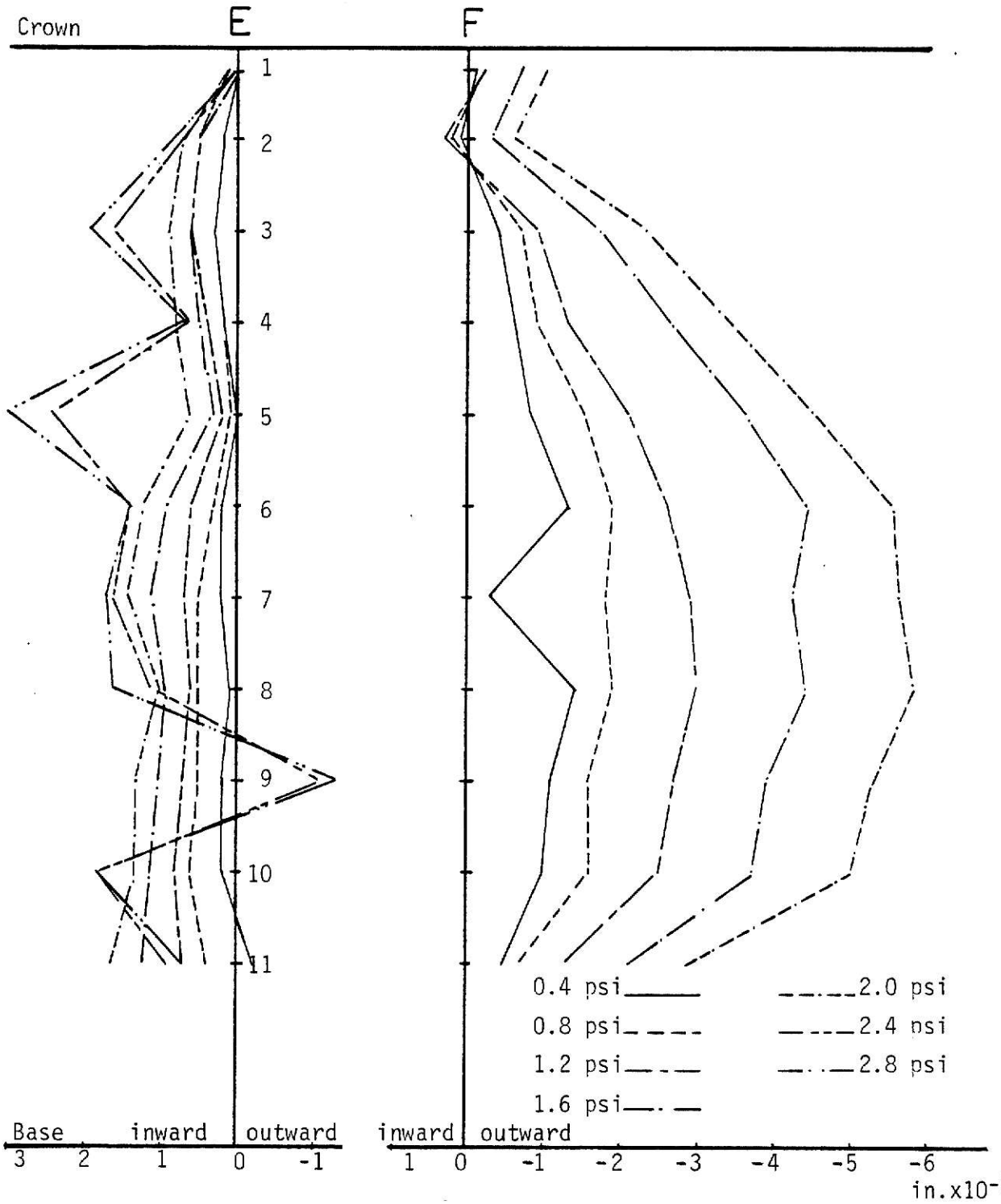

Fig. 28. Deflection Profiles for Lines E and F of Shell No. 1, Tested in Jan.-Feb., 1982, 1 in. = 25.4

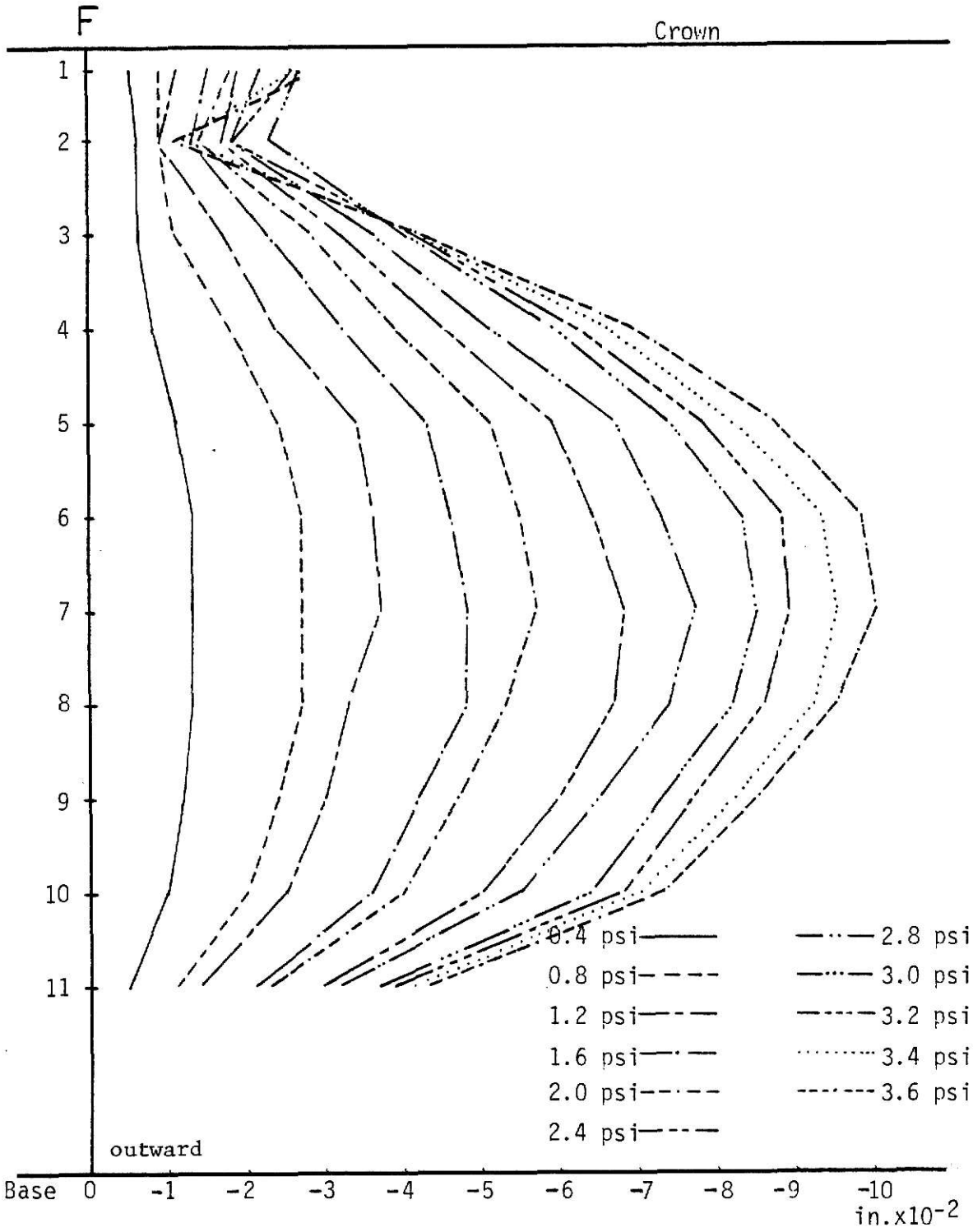

Fig. 29. Deflection Profile for Line F of Shell No. 1, Tested on Feb. 19, 1982, 1 in. = 2.54mm

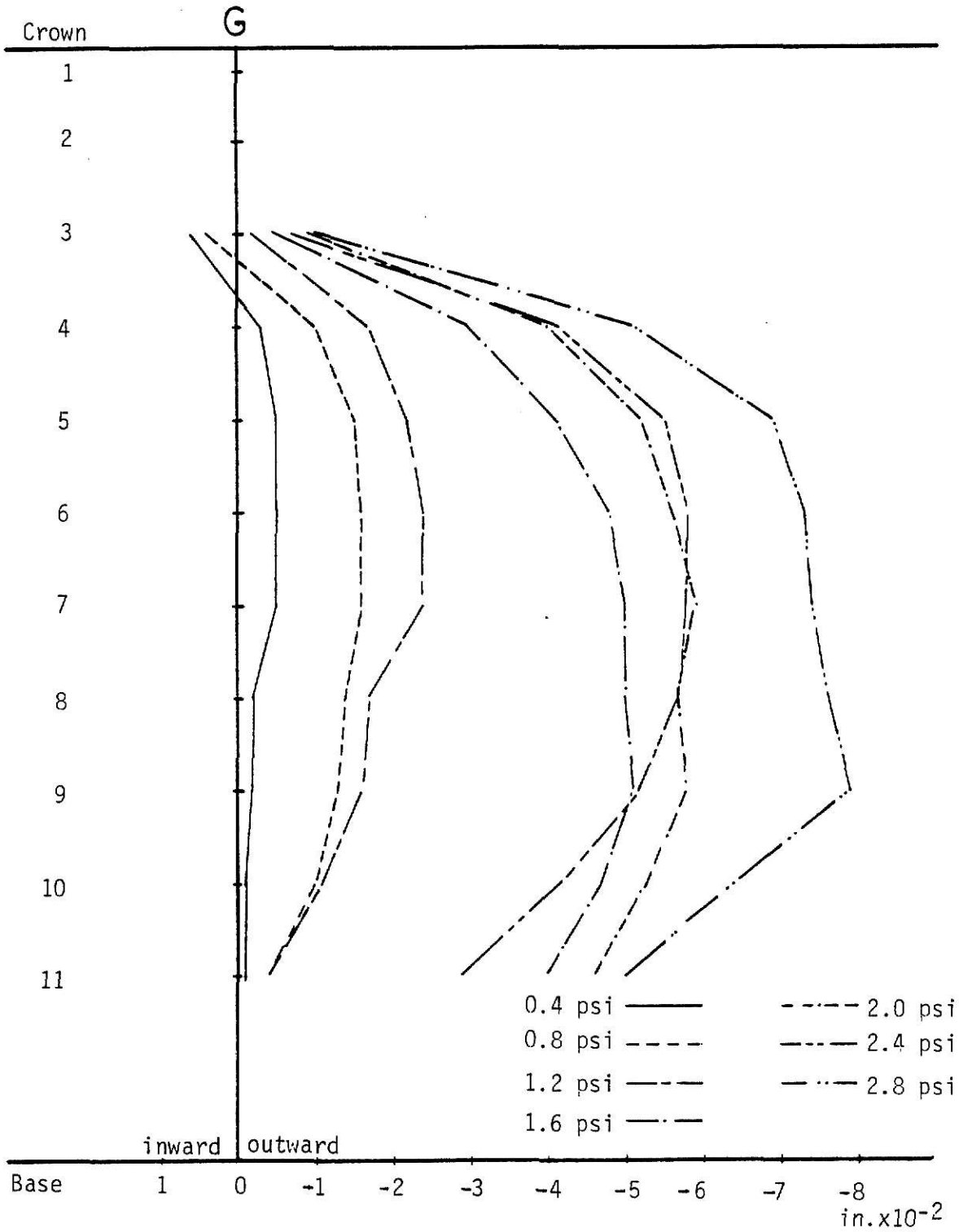

Fig. 30. Deflection Profile for Line G of Shell No. 1, Tested in Jan.-Feb., 1982, 1 in. = 25.4mm

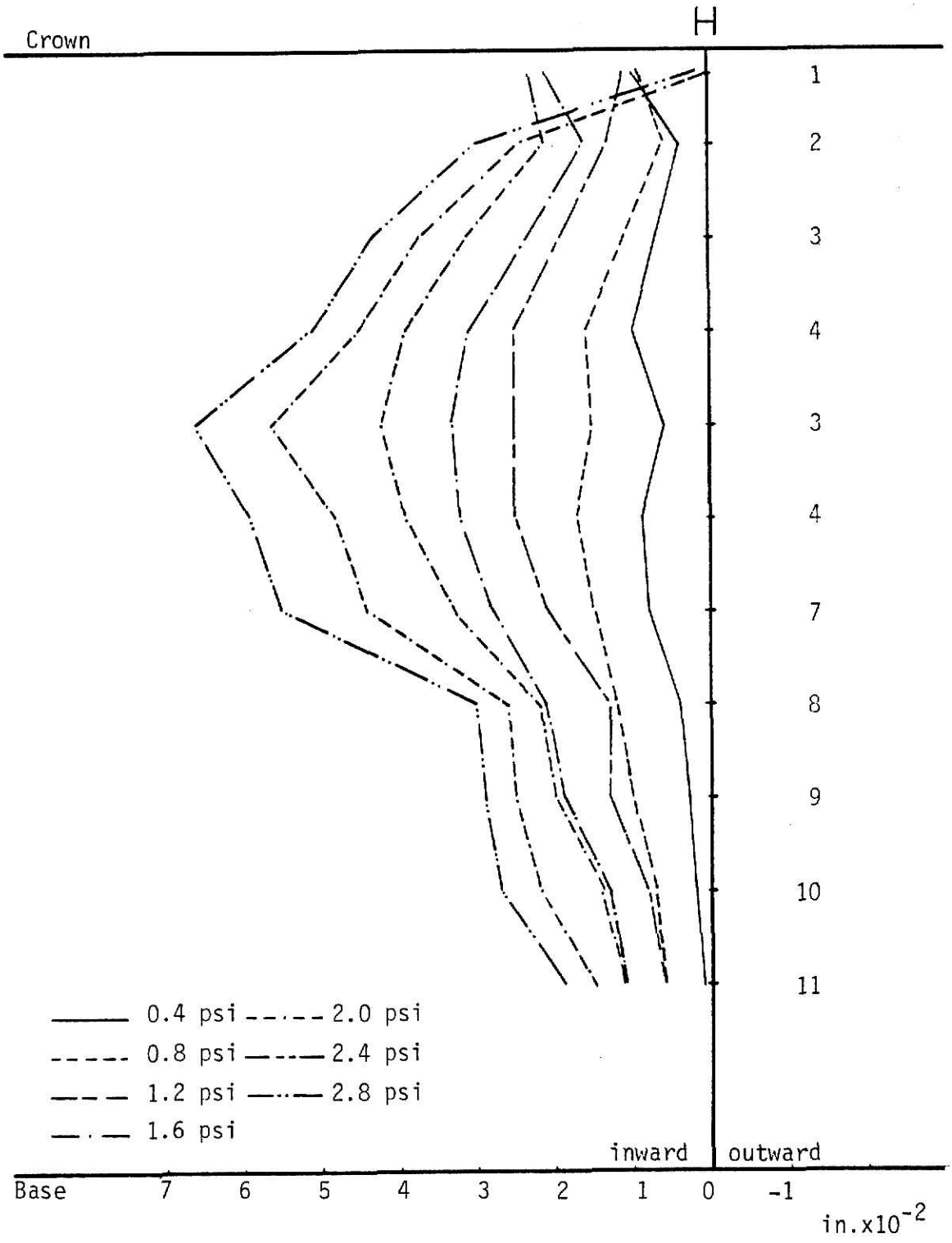

Fig. 31. Deflection Profile for Line H of Shell No. 1, Tested in Jan.-Feb., 1982, 1 in. = 25.4mm

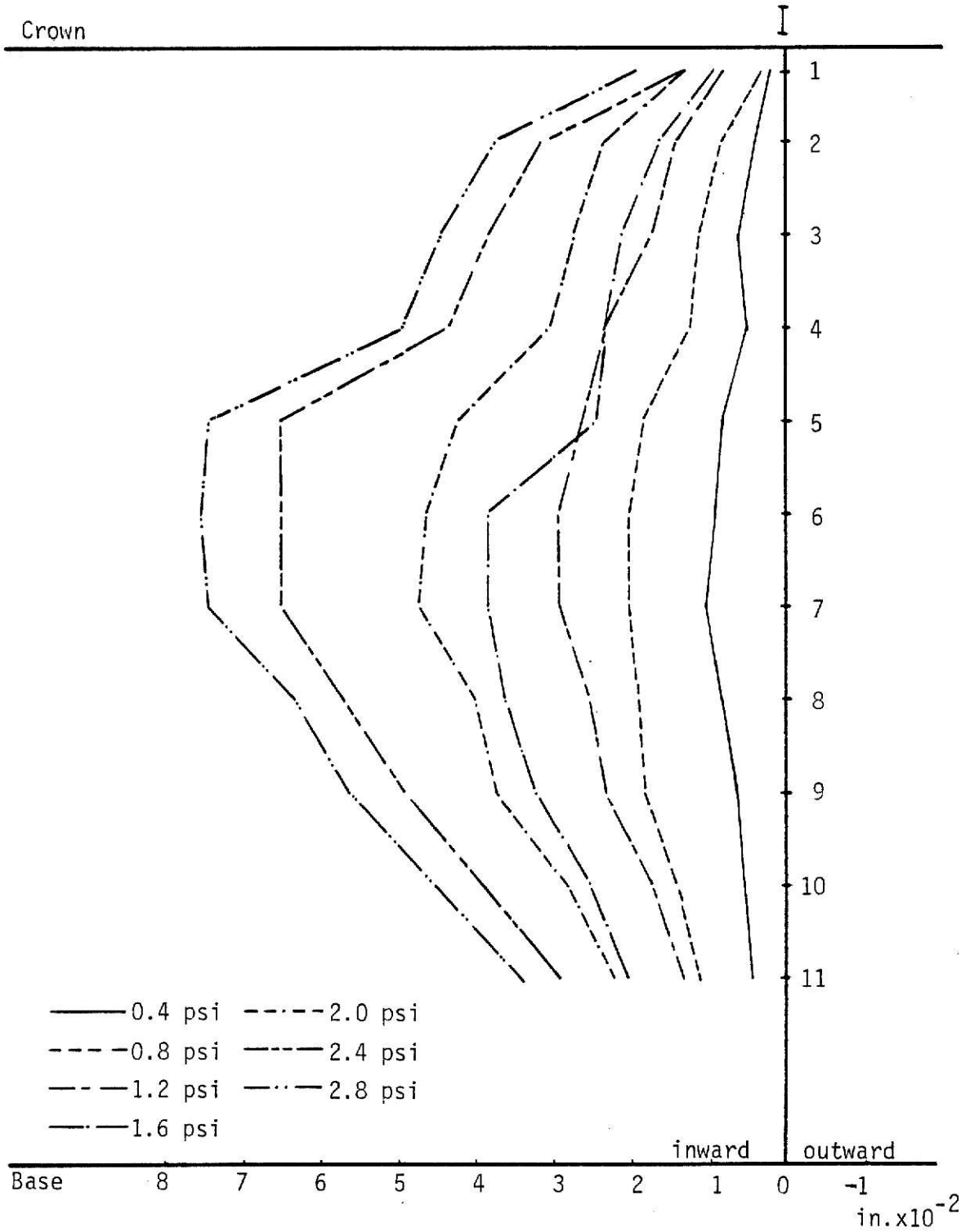

Fig. 32. Deflection Profile for Line I of Shell No. 1, Tested in Jan.-Feb., 1982, 1 in. = 25.4mm

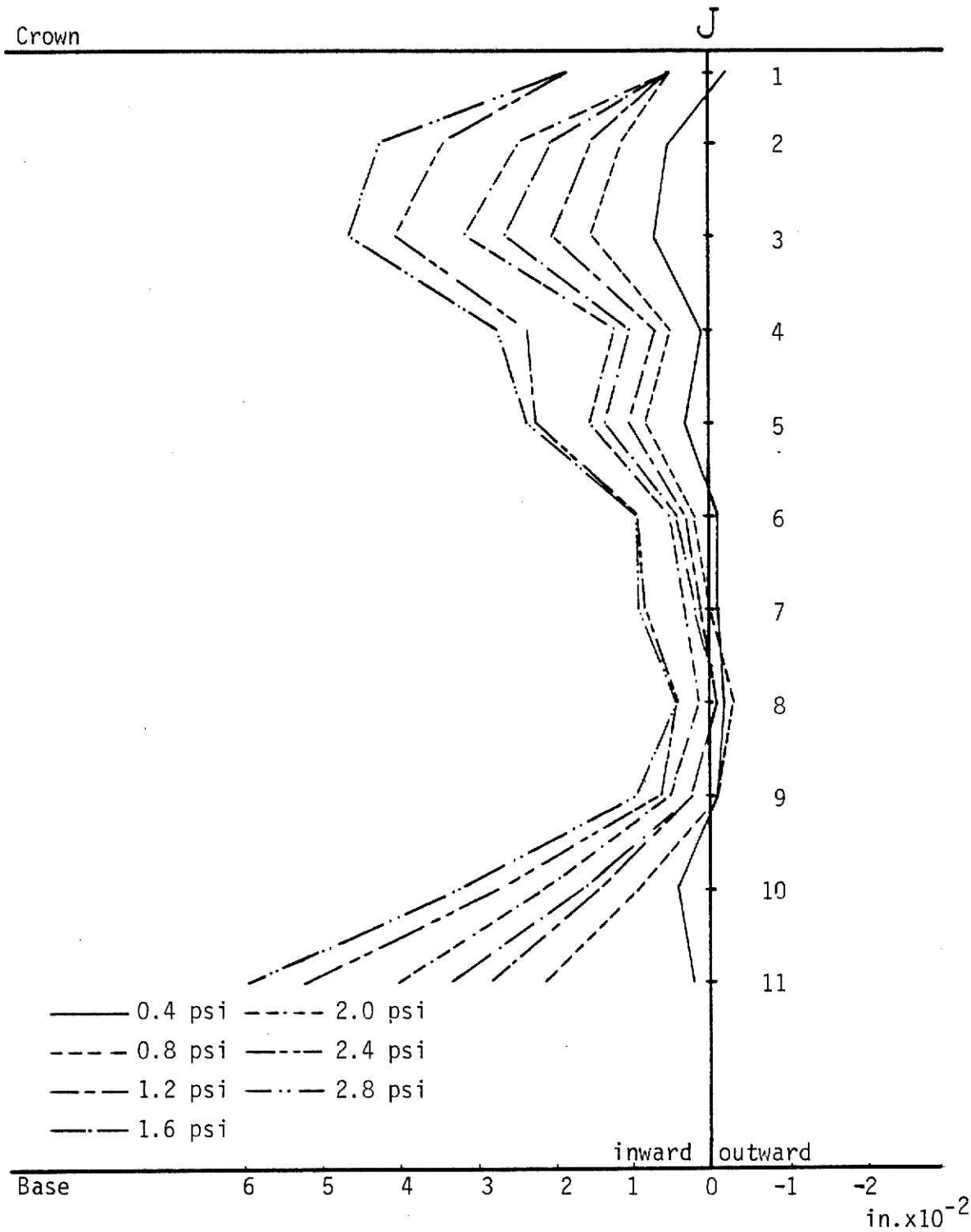

Fig. 33. Deflection Profile for Line J of Shell No. 1, Tested in Jan.-Feb., 1982, 1 in. = 25.4mm

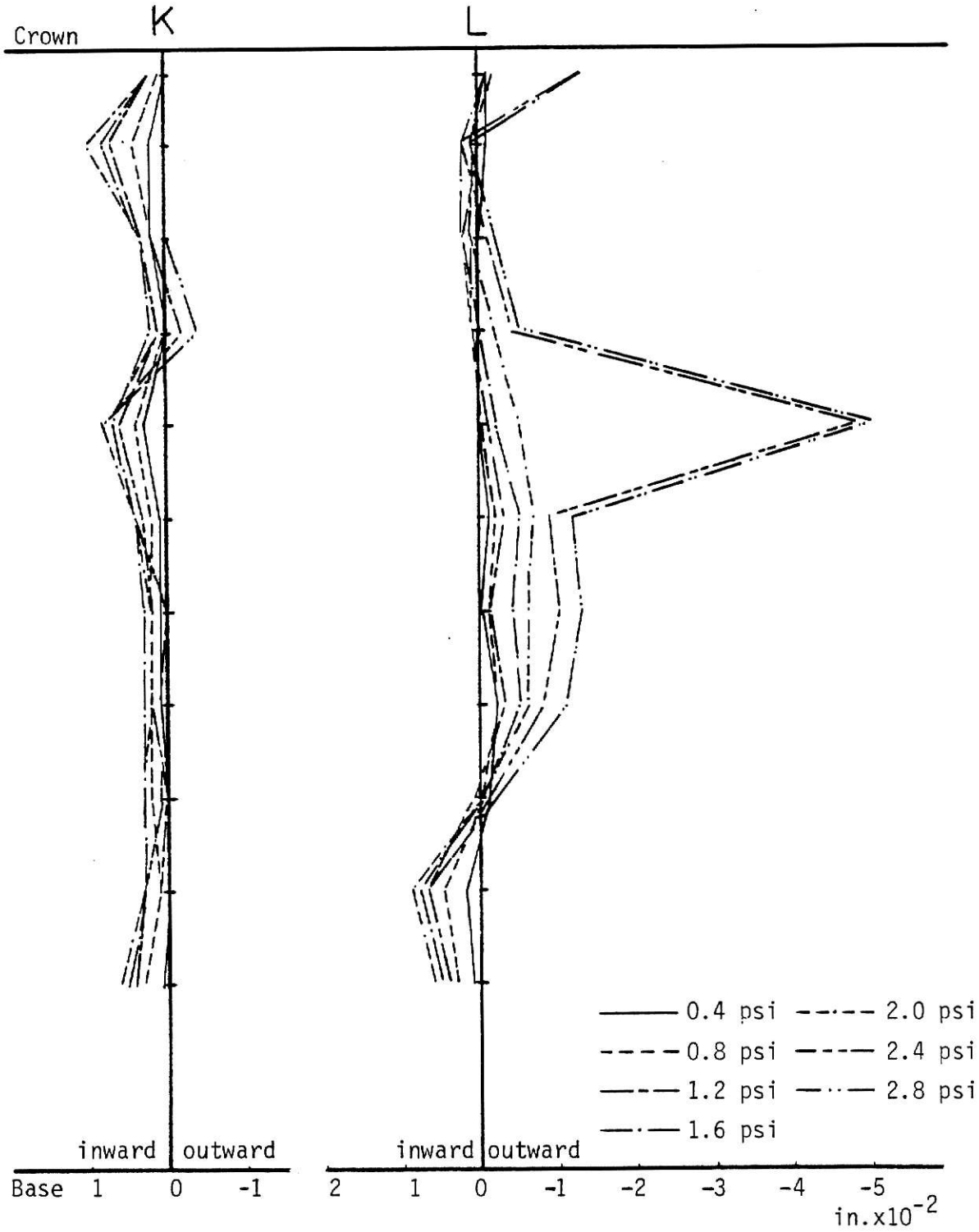

Fig. 34. Deflection Profiles for Lines K and L of Shell No. 1, Tested in Jan.-Feb., 1982, 1 in. = 25.4mm

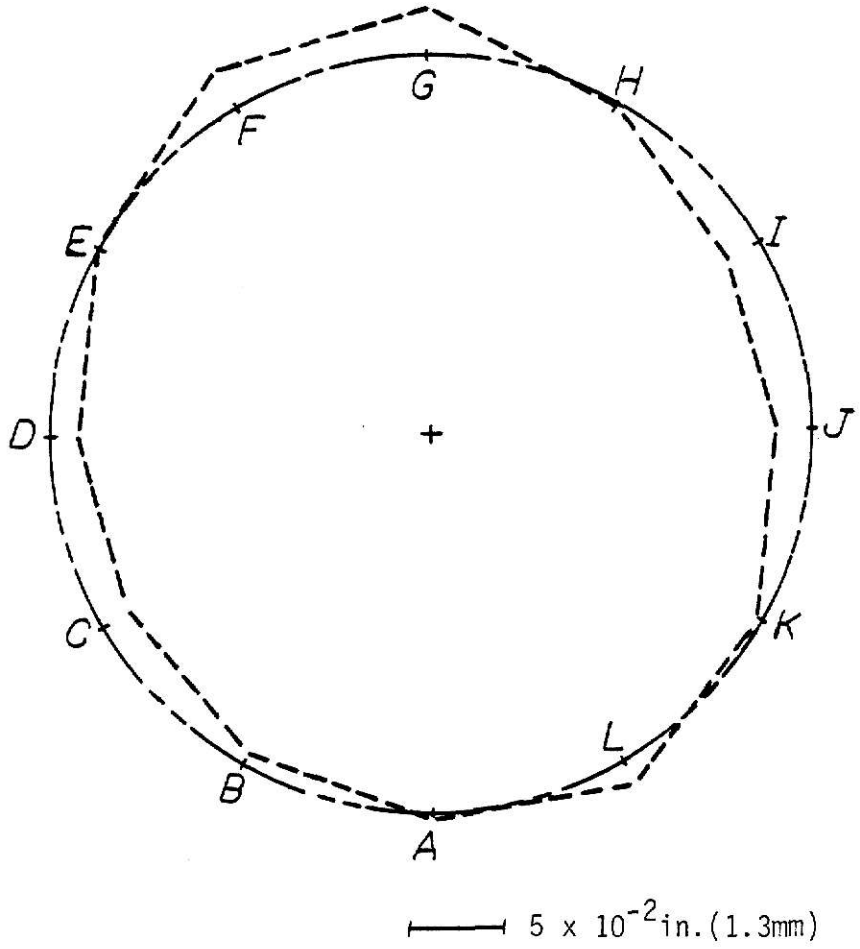

Fig. 35. Deflection Profile for Level No. 1 of Shell No. 1 at 2.8 psi (19.3 KPa), Tested in Jan.-Feb., 1982

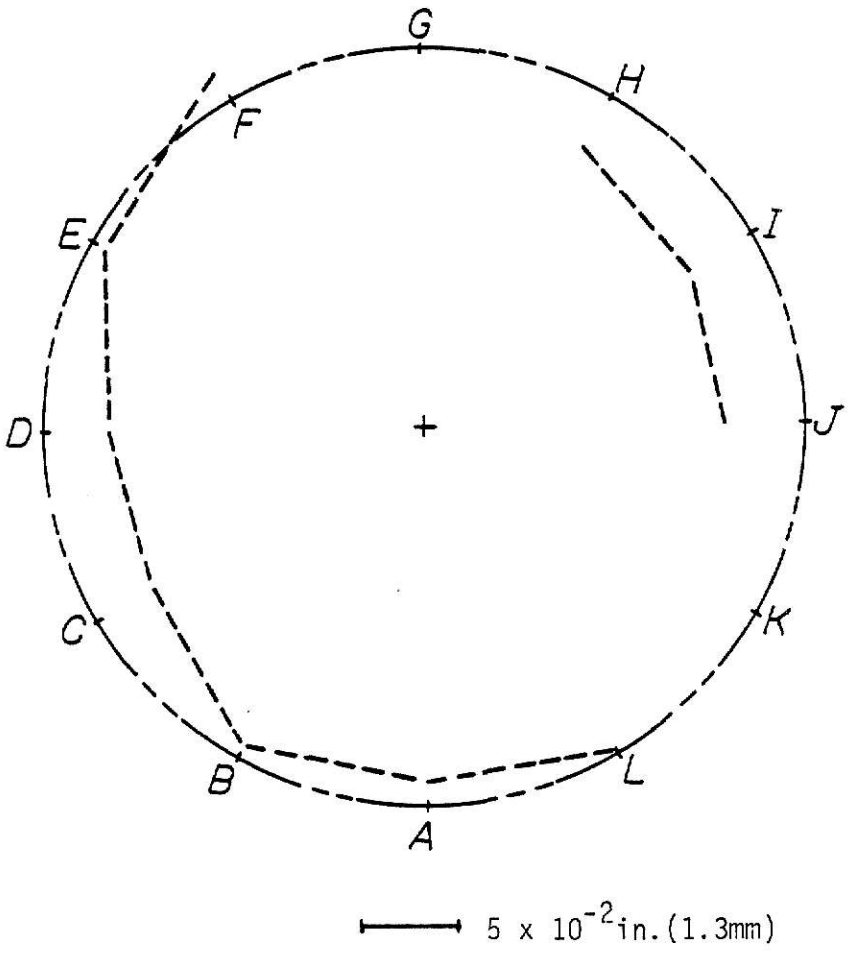

Fig. 36. Deflection Profile for Level No. 2 of Shell No. 1 at 2.8 psi (19.3 KPa), Tested in Jan.-Feb., 1982

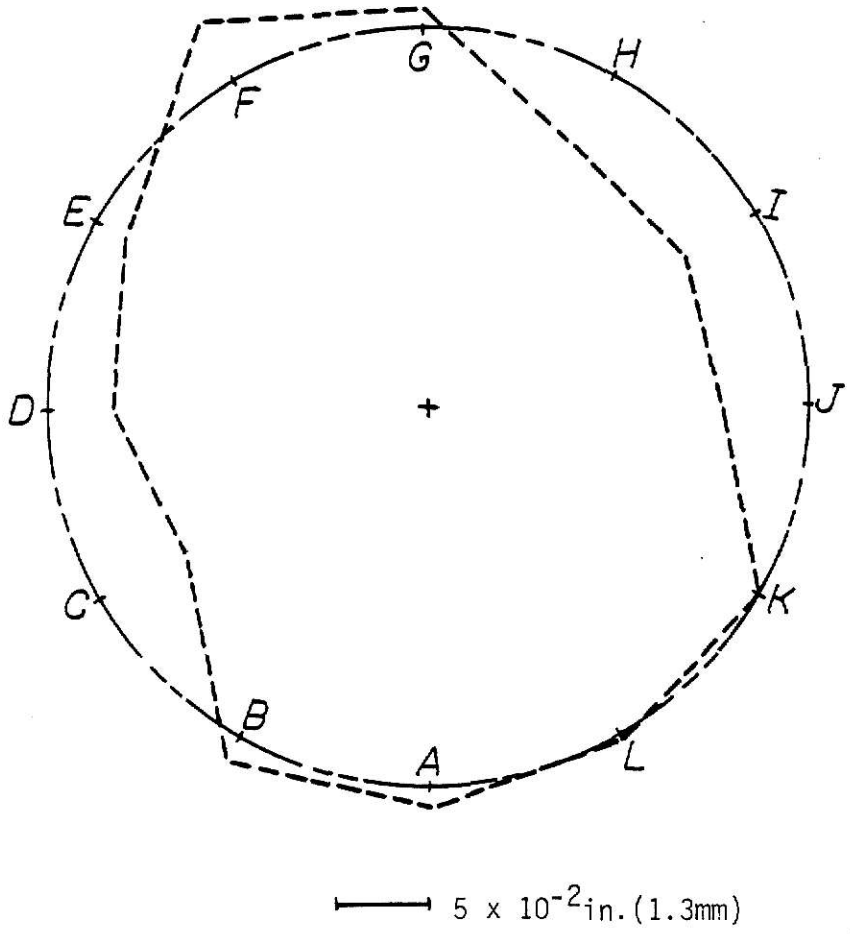

Fig. 37. Deflection Profile for Level No. 3 of Shell No. 1 at 2.8 psi (19.3 KPa), Tested in Jan.-Feb., 1982

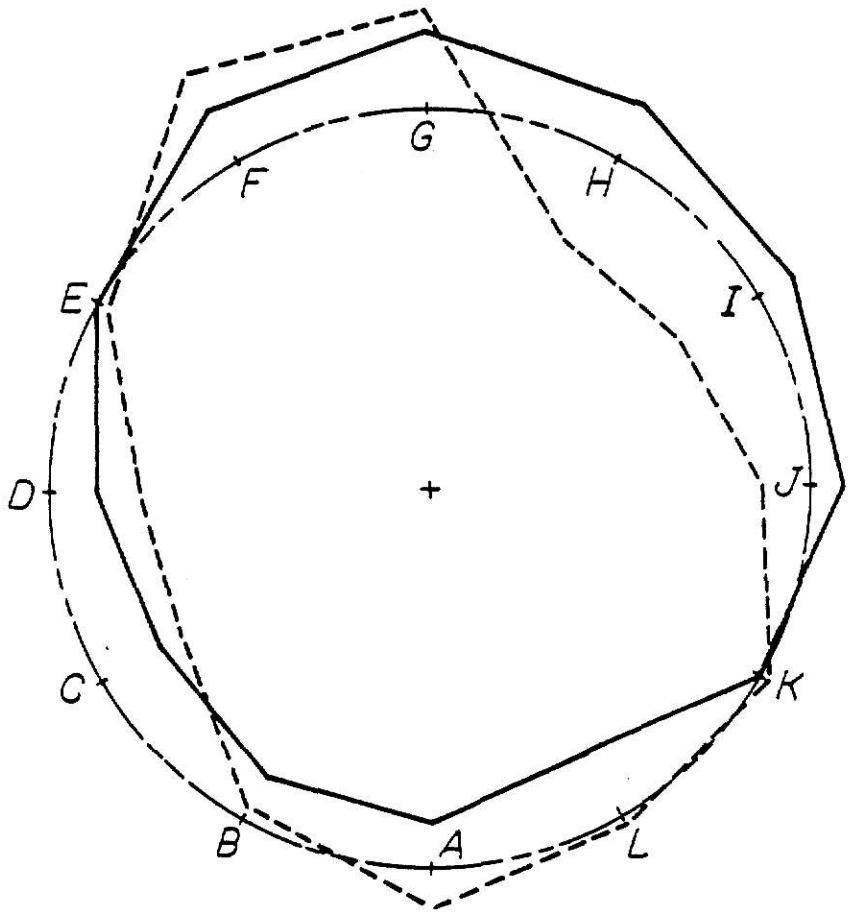

Fig. 38. Deflection Profile for Level No. 4 (Throat) of Shell No. 1 at 2.8 psi (19.3 KPa), Tested in Jan.-Feb., 1982

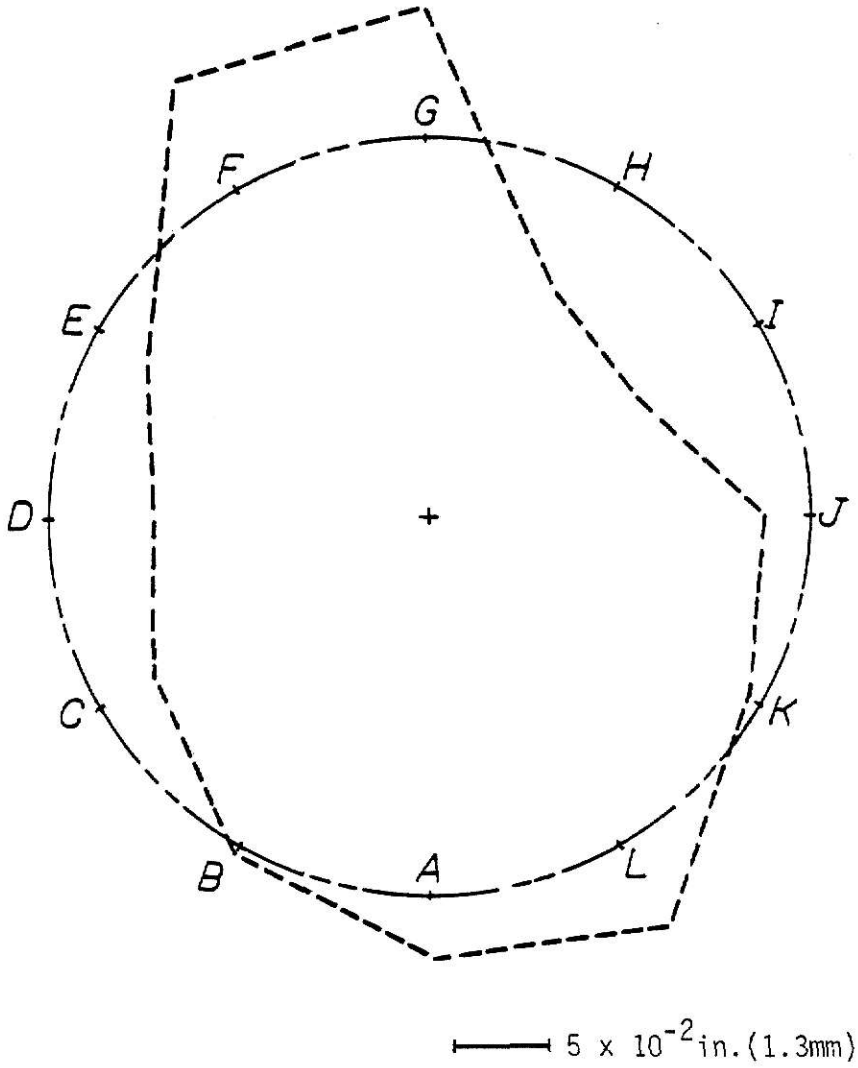

Fig. 39. Deflection Profile for Level No. 5 of Shell No. 1 at 2.8 psi (19.3 KPa), Tested in Jan.-Feb., 1982

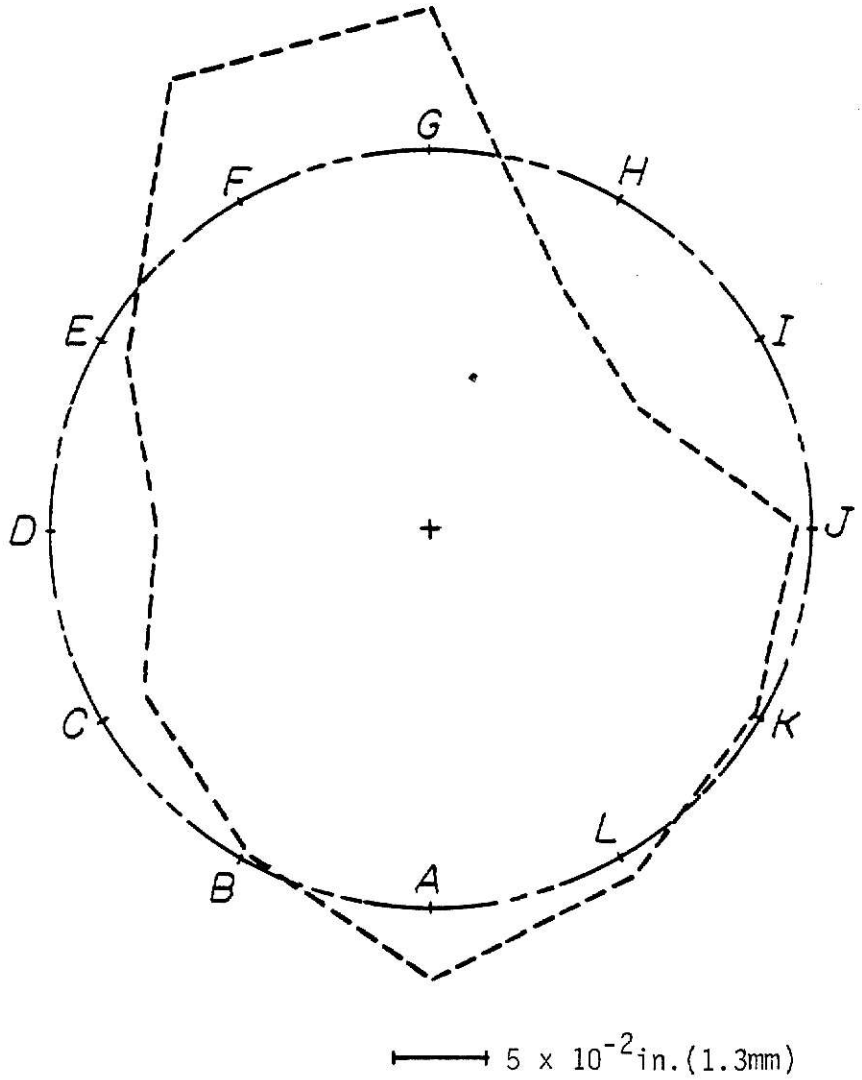

Fig. 40. Deflection Profile for Level No. 6 of Shell No. 1 at 2.8 psi (19.3 KPa), Tested in Jan.-Feb., 1982

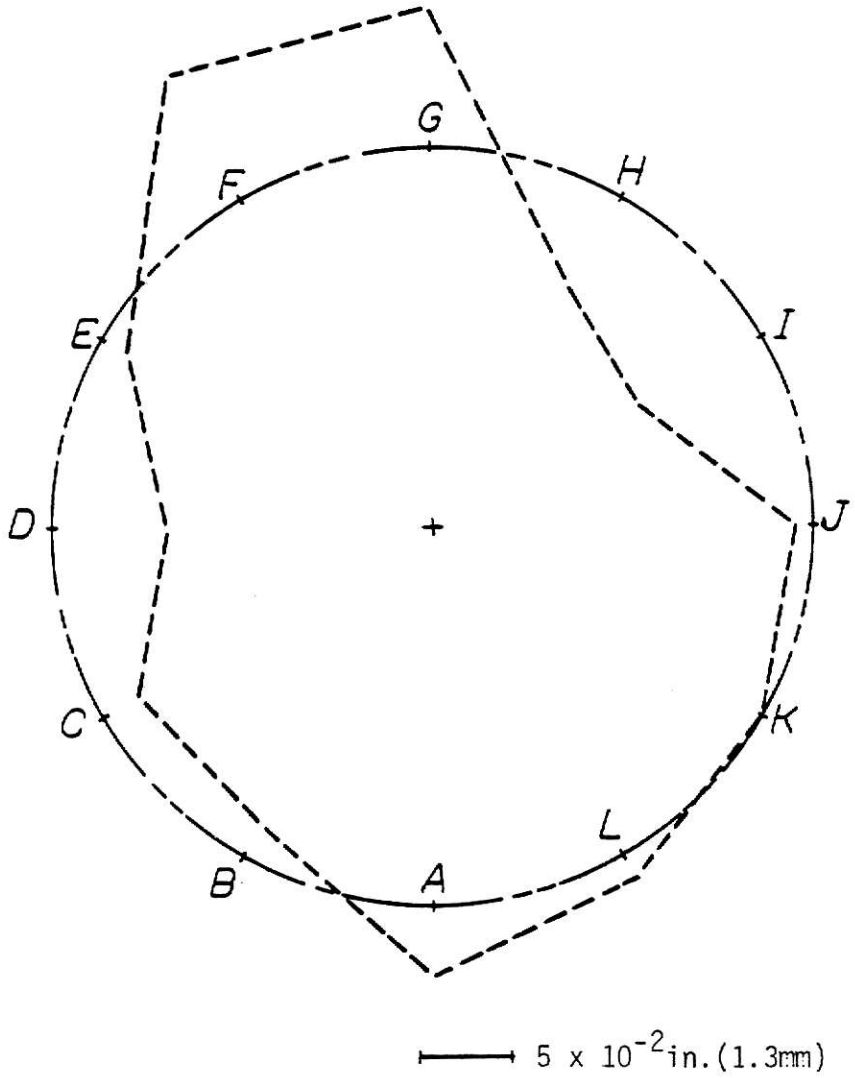

Fig. 41. Deflection Profile for Level No. 7 of Shell No. 1 at 2.8 psi (19.3 KPa), Tested in Jan.-Feb., 1982

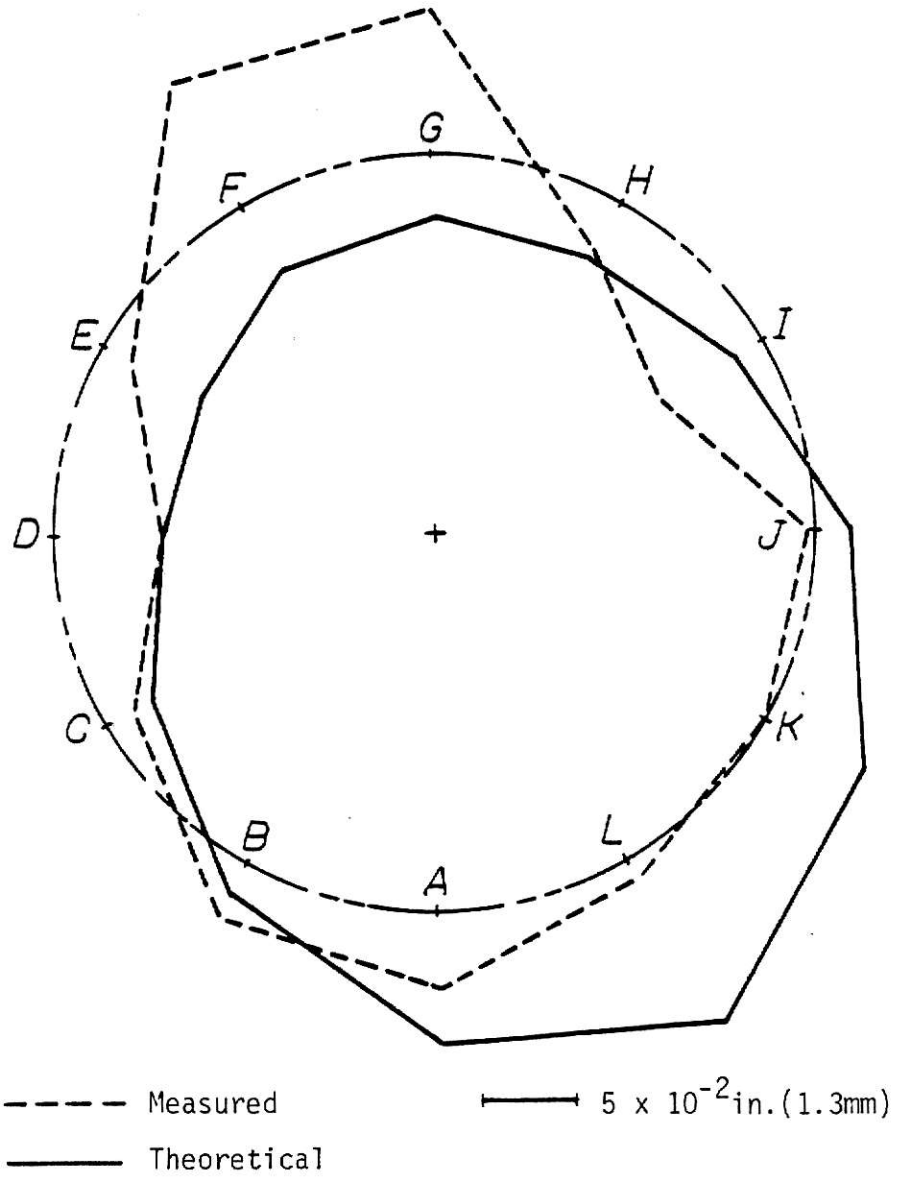

Fig. 42. Deflection Profile for Level No. 8 of Shell No. 1 at 2.8 psi (19.3 KPa), Tested in Jan.-Feb., 1982

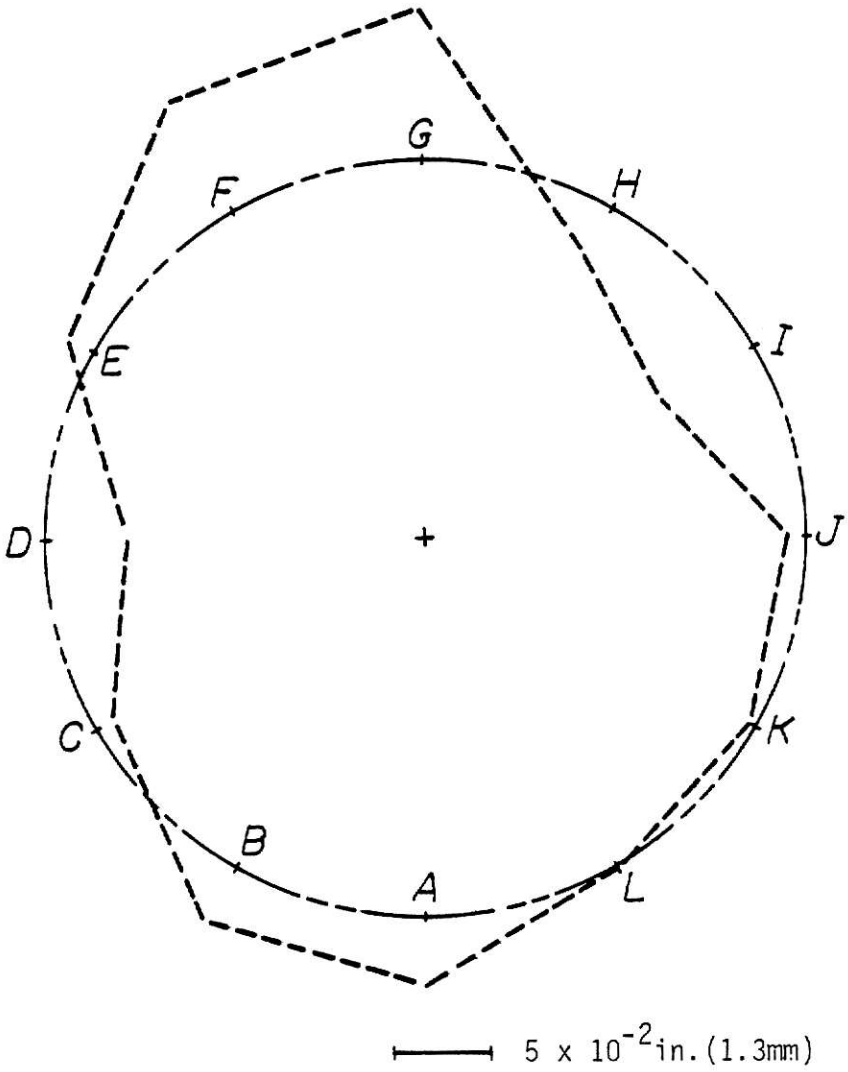

Fig. 43. Deflection Profile for Level No. 9 of Shell No. 1 at 2.8 psi (19.3 KPa), Tested in Jan.-Feb., 1982

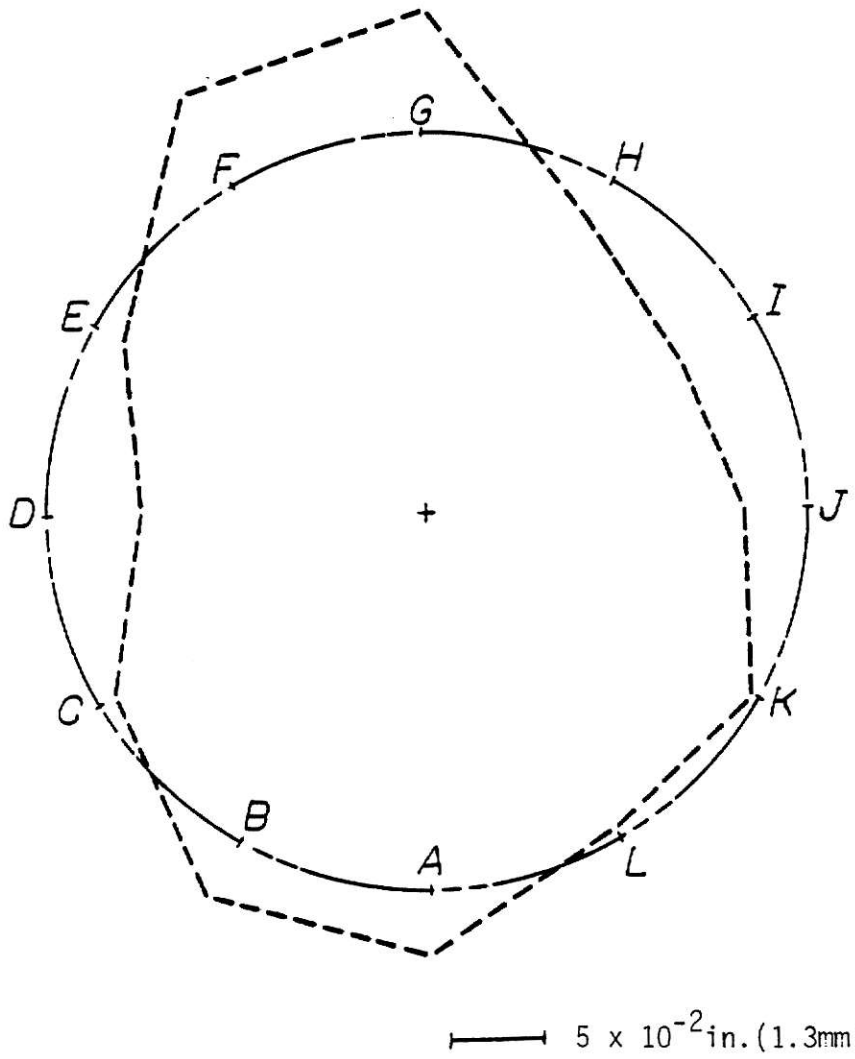

Fig. 44. Deflection Profile for Level No. 10 of Shell No. 1 at 2.8 psi (19.3 KPa), Tested in Jan.-Feb., 1982

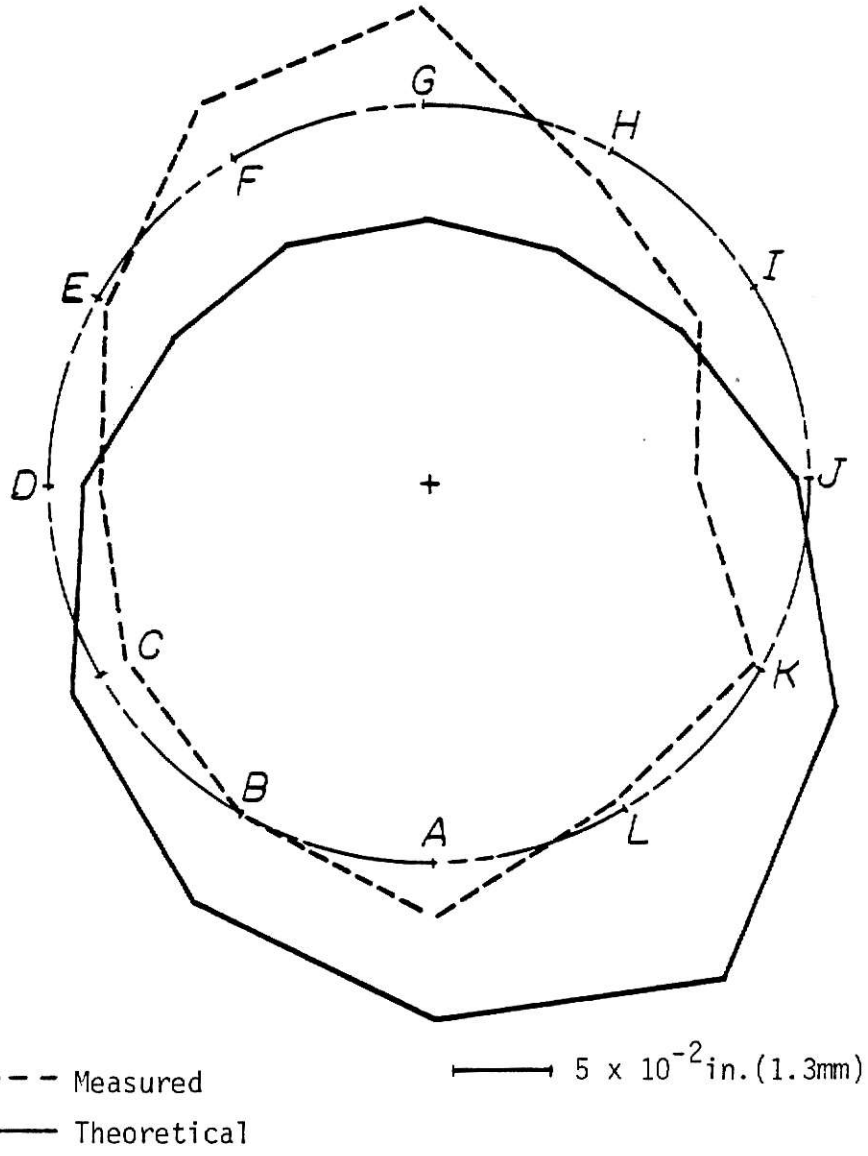

Fig. 45. Deflection Profile for Level No. 11 of Shell No. 1 at 2.8 psi (19.3 KPa), Tested in Jan.-Feb., 1982

Fig. 46. Failed Region From Outside, Shell No. 1, Test No. 2

Fig. 47. Failed Region From Inside, Shell No. 1, Test No. 2

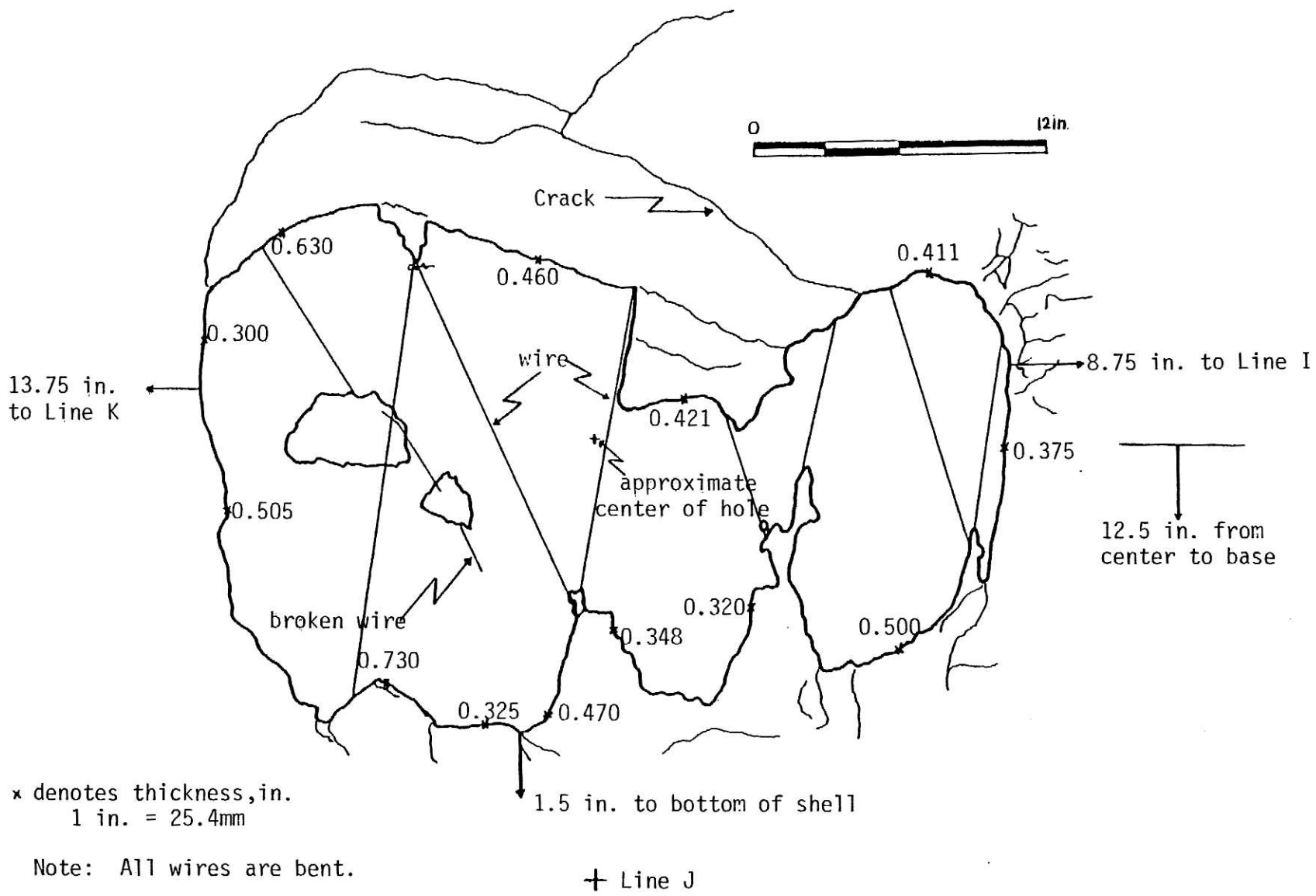

Fig. 48. Outside View of Hole, Shell No. 1,
Test No. 2, 1 in. = 25.4mm

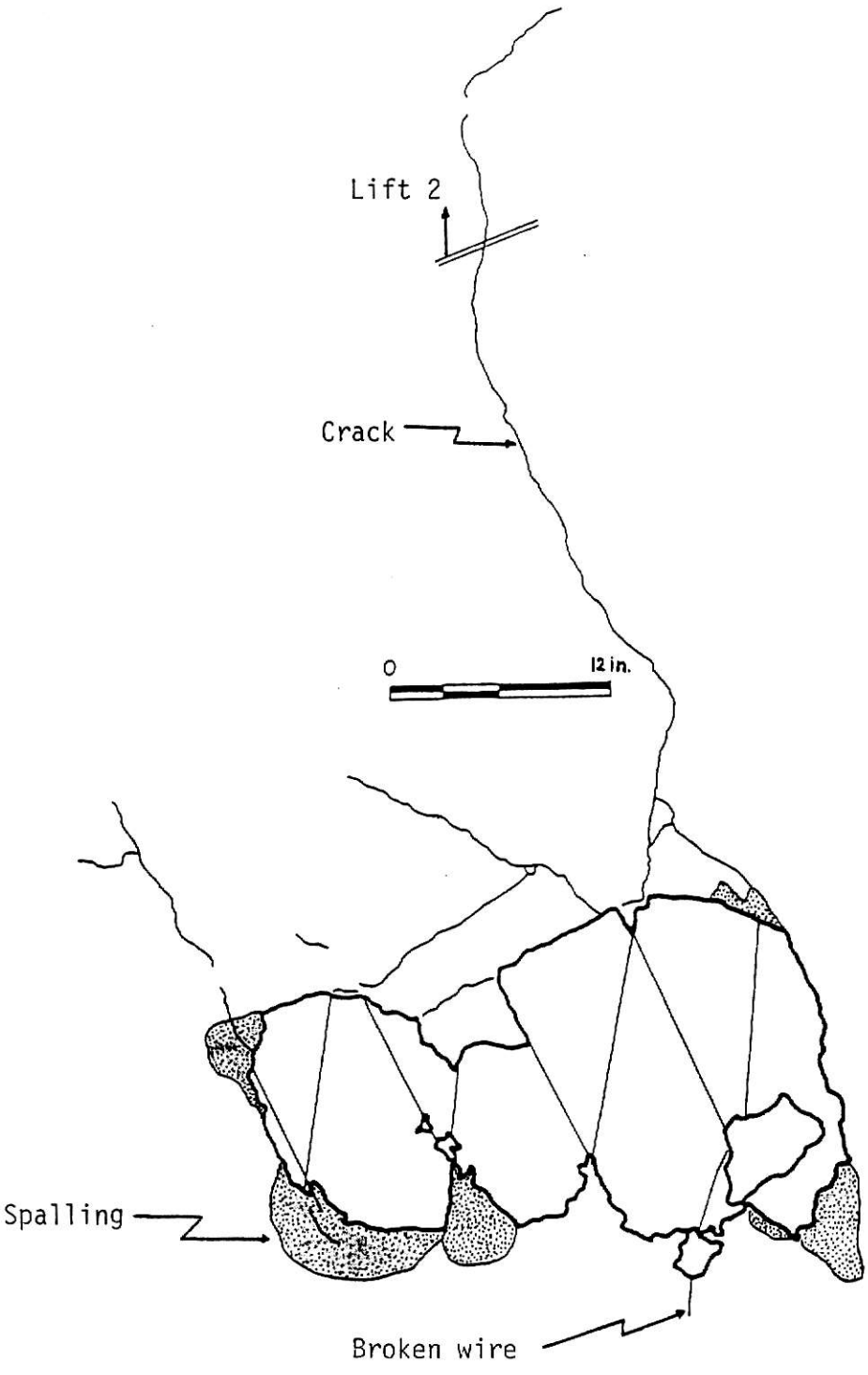

Fig. 49. Inside View of Hole, Shell No. 1, Test No. 2, 1 in. = 25.4mm

Appendix C : Sample Calculations

(a) Sample Calculations for the Improved Deviation Data Considering Actual Thicknesses:

Actual center line radial deviation from ideal geometry is:

$$\Delta r_{ij} = \Delta r_{1ij} + \tfrac{1}{2} \Delta t_{ij}$$

where

Δr_{1ij} = Measured deviation of outer surface, Table 3

Δt_{ij} = Thickness deviation from 0.5 in. (13 mm), Table 4

i = Gage number from 1-11

j = Line number from A-L, i.e., from 1-12

At throat, Line A:

$\Delta r_{141} = -0.83$ (outward)

$\Delta t_{41} = 0.60 - 0.50 = +0.10$ (increase)

$\Delta r_{41} = -0.83 + 0.10/2 = -0.78$

At throat, Line D:

$\Delta r_{144} = +0.62$ (inward)

$\Delta t_{44} = 0.76 - 0.5 = +0.26$ (increase)

$\Delta r_{44} = 0.62 + 0.26/2$

$= 0.75$

(b) Sample Calculations for Membrane Theory Amended by Meridional Imperfection:

At throat, Line H:

$q = 1.0$ psi (6.9 kPa)

$a = R_T = 36$ in. (0.91 m)

$H_T = 108$ in. (2.74 m)

$R_B = 56$ in. (1.42 m)

$R_{Top} = 38.7$ in. (0.98 m)

$t = 0.396$ in. (10.06 mm) - Notice that this number is not that shown in Table 4 (.49). It is the number measured right next to strain gage.

$\mu = 0.16$

$E_c = 3.62 \times 10^6$ psi (24.9 GPa)

$\phi = 90^o$

Uniform external pressure:

$P_\Theta = P_\phi = 0$

$P_N = -q$

$N_{\phi\Theta} = 0 \quad \& \quad \frac{\partial}{\partial \Theta} = 0$

$$b = \frac{R_T H_T}{\sqrt{R_B^2 - R_T^2}} = \frac{36 \times 108}{\sqrt{(56)^2-(36)^2}} = 90.64 \text{ in (2.30 m)}$$

$$R_\phi = \frac{-a^2b^2}{(a^2\sin^2\phi - b^2\cos^2\phi)^{3/2}} = \frac{-(36)^2(90.64)^2}{[(36)^2]^{3/2}} = -228.21 \text{ in. (5.8 m)}$$

$$R_\Theta = \frac{a^2}{(a^2\sin^2\phi - b^2\cos^2\phi)^{1/2}} = \frac{(36)^2}{[(36)^2]^{1/2}} = 36 \text{ in. (0.91 m)}$$

$$\tan\phi = \frac{dz}{dr} = \pm \frac{b}{a}\sqrt{\frac{r^2}{r^2-a^2}} \quad \begin{cases} +\phi < 90^o & (z+) \\ 90 \leq \phi \leq 180 & (z-) \end{cases}$$

$$\text{Tan}\phi_{Top} = -\frac{90.64}{36}\sqrt{\frac{(38.7)^2}{(38.7)^2 - (36)^2}} = -6.86$$

$$\phi_{Top} = -81.70^{\circ} \quad \text{or} \quad \phi_{Top} = 180 - 81.70 = 98.29^{\circ}$$

$$k^2 = 1 + \frac{a^2}{b^2} = 1 + \frac{(36)^2}{(90.64)^2} = 1.158$$

$$\zeta_t = \frac{1}{k^2 \text{Sin}^2\phi_T - 1} = \frac{1}{1.158\ \text{Sin}^2(98.29) - 1} = 7.467$$

$$\zeta = \zeta_{throat} = \frac{1}{1.158\ \text{Sin}^2(90) - 1} = 6.329$$

$$N_\phi = \frac{-qa^2}{2b}\ \frac{\sqrt{\zeta}}{(1 + \zeta)}\ [\zeta - \zeta_t]$$

$$N_\phi = \frac{-(1)\ (36)^2}{2(90.64)}\ \frac{\sqrt{6.329}}{(1 + 6.329)}\ [6.329 - 7.467]$$

N_ϕ = 2.79 lb/in. (0.49 kN/m) due to suction

$$N_\theta = -\frac{R_\theta}{R_\phi} N_\phi - R_\theta q$$

$$N_\theta = -\frac{36}{-228.21}\ (2.79) - 36(1)$$

N_θ = -35.56 lb/in. (-6.23 kN/m) due to suction

P' = Load carried by shell from top cover

$$2\pi R_{Top} P' = \frac{5}{9}\pi R^2_{Top}\ q$$

$$P' = \frac{5}{9}\ \frac{R_{Top}\ q}{2} = \frac{5}{9} \times \frac{1}{2}\ (1)\ (38.7) = 10.75 \text{ lb/in. } (1.88 \text{ kN/m})$$

$$N_\phi = -\frac{R_{Top} P'}{R_\theta\ \text{Sin}^2\phi} = -\frac{38.7 \times 10.75}{36 \times 1}$$

N_ϕ = - 11.56 lb/in. (-2.02 kN/m) due to load at top of shell

$$N_\Theta = \frac{R_{Top} P'}{R_\phi \, Sin^2\phi} = \frac{38.7 \times 10.75}{-228.21 \times 1}$$

N_Θ = -1.82 lb/in. (-.32 kN/m) due to load at top of shell

N_ϕ(total) = 2.79 - 11.56 = -8.77 lb/in. (-1.54 kN/m)

Due to imperfection:

$$\left.\begin{aligned} N_\Theta &= +n_\Theta (2\ D_d)\ k\ R\ N_\phi / H \\ M_\phi &= +m_\phi (2\ D_d)\ N_\phi / (2Hk) \end{aligned}\right\}$$ Plus sign is due to positive imperfection inward

Circular imperfection:

$$n_\Theta = \frac{2}{\bar{k}} \left[1 - 2 \cos \bar{k}\ e^{-\bar{k}} + \cos 2\bar{k}\ e^{-2\bar{k}}\right]$$

$$m_\phi = \frac{2}{\bar{k}} \left[2 \sin \bar{k}\ e^{-\bar{k}} - \sin 2\bar{k}\ e^{-2\bar{k}}\right]$$

Straight Line imperfection:

$$n_\Theta = 1 - (\cos 2\bar{k} + \sin 2\bar{k})\ e^{-2\bar{k}}$$

$$m_\phi = 1 - (\cos 2\bar{k} - \sin 2\bar{k})\ e^{-2\bar{k}}$$

$$k = \left(\frac{3}{R^2 t^2}\right)^{1/4} = 0.3486$$

$$\bar{k} = \frac{kH}{4} = 2.091$$

where

R = horizontal radius = 36 in. (0.91 m)

t = thickness at Line H = 0.396 in. (10.06 mm)

H = height of imperfection (spacing) = 24 in. (60.96 cm)

$\cos \bar{k}$ = -0.49706

$\cos 2\bar{k}$ = -0.50587

$\sin \bar{k} = +0.86772$

$\sin 2\bar{k} = -0.86261$

$e^{-\bar{k}} = 0.12356$

$e^{-2\bar{k}} = 0.015268$

Circular: $n_\Theta = 1.0666$, $m_\phi = 0.2177$

Straight Line: $n_\Theta = 1.0209$, $m_\phi = 0.9946$

$$D_d(ij) = \Delta r_{i+1,\,j} - (\Delta r_{ij} + \Delta r_{i+2,\,j})/2$$

where

D_d = imperfection out of round from the perfect shape in the radial direction

$$\Delta r_{ij} = \Delta r_{1ij} + \tfrac{1}{2}\,\Delta t_{ij}$$

where Δr_{1ij} and Δt_{ij} are obtained from Tables 3 and 4, respectively.

$$D_d(48) = \Delta r_{58} - (\Delta r_{48} + \Delta r_{68})/2$$

$$\Delta r_{58} = \Delta r_{158} + \tfrac{1}{2}\,\Delta t_{58}$$

$$= 0.45 + \tfrac{1}{2}\,(0.32 - 0.5) = 0.36$$

$$\Delta r_{48} = 0.13 + \tfrac{1}{2}\,(0.49 - 0.5) = 0.125$$

$$\Delta r_{68} = 0.31 + \tfrac{1}{2}\,(0.61 - 0.5) = 0.365$$

$$D_d(48) = 0.115$$

Circular:

$$N_\Theta = +1.0666 \times 2 \times 0.115 \times 0.3486 \times 36\ (-8.77)/24$$

$N_\Theta = -1.125$ lb/in. (-0.20 kN/m) due to imperfection

N_Θ(total) = -35.56 - 1.82 -1.125 = -38.5 lb/in. (-6.74 kN/m)

M_ϕ = +0.2177 x 2 x 0.115 (-8.77)/2 x 24 x 0.3486

M_ϕ = -0.026 lb-in./in. (-0.116 N-m/m)

Straight Line:

N_Θ = +1.0209 x 2 x 0.115 x 0.3486 x 36 (-8.77)/24

N_Θ = -1.08 lb/in. (-0.19 kN/m) due to imperfection

N_Θ(total) = -35.56 - 1.82 -1.08 = -38.46 lb/in. (-6.74 kN/m)

M_ϕ = +0.9946 x 2 x 0.115 (-8.77)/2 x 24 x 0.3486

M_ϕ = -0.12 lb-in./in. (-0.534 N-m/m)

$\varepsilon_\phi = (N\phi - \mu N_\Theta)/tE_c$

$= [-8.77 - 0.16 (-38.5)] /(0.396) (3.62 \times 10^6)$

$\varepsilon_\phi = -1.82 \times 10^{-6}$ in./in.

$\varepsilon_\Theta = (N_\Theta - \mu N_\phi)/tE_c$

$= [-38.5 - 0.16 (-8.77)]/(0.396) (3.62 \times 10^6)$

$\varepsilon_\Theta = -25.88 \times 10^{-6}$ in./in.

(c) Equations and Sample Calculations for Experimental Forces and Bending Moments at Maximum Load of 3.7 Psi (25.53kPa).

$\sigma_{i\Theta} = E_c(\varepsilon_{i\theta} + \mu\varepsilon_{i\phi})/(1 - \mu^2)$

$\sigma_{o\Theta} = E_c(\varepsilon_{o\theta} + \mu\varepsilon_{o\phi})/(1 - \mu^2)$

$N_\Theta = (\sigma_{i\Theta} + \sigma_{o\Theta})\ t/2$

$M_\Theta = t^2(\sigma_{o\Theta} - \sigma_{i\Theta})/6$

Similarly

$$\sigma_{i\phi} = E_c(\varepsilon_{i\phi} + \mu\varepsilon_{i\theta})/(1 - \mu^2)$$

$$\sigma_{o\phi} = E_c(\varepsilon_{o\phi} + \mu\varepsilon_{o\theta})/(1 - \mu^2)$$

$$N_\phi = (\sigma_{i\phi} + \sigma_{o\phi})\ t/2$$

$$M_\phi = t^2(\sigma_{o\phi} - \sigma_{i\phi})/6$$

In which,

σ - stress

ε - strain from strain gage data

i - inner face of the shell

o - outer face of the shell

N - membrane force, tension is positive

M - bending moment, positive moment causes tension in the outer layer of the shell

At the patched region:

$t = 0.715$ in. (18.16 mm)

$$\sigma_{i\theta} = 3.62 \times 10^6[(-49\times10^{-6})+0.16(76\times10^{-6})]/[1-(0.16)^2]$$

$\sigma_{i\theta}$ = -136.9 Psi (-944.6 kPa)

$$\sigma_{o\theta} = 3.62 \times 10^6[(-108\times10^{-6})+0.16(-1\times10^{-6})]/[1-(0.16)^2]$$

$\sigma_{o\theta}$ = -401.8 Psi (-2.8 MPa)

N_θ = (-136.9 - 401.8) (0.715)/2

N_θ = -192.6 lb/in. (-33.7 kN/m)

$M_\theta = (0.715)^2\ (-401.8 + 136.9)/6$

$M_\theta = -22.6$ lb-in./in. (-100.6 N-m/m)

$\sigma_{i\phi} = 3.62 \times 10^6\ [76 \times 10^{-6} + 0.16(-49 \times 10^{-6})]/[1-(0.16)^2]$

$\sigma_{i\phi} = 253.2$ Psi (1.7 MPa)

$\sigma_{o\phi} = 3.62 \times 10^{-6}\ [(-1 \times 10^{-6}) + 0.16(-108 \times 10^{-6})/[1-(0.16)^2]$

$\sigma_{o\phi} = -67.9$ Psi (-468.5 kPa)

$N_\phi = (253.2 - 67.9)\ (0.715)/2$

$N_\phi = 66.2$ lb/in. (11.6 kN/m)

$M_\phi = (0.715)^2\ (-67.9 - 253.2)/6$

$M_\phi = -27.4$ lb-in./in. (-121.9 N-m/m)

Appendix D : Notation

Notation

$a = R_T$ - throat radius

b - shell geometry parameter

e - shell radial imperfection(inward positive)(also denoted D_d)

E_c - Young's modulus of concrete

E_T - Tangent modulus

F_θ, F_ϕ - experimental correction factors depending on the shape of the cooling tower shell

f'_c - concrete uniaxial compressive strength

H - distance between three dial gages,24 in. (0.61 m)

H_T - vertical distance from the throat to the base

i - gage number from 1-11

j - line number from 1-12 (A-L)

K, $\bar{K}$ - parameters

$K_{G\theta}$, $K_{G\phi}$ - factors depending on shape and boundary conditions of the cooling tower shell

M - bending moment

m_ϕ - nondimensionalized meridional moment coefficient

N_θ, N_ϕ - membrane forces

n_θ - nondimensionalized hoop force coefficient

P - applied axial load

P_θ, P_ϕ, P_N - load components per unit area of middle surface

q - uniform external pressure

q_{cr} - buckling pressure

Q_θ, Q_ϕ - geometry buckling parameters

Notation (continued)

R - horizontal radius

r - horizontal radius

R_B - base radius

R_{Top} - top radius

S - deviation expressed as slope

w - horizontal displacement (inward positive)

t - shell thickness

Z - vertical coordinate

ϕ - meridional direction

θ - circumferential direction

σ - stress

ε - strain

Δ - net radial deviation of the shell surface(inward positive)

$\Delta_{r_{ij}}$ - center line radial deviation from ideal geometry (inward positive)

μ- Poisson's ratio

Acknowledgements

The author wishes to express his gratitude to Dr. S.E. Swartz for his guidance and invaluable advice in conducting this research project as well as his helpful suggestions in preparation of this manuscript. It was a great opportunity as well as a learning experience to work with him.

Sincere thanks are also extended to Dr. K.K. Hu for his valuable advice, to Dr. P.B. Cooper and Dr. C.L. Huang, his committee members, for their assistance in reviewing this manuscript, and to Dr. R. Snell, head of the department of Civil Engineering, for his support.

The research reported herein was partially supported by the National Science Foundation, grant ENG-7818415. This support is gratefully acknowledged.

Finally, the author wishes to express his words of deepest appreciation to his parents, for that legacy of expectations that they passed on to him. He will always remember and be grateful.

List of References

1. Abel, J.F., Billington,D.P.,Nagy, D.A., and Wiita-Dworkin, C.,"Buckling of Cooling Towers," Journal of the Structural Division, Proceeding of the ASCE, Vol.108, No. ST10, Oct., 1982.

2. Abel, J.F., and Gould, P.L.,"Buckling of Concrete Cooling Tower Shells," ACI Publication SP67-5, "Concrete Shell Buckling," 1981.

3. Al-Dabbagh, A. and Gupta, A.K.,"Meridional Imperfection in Cooling Tower Design," Paper No. 14636, Journal of the Structural Division, Proc. ASCE, No. ST6, June 1979.

4. Billington, D.P. and Harris, H.G.,"Test Methods for Concrete Shell Buckling," ACI Publication SP-67, "Concrete Shell Buckling," 1981.

5. Central Electricity Generating Board, "Report of the Committee of Inquiry into Collapse of Cooling Towers at Ferrybridge," London, England, Nov., 1965.

6. Chien, Karl Chia-Chang, "Costruction and Testing of a Reinforced Concrete Hyperbolic Cooling Tower Model," M.S. Thesis, Dept. of Civil Engineering, Kansas State Univ., Manhattan, Kansas, 1982.

7. Cole, P.P.,"Buckling of Hyperbolic Cooling-Tower Shells," Thesis Presented to Princeton University at Princeton, N.J., in 1973, in partial fulfillment of the requirements for the degree of Master of Science.

8. Cole, P.P., Abel, J.F., and Billington, D.P.,"Buckling of Cooling-Tower Shells: Bifurcation Results," Journal of the Structural Division, ASCE, Vol.101, No. ST6, Proc. Paper 11365, June, 1975.

9. Cole, P.P., Abel, J.F., and Billington, D.P.,"Buckling of Cooling-Tower Shells: State-of-the-Art," Journal of the Structural Division, ASCE, Vol.101, No. ST6, Proc. Paper 11364, June 1975.

10. Croll, J.G.A., Kaleli, F., and Kemp, K.O.,"Behavior of Geometrically Imperfect Cooling Towers," in Process ASCE Engineering Mechanics Division.

11. Croll, J.G.A., Kaleli, F., and Kemp, K.O.,"Meridionally Imperfect Cooling Towers," Journal of the Engineering Mechanics Division, ASCE, Vol.105, No. EM5, Oct. 1979.

12. Croll, J.G.A., Kaleli, F., Kemp, K.O., and Munro, J.,"A Simplified Approach to the Analysis of Geometrically Imperfect Cooling Tower Shells," Engineering Structures, Vol.1, No.1, September 1978.

13. Der, T.J. and Fidler, R.,"A Model Study of the Buckling Behavior of Hyperbolic Shells," Proceedings, Institution of Civil Engineers, Vol.41, London, England, Sept., 1968.

14. Ewing, D.J.F.,"The Buckling and Vibration of Cooling Tower Shells. Part I: Linearized Buckling Theory," Laboratory Report No. RD/L/R1763, Central Electricity Research laboratories, Leatherhead, England, Nov.,1971.

15. Ewing, D.J.F.,"The Buckling and Vibration of Cooling Tower Shells. Part II: Calculations," Laboratory Report No. RD/L/R1764, Central Electricity Research Laboratories, Leatherhead, England, Nov.,1971.

16. Gates, T.,"Design and Construction of Support Facilities for Micro-Concrete Model Shells, Hyperboloids of Revolution," M.S. Thesis, Dept. of Civil Engineering, Kansas State Univ., Manhattan, Kansas, 1981.

17. Gates, T.E., Hu, K.K., McDonald, C.R., and Swartz, S.E., "Construction and Testing of Micro-Concrete Models of Cooling-Tower Shells," Proceeding, Fourth International Congress on Experimental Mechanics, Society For Experimental Stress Analysis, 1981.

18. Gupta, A.K. and Al-Dabbagh, A.,"Meridional Imperfection in Cooling Tower Design-Update," Journal of the Structural Division, Proceedings of ASCE, Vol.108, No. ST8,Aug.,1982.

19. Hayashi, K. and Gould, P.L.,"Some Aspects of the Response of a Wind-Loaded Reinforced Concrete Cooling Tower," Research Report No.63, Structures Program, Dept. of Civil Engineering, Washington University, St. Louis, Missouri, May 1982.

20. Hu, K.K., Kirmser, P.G., Swartz, S.E., and Pan, C.,"On the Matrix Analysis of Non-Linear Buckling of Hyperbolic Cooling Towers," Presented at the Joint ASME/ASCE Mechanics Conference, Boulder, Colorado, June 22-24,1981.

21. Hutchinson, J.W.,"Initial Post-Buckling Behavior of Toroidal Shell Segments," International Journal of Solids and Structures, Vol.3, No.1, Jan.,1967.

22. Langhaar, H.L. and Miller, R.E.,"Buckling of an Elastic Isotropic Cylindrical Shell Subjected to Wind Pressure," Proceedings, Symposium on the Theory of Shells to Honor L. H. Donnell, Houston, Texas, 1967.

23. Mang, H.A., Floegl, H., Trappel, F., and Walter, H.,"Wind-Loaded Reinforced-Concrete Cooling Towers: Buckling or Ultimate Load?," Institute of Structural Analysis and Strength of Materials, Technical University of Vienna, Vienna, Austria, 1981.

24. Mungan, Ihsan,"Buckling of Reinforced Concrete Cooling Tower Shells: BSS Approach," ACI Journal No.5, V.79, Sept-Oct., 1982.

25. Mungan,Ihsan,"Buckling Stresses of Stiffened Hyperboloidal Shells," Journal of the Structural Division, ASCE, Vol. 105, No. 8, August 1979.

26. Mungan, Ihsan,"Buckling Stress States of Hyperboloidal Shells," Journal of the Structural Division, ASCE, Vol. 102, No. ST10, Proc. Paper 12465, October, 1976.

27. Rayleigh,Lord,"The Theory of Sound," Vol.1,2nd ed. London: Macmillan and Co., 1894.

28. Sabnis, G.M., Harris, H.G., White, R.N., and Mirza, M.S., Structural Modeling and Experimental Techniques, Prentice-Hall, Inc., Englewood Cliffs, N.J., 1983.

29. Schnobrich, W.C.,"Analytical and Numerical Evaluation of the Buckling Strength of Reinforced Concrete Shells," ACI Publication SP-67,"Concrete Shell Buckling", 1981.

30. Swartz, S.E.,"Buckling Behavior of Concrete Shells," Summary Report to the National Science Foundation, Grant No. ENG 78-18415, Dec. 1981.

31. Timoshenko, S.,"Strength of Materials, Part I, Elementary Theory and Problems," Robert E.KRIEGER Publishing Company, Huntington, New York, 1958.

32. Vandepitte, Daniel and Rathe, Jacques,"An Experimental Investigation of the Buckling Load of Spherical Concrete Shells Subjected to Uniform Radial Pressure," RILEM International Symposium, Buenos Aires, Argentina, Sept. 13-18, 1971.

33. Veronda, D.R. and Weingarten, V.I.,"Stability of Hyperboloidal Shells: An Experimental and Analytical Investigation," USCCE 009, School of Engineering, Univ. of Southern California, Los Angeles, Calif., March., 1973.

34. Veronda, D.R. and Weingarten, V.I.,"Stability of Hyperboloidal Shells," Journal of the Structural Division, ASCE, Vol.101, No. ST7, Proc. Paper 11446, July, 1975.

35. Veronda,D.R. and Weingarten,V.I.,"Stability of Pressurized Hyperboloidal Shells,"Journal of the Engineering Mechanics Division, ASCE, Vol.101, No. EM5, Proc. Paper 11650, October 1975.

TESTING OF A REPAIRED MICRO-CONCRETE MODEL OF A COOLING TOWER SHELL

by

HOSSEIN MOZAFFARIAN

B.S., Kansas State University, 1980

An Abstract of a Master's Thesis

submitted in partial fulfillment of

the requirements for the degree

MASTER OF SCIENCE

Department of Civil Engineering

Kansas State University

Manhattan, Kansas

1983

ABSTRACT

Hyperbolic natural-draft cooling towers are probably the largest reinforced concrete thin-shell structures. Due to increasing need for electric power the use of taller and larger cooling towers with higher cooling capacities has become necessary. However, there has been little experimental research on the behavior and stability of this type of shells.

The experiment carried out here was to give some evidence on the buckling behavior of this type of shell and observe the effects of geometry and thickness imperfections under axisymmetric pressure (vacuum). The model cooling tower under consideration was 12 ft. (3.65 m) high, 9.33 ft. (2.84 m) in diameter at the base, and had a nominal thickness of 0.5 in. (13 mm).

The model failed explosively at a vacuum pressure of 3.7 Psi (25.53 KPa) and about 1 ft. (30.5 cm) above the base on line J. Both the unusual failure mode and unsymmetrical response of the model could be attributed to imperfections, the out-of-roundness of the shell, and small amount of reinforcing.